STIMULI SENSITIVE CORE-SHELL NANOPARTICLES FOR TARGETED DRUG DELIVERY

CHOOI KAR WAI

NATIONAL UNIVERSITY OF SINGAPORE

2003

STIMULI SENSITIVE CORE-SHELL NANOPARTICLES FOR TARGETED DRUG DELIVERY

CHOOI KAR WAI

(B. Eng. (Hons.), University Science of Malaysia)

A THESIS SUBMITTED

FOR THE DEGREE OF MASTER OF ENGINEERING

DEPARTMENT OF CHEMICAL AND ENVIRONMENTAL ENGINEERING

NATIONAL UNIVERSITY OF SINGAPORE

2003

ACKNOWLEDGEMENT

First of all, I would like to express my deepest gratitude to my supervisors, Dr. Yang Yi-Yan and Dr. Tong Yen-Wah, for their guidance, advice and encouragement. This work could not have been completed without their support.

I extend my sincere gratitude to all my friends and colleagues who have contributed in various ways to this work, especially Dr. Chaw Cheng-Shu and Dr. Kumaresh Soppimath, for offering me their precious time and invaluable suggestions.

I also wish to thank Dr. Liu Xue-Ming and Ms. Wang Li-Shan for their kindness in providing me the precious polymers. Thanks are extended to Mr. Tan Cherng-Wen Darren, Ms. Su Siew-Ping, Ms. Chow Shue-Yin and Ms. Wang Lin for their technical assistance in this project.

Special thanks go to my family members for their greatest love, support and encouragement.

Last but not least, I would like to thank the National University of Singapore for giving me an opportunity to pursue my Master degree, and also Institute of Materials Research and Engineering (IMRE), and Institute of Bioengineering and Nanotechnology (IBN) of Singapore for providing me with necessary financial support, laboratory space and equipments.

TABLE OF CONTENTS

CHAPTER 4 RESULTS AND DISCUSSION

SUMMARY

The development of modulated drug delivery vehicles with remarkable efficacy in recent years has prompted the design of smart polymeric systems that are responsive to external stimuli or changes in the physiological environment. Therefore, two novel polymer systems, such as cholesteryl end-capped poly(*N*-isopropylacrylamide-*co*-*N,N*-dimethylacrylamide) [P(NIPAAm-*co*-DMAAm)] and poly(*N*-isopropylacrylamide-*co*-*N,N*-dimethylacrylamide-*co*-oleic acid) [P(NIPAAm-*co*-DMAAm-*co*-OA)] that are thermally and/or pH responsive were employed to fabricate core-shell nanoparticles for targeted drug delivery. Two hydrophobic drugs with different molecular structures, such as cyclosporin A (CyA) and indomethacin (IMC), were chosen as model drugs.

The blank and drug-loaded core-shell nanoparticles were characterised using various analytical tools. Transmission electron microscopy and dynamic light scattering measurements revealed that the core-shell nanoparticles were spherical, and had a mean diameter less than 200 nm. P(NIPAAm-*co*-DMAAm-*co*-OA) nanoparticles demonstrated a change in particle size with respect of pH. The critical association concentration (CAC) of cholesteryl end-capped P(NIPAAm-*co*-DMAAm) and P(NIPAAm-*co*-DMAAm-*co*-OA) polymers in ultra pure water was estimated as 20.0 and 64.0 mg/L, respectively. The CAC value of cholesteryl end-capped P(NIPAAm-*co*-DMAAm) polymer was reduced to 12.0 mg/L in phosphate buffer saline (PBS), while the CAC of P(NIPAAm-*co*-DMAAm-*co*-OA) polymer remained unchanged in the presence of salts.

The lower critical solution temperature (LCST) of cholesteryl end-capped P(NIPAAm-*co*-DMAAm) and P(NIPAAm-*co*-DMAAm-*co*-OA) core-shell nanoparticles in water was estimated to be 37.0^{o}C and 32.8^{o}C, respectively. However, the presence of salts in PBS, as well as serum proteins in bovine serum albumin (BSA) and fetal bovine serum (FBS), reduced the LCST of both core-shell nanoparticles systems. The LCST of P(NIPAAm-*co*-DMAAm-*co*-OA) polymer was increased with increasing pH. The core-shell nanoparticles demonstrated reversibility of thermoresponsive aggregation and dispersion. Meanwhile, it was also demonstrated that P(NIPAAm-*co*-DMAAm-*co*-OA) core-shell nanoparticles experienced deformation and reformation of structure in heating and cooling thermal cycles through the LCST.

Loading of drug molecules was a complicated process. Various factors that influence drug encapsulation efficiency, such as fabrication temperature, pH, initial drug loading, structure and size of drug molecules, as well as polymer concentration were investigated. Better entrapment was yielded for CyA compared to IMC because of its lower dissolution loss during the fabrication process. Higher drug encapsulation efficiency was obtained at lower fabrication temperatures and pH, but at higher polymer concentrations. However, drug precipitation, which was caused by rapid solvent removal at high temperatures, was the dominant factor that influenced the drug encapsulation efficiency.

In vitro release of drug-loaded core-shell nanoparticles was studied at different temperatures, pH and drug loading level. Cholesteryl end-capped P(NIPAAm-*co*-DMAAm) and P(NIPAAm-*co*-DMAAm-*co*-OA) core-shell nanoparticles showed higher CyA release at temperatures below the LCST than above the LCST.

P(NIPAAm-*co*-DMAAm-*co*-OA) core-shell nanoparticles also demonstrated pH responsive release of CyA and IMC, wherein higher release was obtained at higher pH. Furthermore, an increase in drug loading level resulted in a slower release of IMC.

Hence, the core-shell nanoparticles developed would make a good carrier for targeted drug delivery because they possess a great potential for passive targeting due to their small size, low CAC and good stability against serum proteins, as well as active targeting because of their reversible stimuli responsive character.

NOMENCLATURE

Notation

b	Block copolymer
co	Random copolymer
g	Grafted copolymer
I_1	Intensity of the first band
I_3	Intensity of the third band
M_w	Weight-averaged molecular weight
M_n	Number-averaged molecular weight
T_g	Glass transition temperature
T_m	Melting temperature
v	Volume
w	Weight

Abbreviation

AcN	Acetonitrile
ADR	Adriamycin
AlClPc	Aluminium chloride phthalocyanine
BAN	4-Bromo-1-acetonaphthone
BSA	Bovine serum albumin
CA	Cholic acid
CAC	Critical association concentration
$CaCl_2$	Sodium chloride
$CDCl_3$	Deuterated chloroform

ϵ-CL	ϵ-Caprolactone
CyA	Cyclosporin A
CZ	Clonazepam
Da	Dalton
DCM	Dichloromethane
DLS	Dynamic light scattering
DMAAm	*N,N*-Dimethylacrylamide
DMAc	*N*,*N*-Dimethylacetamide
DMF	*N*,*N*-Dimethylformamide
DMSO	*N*,*N*-Dimethylsulfoxide
DNA	Deoxyribonucleic acid
DOX	Doxorubicin
DSC	Differential scanning calorimeter
DSPE	Distearoyl phosphatidyl ethanolamine
EPR	Enhanced permeation and retention
FBS	Fetal bovine serum
FID	Flame ionisation detector
FTIR	Fourier transformation infra red
GC	Gas chromatography
GI	Gastrointestinal
GPC	Gel permeation chromatography
H	Hydrogen
HCl	Hydrochloride acid
He	Helium
^{1}H NMR	Proton nuclear magnetic resonance

HPLC	High-performance liquid chromatography
IMC	Indomethacin
KBr	Potassium bromide
KRN	KRN 5500: (6-[4-deoxy-4-(2E,4E)-tetradecadienoylglycyl]amino-L-glycero-β-L-manno-heptopyranosyl]amino-9H-purine)
LCST	Lower critical solution temperature
MAA	Methacrylic acid
MDSC	Modulated differential scanning calorimetry
MePEG	Methoxy polyethylene glycol
MPS	Mononuclear phagocyte system
MTD	Maximum tolerated dose
MTX	Methotrexate
NaOH	Sodium hydroxide
NaCl	Sodium chloride
N_2	Nitrogen
Ne	Neon
NIPAAm	*N*-isopropylacrylamide
OA	Oleic acid
ODA	Octadecyl acrylate
PA	Pullulan acetate
PAA	Poly(acrylic acid)
P(Asp)	Poly(aspartic acid)
PBLA	Poly(β-benzyl L-aspartate)
PBLG	Poly(γ-benzyl L-glutamate)

PBMA	Poly(butylmethacrylate)
PBS	Phosphate buffer solution
PCL	Poly(ϵ-caprolactone)
PBMA	Poly(butyl methacrylate)
PDLLA	Poly(D,L-lactide)
PEG	Poly(ethylene glycol)
PEO	Poly(ethylene oxide)
PHAA	Poly(2-hydroxyethyl aspartamide)
P(HAZA)	Poly(*N*-hexyl-L-aspartamide)-Z-acid
PHEA	Poly(2-hydroxyethyl-L-aspartamide)
PHPMA	Poly(*N*-(2-hydroxy-propyl)methacrylamide)
PHSA	Poly(*N*-hexyl stearate L-aspartamide)
PLA	Poly(L-lactic acid)
PLGA	Poly(lactic-co-glycolic acid)
PLL	Poly(L-lysine)
Pluronic	Poly(ethylene oxide)-poly(propylene oxide)-poly(ethylene oxide)
PNIPAAm	Poly(*N*-isopropylacrylamide)
PS	Polystyrene
RES	Reticuloendothelial system
RNA	Ribonucleic acid
S.D.	Standard deviation
SDM	Sulfadimethoxine
TEM	Transmission electron microscopy
TGA	Thermogravimetric analyser

THF	Tetrahydrofuran
UV-VIS	Ultraviolet-Visible

LIST OF FIGURES

LIST OF TABLES

CHAPTER 1 INTRODUCTION

Drug delivery is rapidly becoming an integral part of drug development strategies within the pharmaceutical and biotechnology industries. Global drug delivery market is currently valued at US$50 billion a year, or 12.5% of world total pharmaceutical sales. However, it has been estimated that by the year of 2005, the sales of drug delivery products will reach US$100 billion, as technologies currently being researched and developed reach fruition and are commercialised (Informa Pharmaceuticals, 2000).

Until the early 1970s, drugs were delivered to the human body exclusively *via* oral and injection means. In the case of oral doses, the drug concentration in blood first rises rapidly to a maximum level, and then falls gradually as the drug is metabolised. On the other hand, intravenous injection results in an exponential decrease from the maximum blood concentration (Kaneko et al., 1998). Often the initial maximum concentration is above the therapeutically desirable level, increasing the risk of side effects. Conversely, the minimum concentration may be below the therapeutically effective level, hence repeated administration becomes necessary [Figure 1.1 (a)].

Conventional drug therapy generally involves the periodic dosing of a therapeutic agent that has been formulated in a way to ensure its stability, activity, and bioavailability. For most drugs, conventional methods of formulation are quite effective. However, some drugs are unstable and toxic, and have a narrow therapeutic range, or exhibit extreme solubility problems. Sometimes, they require localisation to a particular site in the body, or strict compliance or long-term use (Linhardt, 1989). Such

problems in conventional drug therapy have prompted the development of controlled drug delivery system to keep drug concentrations in effective ranges for longer periods by a single dose and to deliver drugs only to target sites [Figure 1.1 (b)].

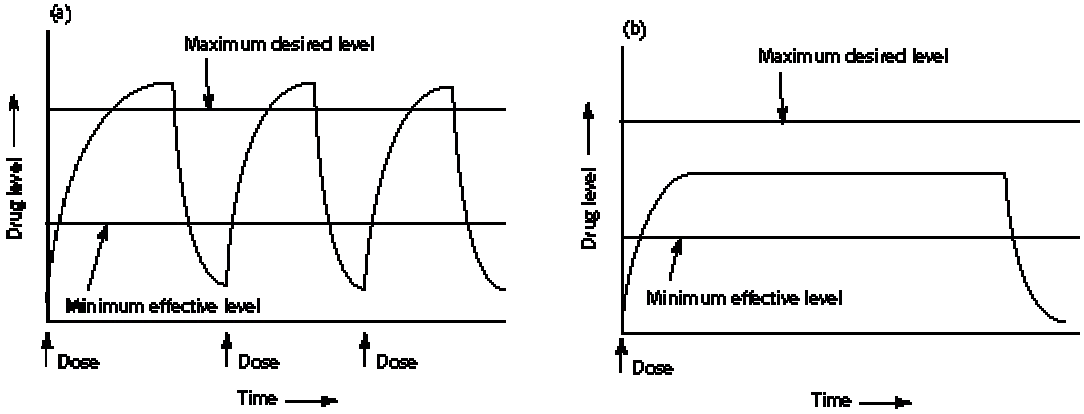

Figure 1.1 Drug levels in the blood with (a) traditional drug dosing and (b) controlled-delivery dosing (Brannon-Peppas, 1997)

The earliest drug delivery systems, first introduced in the 1970s by Yolles and coworkers, were based on polymers formed from lactic acid. Since then, much progress has been made on the design of efficient drug carriers such as liposomes (Lasic, 1996; Tardi et al., 1986; Weinstein, 1987), microparticles (Alonso, 1996; Brannon-Peppas, 1995) and nanoparticles (Cavallaro et al., 1994; Niwa et al., 1995), but many of these delivery vehicles have shown limited therapeutic efficacy in the clinic (Duncan, 1992). The use of liposomes is restricted because they are structurally fragile, and taken up easily by monophagocytes in various tissues of the reticuloendothelial system (RES) (Allen, 1988) and have a low loading efficiency of hydrophobic drugs (Kabanov et al., 1992). On the other hand, microparticles (1 to 5000 μm) are too large to direct the drugs to target tissues across the mucosal membrane or *via* systemic circulation (Kreuter, 1983; Schroeder et al., 1978).

To overcome these problems, polymeric nanoparticles are proposed as an alternative drug carrier. Due to their small size, nanoparticles may be useful as sustained-release injections for the delivery of drugs to a specific organ or target site. However, since most drugs are relatively hydrophobic, conjugation of drugs with polymeric nanoparticles formed from homopolymer, statistical copolymer or natural polymer often leads to precipitation because of a high local concentration of hydrophobic drug molecules bound along the polymer chain. Polymeric core-shell nanoparticles can solve these problems associated with the conventional polymeric nanoparticles due to their unique properties (Harada and Kataoka, 1998; Yokoyama et al., 1990; Yokoyama et al., 1994b).

Polymeric core-shell nanoparticles, a colloidal drug delivery system, can be easily fabricated, and their chemical as well as physical properties can be readily controlled *via* molecular synthesis. Besides, they can also protect the drugs having short *in vivo* half-lives, and improve the bioavailability of drugs having poor aqueous solubility. The drug in the carrier is unchanged, therefore its absorption, distribution, metabolism and excretion after being released from the carrier is similar to that of the native drug. Moreover, its biological efficiency when released from the carrier is the same as that when used alone. In addition, polymeric core-shell nanoparticles can be localised to a desired site, reducing systemic toxicity, and this localisation can increase the drug potency.

In recent years, controlled drug delivery formulations and the polymers used in these systems have become much more sophisticated, with the ability to do more than sustained release for a particular drug. For example, controlled-release systems have

been developed to respond to changes in the biological environment, and thus alter the drug-release process accordingly. The release of the drug may be constant or cyclic over a long period, or it may be triggered by the environment or other external stimuli such as pH (General and Thünemann, 2001; Govender et al., 2001; Kang and Bae, 2001; Leroux et al., 1996; Leroux et al., 2001), electricity (Eisenberg and Grodzinsky, 1984; Kwon et al., 1991), temperature (Chung et al., 1998; Huang et al., 1994; Kim et al., 2000a; Kohori et al., 1998; Meyer et al., 2001), ultrasound (Husseini et al., 2002; Marin et al., 2001) and electrochemicals (Takeoka et al., 1995) (Brannon-Peppas, 1997). Stimuli-sensitive drug carriers are more advantageous in some cases. For instance, during the 1980s, diabetes, which requires fluctuating levels of insulin to mimic the natural biofeedback mechanism, became a widely investigated "test case" for the application of a modulated release system (Sinko and Kohn, 1993).

Therefore, the design of stimuli-sensitive core-shell nanoparticles that are able to selectively recognise their physiological objective is of great interest. These core-shell nanoparticles are expected to present a double targeting character, which are the passive targeting resulting from both their small size and highly hydrated shell structure, and active physical affinity targeting resulting from their stimuli-responsive properties.

In the next chapter, a review of the research work done in polymeric core-shell nanoparticles as drug carriers will be presented. An understanding of this will then bring into focusing the objectives of this project. Chapter 3 describes the methodology of this research project while the results obtained are presented and discussed in Chapter 4. The conclusions and recommendations will be in Chapter 5.

CHAPTER 2 LITERATURE REVIEW

2.1 Introduction to polymeric core-shell nanoparticles

Polymeric core-shell nanoparticles are known to exhibit micellar behaviour (Kwon et al., 1995; Kwon et al., 1993a; Bahadur et al., 1988) and were first proposed as drug carriers by Bader et al. (1984). They have emerged as potential drug carriers for poorly soluble drugs because they mimic aspects of natural carriers, such as viruses and serum lipoproteins, in terms of structure and function. Table 2.1 lists various polymeric core-shell nanoparticle systems developed recently. Core-shell nanoparticles as drug carriers are able to provide a number of advantages. They can solubilise hydrophobic drugs and thus increase their bioavailability by protecting the drugs from possible non-specific tissue adsorption and inactivation under the effect of biological surroundings. They also offer attractive characteristics, particularly a small size, which is in the range of 10-200 nm that allows them to stay in the body (in the blood) long enough to provide gradual accumulation in the required area and body regions with leaky vasculature. Furthermore, this size range allows for easy sterilisation because the nanoparticles can easily pass through the 0.22 to 0.45 μm filters commonly used for filtration sterilisation (Yokoyama, 1998). Additionally, these core-shell nanoparticles can be targeted using stimuli-responsive polymers or attaching specific ligands to the outer surface.

Polymeric core-shell nanoparticles consist of two phases, which are the inner core phase and the outer shell phase. Each phase plays a different role and the functions required for drug delivery systems can be shared by these structurally separated phases.

Table 2.1 Core-shell nanoparticles used for drug delivery

Types of system	**Copolymers**	**Incorporated drugs**	**Reference**
Drug conjugates	PEG-P(Asp)	ADR	Yokoyama et al., 1993; Yokoyama et al., 1998b
	PHPMA	DOX	Ulbrich et al., 2003
	PEO-*b*-P(HAZA)	Amphotericin B	Adam and Kwon, 2003
	Acetal-PEG-PDLLA	Charged peptides	Yamamoto et al., 1999; Yamamoto et al., 2001
	PEO-*b*-PHAA	MTX	Yu and Kwon, 1999
	PEO-*b*-PHEA	MTX	Yu and Kwon, 2000
	PLGA-PEG	DOX	Yoo et al., 2002; Yoo and Park, 2001
	PEO-P(Asp)	ADR	Yokoyama et al., 1994a; Kwon et al., 1994a
	PEG-P(Asp)	Cisplatin	Mizumura et al., 2001
Nano-containers	PNIPAAm-PBMA and PNIPAAm-PS	ADR	Chung et al., 1999; Chung et al., 2000
	PEG-P(Asp)	ADR and ADR dimer	Fukushima et al., 1999
	PEO-PBLA	ADR	Kwon et al., 1995
	PEO-*b*-PHSA	Amphotericin B	Lavasanifar et al., 2000; Lavasanifar et al., 2002b; Lavasanifar et al., 2001a
	Pluronic	DOX	Marin et al., 2002
	CA/PNIPAAm	IMC	Kim et al., 2000c
	PLA/ PNIPAAm	IMC	Kim et al., 2000b
	PEG-PBLA	DOX	Kataoka et al., 2000
	PEG-PBLA	KRN	Yokoyama et al., 1998a
	PEG-DSPE	Protein	Weissig et al., 1998
	MePEG/ϵ-CL	IMC	Shin et al., 1998
	P(NIPAAm-*co*-MAA-*co*-ODA)	AlClPc	Taillefer et al., 2000
	PBLG/PEO	CZ	Jeong et al., 1998
	PA/SDM	ADR	Na et al., 2003
	PEG-P(Asp)	Cisplatin	Yokoyama et al., 1996
	Pluronic/PCL	IMC	Kim et al., 2000a
Polyion complex	P(Asp)-PEG	Diminazene aceturate	Govender et al., 2001
	PLL-*g*-PLGA	Plasmid DNA	Jeong and Park, 2002
	PEG-P(Asp)	Lysozyme	Harada and Kataoka, 2001; Harada and Kataoka, 1998; Harada and Kataoka, 1999
	PEG-PLL	Plasmid DNA	Katayose and Kataoka, 1997

As shown in Figure 2.1, the nanoparticles core serves as a microreservoir for the incorporation of hydrophobic drugs and they are also responsible for pharmacological activities through drug loading and release. On the other hand, the outer shell is responsible for core-shell nanoparticles stabilisation of the interface between the hydrophobic core of the nanoparticles and the external environment; and also interactions with the biocomponents such as proteins and cells. These interactions determine pharmacokinetic behaviour and biodistribution of drugs. Therefore, *in vivo* delivery of drugs may be controlled by the outer shell segment independently of the inner core of the nanoparticle (Yokoyama, 1998).

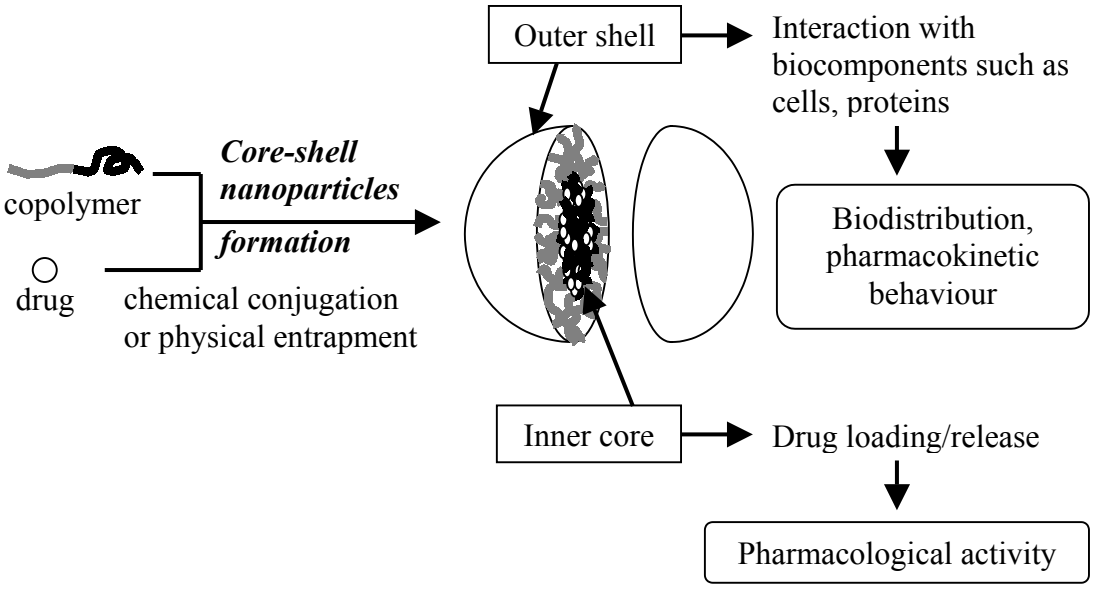

Figure 2.1 The concept and functionality of a core-shell nanoparticle as a drug carrier (Adapted from Yokoyama, 1998)

2.2 Amphiphilic copolymers

Polymeric core-shell nanoparticles represent a different class of micelles and are formed from copolymers containing both hydrophilic and hydrophobic monomer units. The hydrophobic segment forms the hydrophobic core of the nanoparticles, while the

hydrophilic segment surrounds the core as a hydrated outer shell. There are several classifications of polymers, as presented in Figure 2.2. Unlike homopolymer made of identical monomeric units, copolymers are formed from two types of monomeric units differing in their solubility. Following polymerisation, these monomeric units can be organised into a polymeric chain in different positions depending on the type of copolymer desired, such as random, block and graft copolymers.

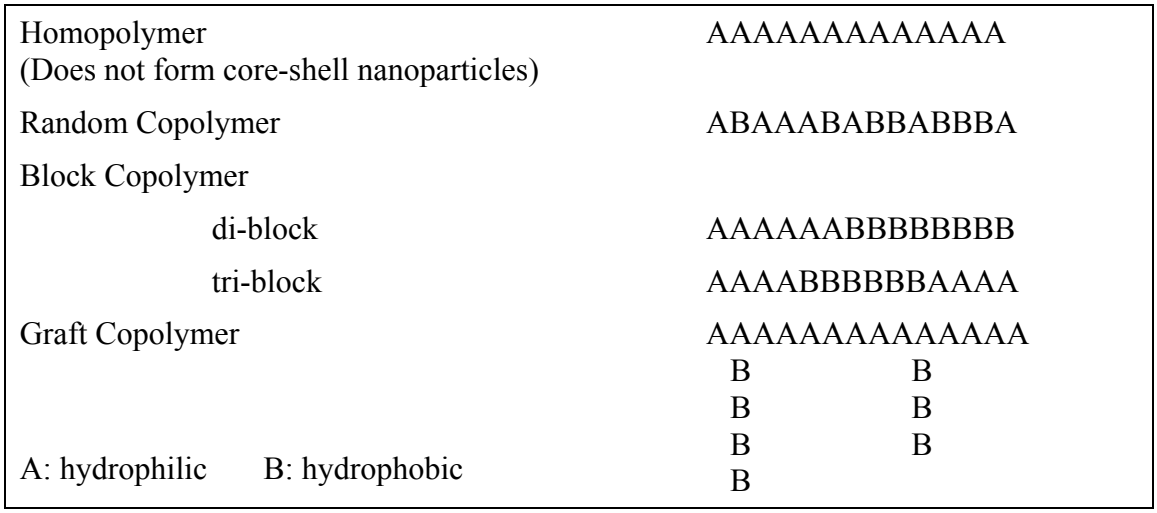

Figure 2.2 A schematic presentation of different polymers which can be created depending on the number of types of repeat units; homopolymer (one type), copolymer (two or more types) (Adapted from Torchilin, 2001)

The copolymer materials used in the preparation of drug carriers are often block copolymers, comprising a block or sequence of one repeat unit coupled to a block of another repeat unit (Cowie, 1994). This can be observed from the rapid development of research on core-shell nanoparticles made from block copolymers as shown in Figure 2.3. The advantage of using block copolymers over random copolymer materials is the much narrower total molecular weight and sequence distributions for block copolymers (Cowie, 1994; Wilczek-Vera, 1996). The versatility afforded by the use of copolymers is largely due to the easily controlled of the material properties, such as copolymer ratio, molecular weight, molecular weight distribution and block

composition. Therefore, polymeric core-shell nanoparticles can be tailor-made to suit a particular application through careful manipulation of the properties of the copolymer materials from which they are formed.

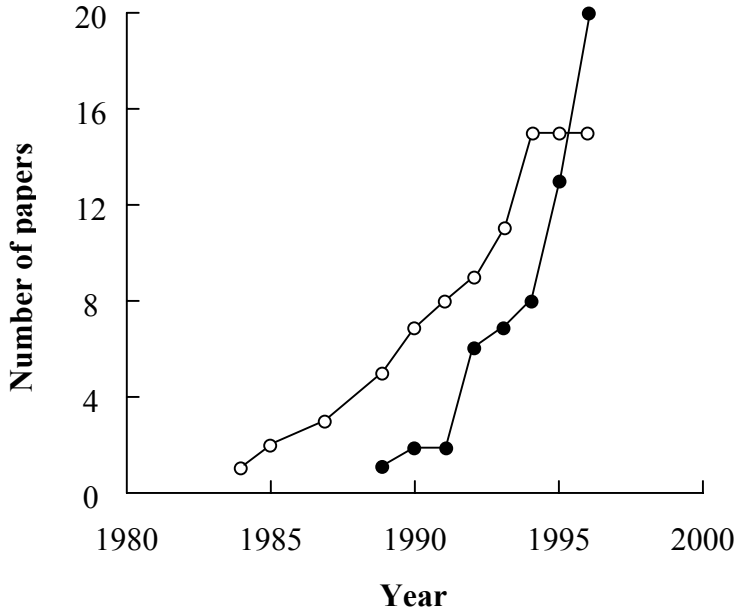

Figure 2.3 Development of work on (○) block copolymer-drug conjugates and (●) block copolymer core-shell nanoparticles for non-covalently incorporated drugs (Kabanov and Alakhov, 2000)

Some polymers may exhibit a stimuli-responsive character, wherein small changes in pH (Katayama and Ohata, 1985; Kim et al., 1994; Liu et al., 2002; Kyriakides et al., 2002; Serres et al., 1996; Taillefer et al., 2000 ; Ulbrich et al., 2003), temperature (Christova et al., 2003; Eekman et al., 2003; Feil et al., 1993; Kim et al., 1994; Serres et al., 1996; Urry, 1997), metabolites (Cartier et al., 1995), or the application of an ultrasound (Husseini et al., 2000; Marin et al., 2002; Rapoport et al., 1999), pressure (Tanaka et al., 1998), or light (Gerasimov et al., 1999; Suzuki and Tanaka, 1990) can cause sharp changes in the polymer volume and shape reversibly (Mikos et al., 1993).

For examples, chemical signals, such as pH, metabolites and ionic factors will change the molecular interactions between the polymer chains or between polymer chain and

solutes present in the system. On the other hand, physical stimuli such as temperature or electrical potential may provide various energy sources for molecular motions and altering molecular interactions. These interactions will change the properties of the polymer materials, such as swelling, solubility, configuration or conformation change, redox states and crystalline/amorphous transition (Audus, 1991; Junginger, 1992; Park, 1997).

Hence, due to the potential applications of such polymers in the normal physiological process, many research groups have been developing drug delivery systems based on these responsive polymers in the last few decades. Among them, the most commonly studied polymers having environmental sensitivity are either pH or temperature sensitive.

2.2.1 Temperature-responsive polymers

Poly(*N*-isopropylacrylamide) (PNIPAAm) and its copolymers are the most frequently studied temperature-sensitive polymers (Dhara and Chatterji, 2000). It exhibits a lower critical solution temperature (LCST) of around 32°C in water. The polymer has a deceptively simple structure with a hydrophobic backbone, containing a strong hydrophilic amide group ($–CONH_2$) substituted with a hydrophobic isopropyl group. The isopropyl group tends to pull away from the water molecules, while the amide group prefers to be in water because of its strong hydrogen-bonding capacity with water molecules. It is generally believed that this hydrophilic-hydrophobic push-pull is responsible for the LCST behaviour of PNIPAAm in water (Dhara and Chatterji, 2000).

At low temperatures (below the LCST), the polymer has a good solubility in water due to its strong hydrogen bonding between the hydrophilic groups and water, which outweighs the unfavourable free energy correlated to the exposure of hydrophobic groups to water. Then, as the temperatures increase, the hydrophobic interactions between hydrophobic side groups become more intense as the hydrogen bonding weakens. Above the LCST, interactions between hydrophobic groups become dominant, leading to an entropy-driven polymer collapse and phase separation (Figure 2.4). The decreased motional freedom of the polymer chain is compensated by an increase in entropy due to the release of structured water around the hydrophobic groups of the polymer (Feil et al., 1993).

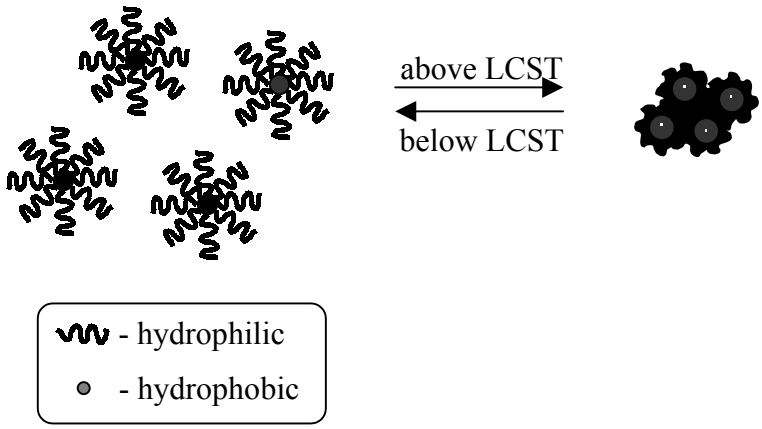

Figure 2.4 Structural changes occurring when the solution temperature is cycled through the LCST of PNIPAAm core-shell nanoparticles
(Adapted from Chung et al., 1998)

2.2.2 pH-responsive polymers

The variation in pH along the gastrointestinal tract (Evans et al., 1988) and also the small but clear difference in pH between tumours and normal tissues (about 7.0 in tumours and 7.4 in normal tissues) (Van den Berg et al., 1982) has motivated many researchers to develop pH-responsive polymeric drug delivery systems. Studies have

been performed on polymers containing weakly acidic or basic groups in the polymeric backbone. For instance, while anionic pH-sensitive polymers contain the carboxylic (Benrebouh et al., 2001; Chiu et al., 2001) and sulfonate or sulfate groups (Kathmann et al., 1997), primary or tertiary amine monomers (Sakata et al., 2001; Yuk et al., 1997) have been used as typical groups in cationic copolymers.

The charge density of the polymers depends on the pH and ionic composition of the outer solution to which the polymer is exposed. Altering the pH of the solution will cause swelling or deswelling of the crosslinked polymer matrices (Figure 2.5). Polyacidic polymer matrices will be swollen at high pH, because the acidic groups will be deprotonated and hence ionised. The opposite holds for polybasic polymer matrices, because the ionisation of the basic groups will increase with decreasing pH (Kost, 1999**)**.

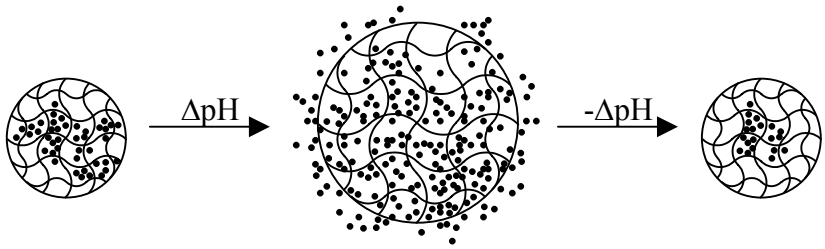

Figure 2.5 A schematic presentation of pH controlled drug delivery systems. Small dots represent drugs; lines represent polymer chains (Δ can be positive or negative) (Kost, 1999)

Based on the unique properties of pH and temperature-sensitive polymers, researchers have used them as a hydrophilic block, and built them into a hydrophobic polymer backbone to form amphiphilic block copolymers. The nanoparticles made from the stimuli-sensitive block copolymers can be employed to achieve both passive and active drug targeting. The details will be introduced later.

2.3 Preparation of core-shell nanoparticles

Basically, there are two methods for the preparation of core-shell nanoparticles, which are the direct dissolution method and the dialysis method, as illustrated in Figure 2.6. The choice of a method mostly depends on the solubility of the copolymer used in water. For instance, if the copolymer is marginally soluble in water, the direct dissolution method is employed, whereas if the copolymer is poorly water-soluble, the dialysis method is preferred (Kim et al., 2000a, Yokoyama et al., 1998a, Shin et al., 1998, Cammas et al., 1997, Ha et al., 1999, Lavasanifar et al., 2001b).

The direct dissolution method merely involves the addition of copolymer into water or other aqueous medium such as phosphate buffer saline (PBS) (Kabanov et al., 1995). In the case of dialysis method, the copolymer is first dissolved in an organic solvent that is miscible with water, such as *N*,*N*-dimethylformamide (DMF) (Fukushima et al., 1999; Lavasanifar et al., 2001a; Kwon et al., 1995; Kim et al., 1998; Yokoyama et al., 1998a), tetrahydrofuran (THF) (Kim et al., 1998), *N*,*N*-dimethylsulfoxide (DMSO) (Jeong and Park, 2002; Lavasanifar et al., 2002b; Yokoyama et al., 1998a), *N*,*N*-dimethylacetamide (DMAc) (Allen et al., 1999b; Chung et al., 2000; Kim et al., 1998; Lavasanifar et al., 2000; Yamamoto et al., 2002) and *N*-ethylacetamide (Chung et al., 1999; Chung et al., 2000;). The copolymer-solvent mixture is stirred, and then dialysed against water. During the dialysis, the organic solvent is removed, and the core-shell nanoparticles are formed.

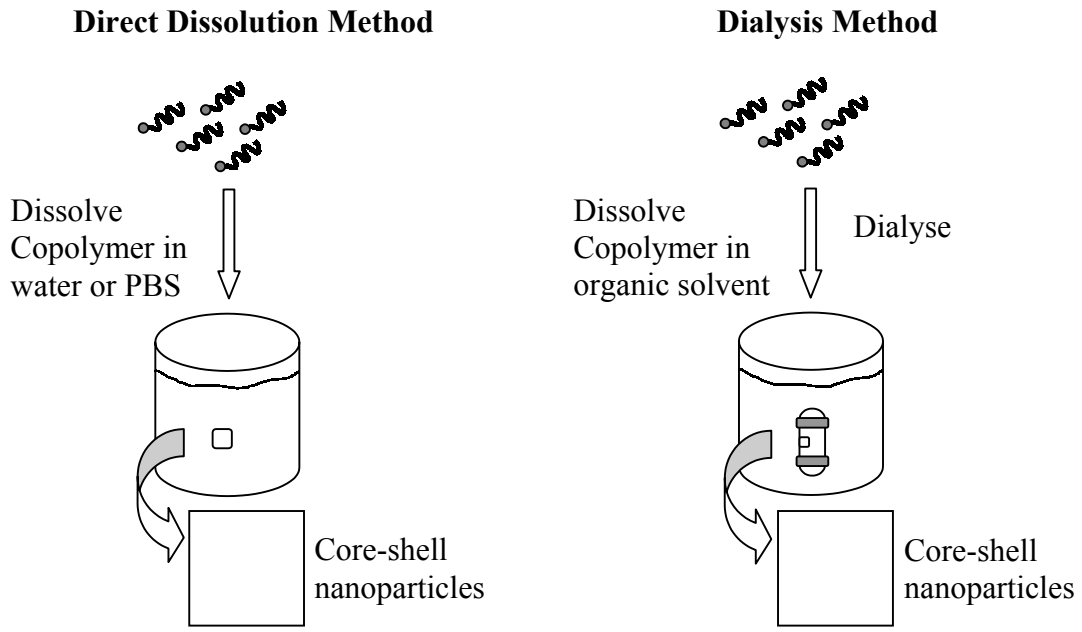

Figure 2.6 A schematic presentation of the direct dissolution and dialysis methods employed for the preparation of polymeric core-shell nanoparticles

2.4 Drug incorporation

Hydrophobic drugs can be incorporated into polymeric core-shell nanoparticles by chemical conjugation (Kataoka, 1994; Yoo et al., 2002) or physical entrapment (Kataoka et al., 1993; Kwon and Okano, 1996; Kwon and Okano, 1999; La et al., 1996). However, in some cases, incorporation of the hydrophobic drug has been employed using both chemical conjugation and physical entrapment. For instance, Yokoyama et al. (1998b) found that the physical entrapment of adriamycin was higher in micelles formed from adriamycin-conjugated poly(ethylene glycol)-*b*-poly(aspartic acid) [PEG-*b*-P(Asp)] than in micelles formed from the PEG-*b*-P(Asp) copolymer alone.

If a drug is chemically attached to the hydrophobic block of the copolymer, its incorporation into the inner core proceeds simultaneously with the formation of

nanoparticles. However, different protocols are used for physical drug incorporation, depending on the method for the preparation of core-shell nanoparticles (Figure 2.6). For example, in the direct dissolution method, copolymer solution in water is added to a drug, which is dried from an organic solvent, or alternatively the drug in an organic solvent, which is immiscible with water (e.g. chloroform), is added to the water solution of preformed nanoparticles. The entrapment of the drug is achieved with solvent evaporation (Kataoka et al., 2000; Kwon et al., 1997). For the dialysis method, the drug is dissolved together with the copolymer in an organic solvent. In some cases, the oil-in-water emulsion dialysis method is also used for the incorporation of hydrophilic drugs into nanoparticles (Kwon and Okano, 1996).

Chemical conjugation of hydrophobic drugs requires a covalent bond, such as an amide bond, between the specific groups of the drug and the hydrophobic block of the copolymer. Therefore, physical encapsulation of drugs within the polymeric core-shell nanoparticles is generally a more attractive approach than polymer-drug conjugates since many drug molecules do not bear reactive functional groups (e.g. carboxyl, hydroxyl or amino groups) for chemical conjugation, and the free functional site is sometimes required for the pharmacological effectiveness of the drug. In addition, conjugates of drugs may show distinctly different biological properties relative to the parent drugs. This can cause inherent difficulties in characterisation and regulatory approval even for already approved drugs (Lavasanifar et al, 2002a).

However, there are some drawbacks for physical encapsulation of drugs, including low encapsulation capacity and rapid release of encapsulated drugs (i.e. dose dumping). Alternatively, attaching the drugs to the core-forming block allows for greater drug

loading efficiency and amount within the core of the nanoparticles (Yoo and Park; 2001). In addition, drug conjugation increases the stability of drugs. For example, the PLGA-*b*-PEG micelles containing chemically conjugated doxorubicin showed a more sustained release profile of doxorubicin over a longer period, and were more effectively transported within cells by endocytosis compared to those containing non-conjugated doxorubicin (Yoo and Park; 2001).

Furthermore, core-shell nanoparticles formed from the conjugate are rather stable *in vivo*, and their disintegration takes hours. This is attributed to the covalent bonds, which are resistant to enzymatic cleavage mainly because of the steric hindrance, and cannot be readily hydrolysed (Duncan and Kopechek, 1984; Ulbrich et al., 1987). It was reported that upon intravenous injection, there was an increased circulation time in the blood for the conjugates of doxorubicin with PEG-*b*-P(Asp) copolymer compared to non-conjugated doxorubicin (Kwon et al., 1993b). In another study, PEG-*b*-P(Asp) micelles containing only chemically conjugated doxorubicin were found to have no anti-tumour activity, which is attributed to the slow release of free drug from the micelles (Yokoyama et al., 1998b).

2.5 Loading capacity

The factors that influence the extent of incorporation of drugs into the core-shell nanoparticles have been extensively investigated. One of the important factors is the compatibility between the drug and the core-forming block. This compatibility is based on drug characteristics such as molecular volume, interfacial tension against water,

polarity, hydrophobicity, charge and degree of ionisation (Allen et al., 1999a; Nagarajan et al., 1986).

Aside from polymer-drug compatibility, the length of the core-forming and shell-forming blocks can also play an important role in loading capacity. Increasing the length of hydrophobic block has been found to provide a larger core size per nanoparticle and thus greater ability to entrap hydrophobic drugs (Gadelle et al., 1995). On the other hand, a significant increase in the length of the hydrophilic block decreases the aggregation number, leading to a decrease in the degree of solubilisation since there is only a small hydrophobic volume for drug incorporation (Xing and Mattice, 1997).

There is also evidence that polymer and drug concentration can affect drug solubilisation. Xing and Mattice (1997) reported that an increase in the polymer concentration increased the solubilisation capacity of drug to the saturation level. This phenomenon can be explained from the hydrophobic interactions between the drug and the core-forming block. Stronger interactions can be achieved with more core-forming blocks. Similarly, the presence of a hydrophobic drug can enhance the aggregation of amphiphilic copolymer molecules, and thus lower the critical association concentration (CAC). This further leads to an increased number of core-shell nanoparticles present in the solution (Gadelle et al., 1995; Xing and Mattice, 1997), and provides more hydrophobic cores for drug incorporation. Increasing the drug concentration was reported to produce larger nanoparticles, which in turn increased the solubilisation capacity of nanoparticles (Xing and Mattice, 1997).

2.6 Formation of core-shell nanoparticles

The self-association process of amphiphilic copolymers is similar to that of low molecular weight surfactants. At very low concentrations, the polymers only exist as single chain and have a strong tendency to be adsorbed at the air-water interface. An increase in amphiphile concentration leads to the decrease of the surface tension, which will then become constant as the polymer concentration reach a critical association concentration (CAC), evidencing the saturation of the interface with amphiphile molecules and core-shell nanoparticles formation in the bulk phase (Torchilin, 2001) (Figure 2.7).

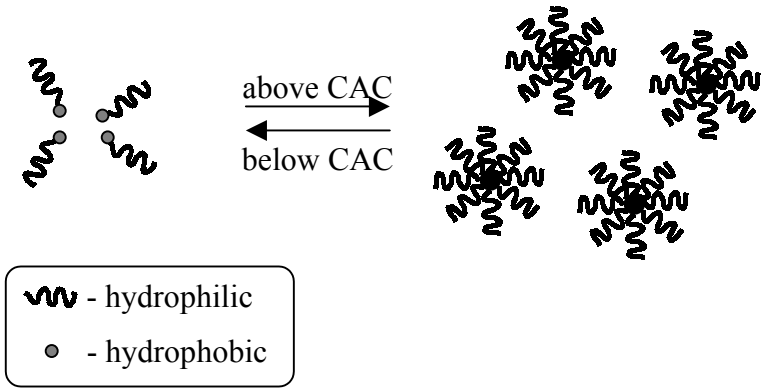

Figure 2.7 Self-assembly and disassembly of core-shell nanoparticles at concentrations above/below the CAC (Adapted from Chung et al., 1998)

At the CAC, a significant amount of solvent can be found inside the hydrophobic core and the core-shell nanoparticles are described as loose aggregates. Further increase in polymer concentration allows core-shell nanoparticles to be in a low-energy configuration, and the remaining solvent is slowly released from the hydrophobic core, resulting in a decrease in the size of nanoparticles (Jones and Leroux, 1999).

Core-shell nanoparticles are formed as a result of two forces. One is an attractive force that leads to the association of molecules while the other, a repulsive force, prevents

unlimited growth of the core-shell nanoparticles to a distinct macroscopic phase (Astafieva et al., 1993; Price, 1983).

The driving force for self-association of amphiphilic copolymers is the inner-core cohesive interactions such as hydrophobic, electrostatic and π-π interactions, as well as hydrogen bonding (Yokoyama, 1998). Hydrophobic interactions are probably the most common driving force for the incorporation of hydrophobic drugs (Kim et al., 1999; La et al., 1996; Na et al., 2000). On the other hand, the electrostatic interaction may be applied to macromolecules with electric charges in high density such as DNA and RNA, because of their anionic phosphodiester bonds existing in each repeating unit, and may also be applied to highly charged proteins such as aspartic acid and lysine residues (Berti et al., 2000; Harada and Kataoka, 1998; Katayose and Kataoka, 1996; Kataoka et al., 1996; Seymour et al., 1998). Hydrogen bonding and π-π interactions may work in association with other cohesive interactions. For example, drugs with aromatic rings are incorporated into the nanoparticles based on π-π and hydrophobic interactions (Kataoka et al., 2000; Kwon et al., 1993b). Table 2.2 lists various cohesive interactions for incorporation of corresponding drugs.

Table 2.2 Cohesive interactions for formation of core-shell nanoparticles and drug incorporation (Adapted from Yokoyama, 1998)

Interactions*	**Incorporated drug**
Hydrophobic	Hydrophobic drug
Electrostatic	DNA, RNA, highly charged proteins
Hydrogen bonding	Proteins
π-π	Aromatic ring-rich drugs
Others	Cisplatin (interchain cross-link)

* Two or more interactions may occur simultaneously.

Generally, core-shell nanoparticles can be formed using two types of amphiphilic copolymers in which the hydrophobic chain is either randomly bound to the hydrophilic polymer or grafted to one end of the hydrophilic polymer. Core-shell nanoparticles fabricated from the randomly modified polymer are smaller than the end-modified polymer. The particle size is mainly determined by the hydrophobic forces that sequester the hydrophobic chains in the core. The excluded volume repulsion between the hydrophobic chains limits their size (Winnik et al., 1992).

When terminal hydrophobic groups associate to form core-shell nanoparticles, the water clusters immobilised around the hydrophobic segments are excluded from the core. Nonetheless, there is no direct interaction between the core and the hydrophilic shell, which remains as mobile linear chains in the core-shell nanoparticle structure (Chung et al., 1998; Winnik et al., 1992). On the other hand, randomly modified polymers associate in such a way that the hydrophobic and hydrophilic parts of the polymer are entangled together, allowing possible contact between the core and the aqueous media. In this case, the hydrophilic chains forming the shell are less mobile (Chung et al., 1998).

2.7 Stability of core-shell nanoparticles

Polymeric core-shell nanoparticles possess high structural stability provided by entanglement of polymer chains in the inner core. However, the nanoparticles should be stable just enough to provide a sufficient time for drug delivery and accumulation in the target region, and simultaneously be able to slowly dissociate into single chains to provide their easy and problem-free elimination from the body (Torchilin, 2001).

Stability of core-shell nanoparticles both *in vitro* and *in vivo*, as well as their clearance from the body depends on the critical association concentration (CAC) values.

The stability of core-shell nanoparticles consists of two different aspects: thermodynamic stability and kinetic stability (Lavasanifar et al., 2002a). A core-shell nanoparticle is thermodynamically stable relative to disassembly to single chains in pure water if the total copolymer concentration is above the CAC. However, even if a nanoparticle system is below its CAC, it may still be kinetically stable and survive at least for a certain period of time, if the core is large and the core is in a glassy state or if it is crystalline and thus physically crosslinked. Table 2.3 shows factors influencing the stability of core-shell nanoparticles as a drug delivery vehicle.

Table 2.3 Factors influencing the thermodynamic or kinetic stability of core-shell nanoparticles (Allen et al., 1999a)

Parameters		**Nanoparticles stability**	**References**
CAC	Low	↑	Wilhelm et al., 1991
	High	↓	
T_g	Low	↓	Kwon et al., 1994b; Kwon and Kataoka, 1995; Kwon and Okano, 1996
	High	↑	
Hydrophobic-hydrophilic block ratio	Low	↓	Alexandridis et al, 1994; Creutz et al., 1998; Nagarajan and Ganesh, 1989
	High	↑	
Conjugated drug content	Low	↓	Yokoyama et al., 1998b
	High	↑	

2.7.1 Thermodynamic stability

Thermodynamic stability is described by an equilibrium constant between a single polymer chain and the core-shell nanoparticles structure, or more conveniently called

the CAC. In general, polymeric core-shell nanoparticles have much smaller CAC values than that of micelles forming from low molecular weight surfactants.

The CAC value is determined by many factors, including the nature and length of the core-forming block, length of the hydrophilic block and the presence of hydrophobic solubilisates. However, the nature and length of the core-forming block have the greatest effect on the CAC. Amphiphilic polymers, containing a highly hydrophobic block have lower CAC values in water than those having less hydrophobic blocks. Large molecular dimensions of the core-forming segment in the polymers induce a strong tendency for aggregation, thus this pushes the CAC to a very small level (Kataoka, 1994; Kwon et al., 1993a). For instance, the CAC values for poly(styrene)-*b*-poly(ethylene oxide) (PS-*b*-PEO) copolymers, containing highly hydrophobic polystyrene block ranged between 1 and 5 ppm (Wilhelm et al., 1991).

A delivery system is subject to 'sink conditions' or severe dilution upon intravenous injection into an animal or human subject. Therefore, core-shell nanoparticles with high CAC may not be suitable as drug targeting carriers since they are unstable in an aqueous environment and easily dissociate upon dilution. In some cases, injecting a larger volume or a more concentrated nanoparticle solution would prevent the copolymer concentration from falling below the CAC immediately upon injection (Allen et al., 1999a).

2.7.2 Kinetic stability

Kinetic stability is described by low dissociation rates of core-shell nanoparticles above/below the CAC and may be more important than the thermodynamic stability in physiological environments where metabolism and excretion take place, and interactions with biological components (e.g. cells, proteins, and lipids) exist, which can destroy core-shell nanoparticles structure. Yokoyama et al. (1993) reported that PEO-P(Asp/DOX) micelles had a very low rate of dissociation in water and PBS, but the dissociation was accelerated in presence of serum.

The rate of disassembly depends upon the physical state of the hydrophobic core. The copolymers are unable to dissociate freely from polymeric core-shell nanoparticles with solid-like core, e.g. those with high glass transition temperatures (Kwon and Okano, 1996). Therefore, core-shell nanoparticles formed from copolymers containing a hydrophobic block, which has a high glass transition temperature, tend to disassemble more slowly than those with a low glass transition temperature. The polymeric nanoparticles with poly(styrene) core (Prochaska et al., 1992; Wang et al., 1992) are a good example. Since the core is likely in a glassy state at room temperature, the nanoparticles are unable to dissociate into single chains for exchange between core-shell nanoparticles at room temperature (Wang et al., 1992).

The rate of disassembly is also influenced by the same factors that affect the rate of unimers exchange between the nanoparticles, such as solvent inside the core, the hydrophobic content of the copolymer and the lengths of both hydrophobic and hydrophilic blocks. For example, Creutz et al. (1998) discovered that for micelles

formed from poly((dimethylamino)alkyl methacrylate-*b*-sodium methacrylate), the rate of unimers exchange decreased with an increase in the hydrophobic/hydrophilic balance of the copolymer.

Moreover, the incorporation of hydrophobic compounds into the core-shell nanoparticles may enhance the stability of nanoparticles. Yokoyama et al. (1998b) reported that both physical entrapment and chemical conjugation of adriamycin (ADR) into the micelle core increased the structural stability of PEG-*b*-P(Asp) micelles. They suggested that the presence of both physically entrapped drug and chemically conjugated drug increased the hydrophobic interactions within the core, producing micelles that were more tightly packed.

2.8 Drug release kinetics

The release of drug from polymeric core-shell nanoparticles depends upon the rate of drug diffusion from the nanoparticles, the stability of nanoparticles and the rate of polymer biodegradation. If the nanoparticles are stable and the rate of biodegradation of the copolymer is slow or non-biodegradable, drug release rate is mainly influenced by the strength of interactions between the drug and the core-forming block (La et al.; 1996), the physical state of the inner core (Kwon et al., 1997), the amount of drug loaded (Kim et al., 1998), the molecular volume of the drug, the length of the core-forming block (Kim et al., 1998) and the localisation of the drug within the core-shell nanoparticles.

2.8.1 Polymer-drug interactions

Strong polymer-drug interactions can enhance drug loading and hinder drug release from the nanoparticles. Therefore, a compromise must be achieved such that both the loading level and the release kinetics of the drug are optimised. Conditions that weaken the hydrophobic-hydrophobic interactions between the drug and the nanoparticles core can accelerate the drug release rate. La et al. (1996) found that the release of indomethacin from poly(ethylene oxide)-poly(*β*-benzyl L-aspartate) micelles was greatly enhanced when the pH value of the external medium was changed from 1.2 to 7.4 at 37^{o}C. At a pH value below the pK_a (4.5) of indomethacin, indomethacin in the nanoparticles remained unionised with little tendency for release. As the pH value of the medium was increased, more of the carboxylic acid groups in the polymer and the carboxylic acid group in indomethacin became ionised, and the hydrophobic-hydrophobic interactions that held indomethacin within the poly(*β*-benzyl L-aspartate) core weakened, resulting in faster indomethacin release.

In the case of drug conjugates, the drug is only released when the covalent bond between the drug and the polymer has cleaved. Water penetration and hydrolysis of the liable bonds in the nanoparticles core (bulk erosion), followed by drug diffusion may occur in relatively hydrophilic liquid-like core structures. However, for rigid core structure, drug release is dependent on the rate of nanoparticles dissociation since water diffusion into hydrophobic core is restricted (Lavasanifar et al., 2002a). The slow dissociation of nanoparticles into single polymeric chains and further hydrolysis of the liable bonds may result in a sustained drug release (Li and Kwon, 2000). The

drug release may be delayed until the carrier reaches the target sites, if the nanoparticles structure is sufficiently stable.

2.8.2 Drug localisation

The incorporated drug may lie within the hydrophobic core or shell itself, or at the interface between the core and shell. The localisation of the drug depends on its physical properties and the interactions between the drug and core/shell-forming blocks (Hruska et al., 1993; Teng et al., 1998). Less hydrophobic drugs are localised in the shell or the interface, while more hydrophobic drugs are entrapped most likely in the inner core. The release rate of drug is a function of its localisation within the nanoparticles. The outer shell region of the nanoparticles is quite mobile, and drug release from this area is rapid. Therefore, the release of drug localised in the corona or at the interface is responsible for the 'burst release' (Teng et al., 1998).

2.8.3 Physical state of the hydrophobic core

The rate of drug release is also controlled by the state of the nanoparticles core (e.g solid or liquid-like) (Kwon et al., 1997). The physical state of the core under physiological conditions ($37^{o}C$) is largely dependent upon the glass transition temperature of the core-forming block as well as the degree of its crystallinity (Allen et al., 1999a). According to Cowie (1994), the nanoparticles have a glassy core if the glass transition temperature of the core-shell nanoparticles is higher than that of the core-forming block; conversely, the nanoparticles have a liquid-like core. The lower

glass transition temperature is attributed to the plasticisation of the solvent or drug molecules incorporated.

The design of polymeric nanoparticles with glassy cores would yield drug release in a sustained manner. Teng et al. (1998) reported that pyrene release from glassy cores formed from poly(styrene) and poly(tert-butyl acrylate) was well sustained. In contrast, pyrene was released too rapidly to be measured from the swollen cores of poly(2-vinylpyridine), which were liquid-like under the experimental conditions.

2.8.4 Length of the core-forming block

The properties of the nanoparticles core, such as the core radius, also influence drug release rate, which is localised inside the hydrophobic core. Longer core-forming block produces larger core, resulting in slower drug release (Allen et al., 1999a). However, if the drug is located at the core-shell interface or in the outer shell, it does not have to diffuse through the core. In this case, drug release is not influenced by the core radius or length of the core-forming block. For example, Hruska et al. (1993) found that the exit rate coefficient for the fluorescent probe BAN was independent of the size of the micelle since it resides close to the core surface.

2.8.5 Molecular volume of the drug

The size or molecular volume of the drug affects its diffusion from the core-shell nanoparticles (Teng et al., 1998). Drugs with larger molecular volumes have a smaller diffusion coefficient, resulting in a decreased release rate. However, the release of

drugs localised at the surface of the nanoparticles should be independent of the molecular volume (Allen et al., 1999a).

2.8.6 Physical state of the drug in the nanoparticles

The physical state of the drug within the core-shell nanoparticles can have a significant effect on drug release kinetics. The incorporated drug may be either well solubilised or undissolved in the hydrophobic core. If the drug is molecularly dissolved within the core, it may act as a plasticiser and lower the glass transition temperature of the core-forming block. This in turn may accelerate the release of the drug from the nanoparticles.

On the other hand, if the drug is undissolved in the core, it may exist instead as a crystal within the nanoparticles core (Benoit et al., 1986; Donbrow, 1991). The present of the drug as a crystal may act as reinforcing filler. In particular, if strong interactions between the polymer and the surface of the crystallite are present, an increase in the glass transition temperature may occur. A sustained release of drug may be yielded (Allen et al., 1999a).

2.9 Morphology

Most of the polymeric core-shell nanoparticles designed was reported to be spherical (Gref et al., 1994; Jeong et al., 1998; Li and Kwon, 1999; Li and Kwon, 2000). However, morphologies other than spheres are of interest because of their different applications in drug delivery. For instance, rod-like core-shell nanoparticles have

different loading capacity and drug release kinetics compared to the spherical core-shell nanoparticles. The rod-like nanoparticles may be the most useful in the preparation of aerosol formulations because they have been shown to be more suitable than spheres (Ding and Liu, 1998). A transfer to rod, vesicles, ellipsoid and lamellar core-shell nanoparticles may occur as the copolymer composition and concentration, type and concentration of added ions and the nature of the common solvent used in the preparation of core-shell nanoparticles are altered (Table 2.4).

Table 2.4 Morphogenic factors that control the morphology of core-shell nanoparticles and examples of each (Adapted from Allen et al., 1999a)

Morphogenic factors	**Block copolymers**	**Morphology**	**References**
Copolymer composition	PS-*b*-PAA 200-*b*-21 200-*b*-15 200-*b*-8	 Spheres Rods Vesicles	Zhang and Eisenberg, 1996b
Copolymer concentration	PS-*b*-PAA 410-*b*-25 2.0 w % 2.6 w % 4.0 w %	 Spheres Rods Vesicles	Zhang and Eisenberg, 1997
Presence of added acid, base or salt	PS-*b*-PAA 410-*b*-25 (1 w %)	 Spheres	
Acid	+ HCl (210 μM) (240 μM)	Rods Vesicles	Zhang et al., 1996a
Base	PS-*b*-PAA 410-*b*-13 (2 w %) + NaOH (28 μM) (56 μM) (115 μM)	 Vesicles Spheres (D = 38 nm) Spheres (D = 35 nm) Spheres (D = 33 nm)	Zhang and Eisenberg, 1996a
Salt	PS-*b*-PAA 410-*b*-25 (1 w %) + $CaCl_2$ (120 μM)	 Vesicles Spheres	Zhang et al., 1996a
Organic solvent	PS-*b*-PAA 390-*b*-40 DMF Dioxane	 Spheres Vehicles	Yu et al., 1997; Yu and Eisenberg, 1997

2.9.1 Copolymer composition

Changing the copolymer composition can have a significant effect on the degree of core-stretching and inter-shell interactions. The degree of stretching of the core-forming blocks decreases when there is an increase in the length of the core and/or shell-forming blocks, while keeping the other block constant. For example, in spherical micelles containing a long poly(acrylic acid) (PAA) block and a polystyrene block of some particular length, when the length of the poly(acrylic acid) was decreased, the degree of core-stretching increased, and the morphology was changed to rod shape (Allen et al., 1999a).

On other hand, an increase in the length of either block leads to an increase in the inter-shell chain repulsions (Allen et al., 1999a). For example, in spherical micelles formed from PS-*b*-PAA copolymers with a long PAA block, in which the aggregation number was restricted by inter-shell repulsion, as the PAA block length was decreased, the inter-shell repulsions became less important. Thus, the aggregation number was restricted by the degree of stretching of the core-forming blocks. Eventually, a further decrease in the length of the PAA block led to a change in morphology from spheres to rods and even to vesicles (Zhang and Eisenberg, 1996b).

2.9.2 Copolymer concentration

An increase in the copolymer concentration increases the aggregation number of the core-shell nanoparticles (Zhang and Eisenberg, 1997). The increased aggregation

number resulted in the production of rods and vesicles under the conditions that previously produced spheres and rods, respectively.

2.9.3 Presence of added acid, base or salt

The presence of ions influences the morphology by affecting the inter-shell chain interactions (Zhang et al., 1996a; Zhang and Eisenberg, 1996a). The addition of electrolytes to the solution of core-shell nanoparticles was found to either strengthen or weaken the inter-corona repulsive interactions, depending on the nature of the ions added. For example, in the PS-*b*-PAA solution (DMF/water), PAA is slightly ionised, therefore the addition of HCl protonates the ionic sites, resulting in a decrease in the inter-shell repulsions, which in turn caused a morphology change from spheres to rods or vesicles (Zhang et al., 1996a).

2.9.4 Organic solvent

The choice of organic solvent has a profound effect on the morphology of nanoparticles (Allen et al., 1999a). It is difficult to predict the morphology when different organic solvents or precipitants are employed. However, an intermediate morphology can be obtained using a mixture of two organic solvents, in which the morphology produced by the individual solvent is known.

2.10 Targeting

The concept of selective delivery of drugs to specific physiological sites, organs, tissues or cells, where pharmacological activities of drugs are required, was first introduced by Erhlich (1906) in the early 20th century. He proposed the 'magic bullet', i.e. carriers with specific affinity for certain organs, tissues or cells for drug targeting. However, among different drug carriers, polymeric core-shell nanoparticles find the most practical applications in a variety of pharmaceutical fields, from oral delivery to sustained release and site-specific drug targeting (Jones and Leroux, 1999). This is owed to the structural similarity of polymeric core-shell nanoparticles to natural carriers, e.g. viruses and serum lipoproteins.

Targeting the drug to the desired site of action would not only improve the therapeutic efficiency but also enable lower accumulation of the drug in healthy tissues, thus minimising unwanted toxic effects. For example, it was shown that adriamycin-loaded micelles accumulated much better in tumours than in non-target tissues (e.g. heart) (Kwon et al., 1994a). Polymeric core-shell nanoparticles are also associated with a lower toxicity, which allows for the administration of higher doses that are found to be toxic. For instance, the activity of DOX on tumours is limited by its toxicity, thus the maximum tolerated dose (MTD) is estimated to be 10 mg/kg. However, incorporation of DOX in PEO-*b*-P(Asp) micelles permitted the administration of DOX doses as high as 50 mg/kg (MTD) (Yokoyama et al., 1998b).

Targeting can be divided into two categories, which are the passive and active targeting.

2.10.1 Passive targeting

Passive targeting involves the random movement of the delivery system through the body. Passive targeted systems use natural flow in areas such as blood stream or gastrointestinal tract, and at a specific physiological site of uptake, the drug is released. The primary advantage of polymeric core-shell nanoparticles following intravenous administration is the ability to achieve a prolonged systemic circulation time in the bloodstream. They can effectively evade non-specific capture at the reticuloendothelial systems (RES) since the size of the core-shell nanoparticles (< 200 nm) is smaller than the threshold (approximately 200 nm) for the capture of RES. In addition, their hydrophilic shell can induce steric repulsive forces and stabilise the nanoparticles interface, preventing the adsorption of proteins and adhesion of cells that can cause recognition and uptake by the mononuclear phagocyte system (MPS).

On the other hand, the nanoparticles are expected to show low renal clearance because their size is much larger than the pore size for renal filtration, unless the core-shell nanoparticles structure dissociates to unimers (Kwon et al., 1993b; Xu et al., 1991). Even if polymer molecular weight is lower than the critical molecular weight for renal filtration, they can also escape renal excretion because of the high molecular weight of nanoparticles (> 10^6 $gmol^{-1}$) (Jones and Leroux, 1999). It was reported that intact core-shell nanoparticles were recovered from plasma several hours after intravenous injection (Kwon et al., 1994a; Roland et al., 1992).

The nanoscopic size of the core-shell nanoparticles is also advantageous for extravasation, which is an essential process for the carrier to reach the target tissues

such as solid tumours and sites of inflammation (Siegal et al., 1995; Yuan et al., 1994) that is located outside of the capillaries (Weinstein and van Osdol, 1992). Due to its small size and highly hydrated as well as flexible shell, nanoparticles can slowly accumulate (so-called enhanced permeability and retention effect, EPR, also known as accumulation *via* an impaired filtration mechanism) in pathological sites with affected and leaky vasculature (e.g. tumours, inflammations and infected areas), improving the efficacy of drug and reducing unwanted side effects (Gabizon, 1995; Matsumura and Maeda, 1986; Maeda et al., 2000; Palmer et al., 1984). For example, micelles of PEO-*b*-P(Asp)-DOX conjugates passively accumulated at solid tumours of mice with plasma levels higher than free DOX. After one day, the plasma levels of conjugate were about 10-fold higher than that of the drug itself (Kwon et al., 1994a).

2.10.2 Active targeting

Drug targeting could be further improved by utilising actively targeted drug delivery systems. The purpose of active targeting is to alter the natural distribution pattern of drugs to direct drugs to specific organs, and to control interactions with target sites. This can be achieved by binding pilot molecules such as antibodies (Kabanov et al., 1989; Ulbrich et al., 2003) or sugar moieties (Cho et al., 1998; Yasugi et al., 1999) to the core-shell nanoparticles. Without creating any steric hindrances for the antibody, the antibody or its fragment can be chemically attached to an activated water-exposed free terminus of hydrophilic block of core-shell nanoparticles. Kabanov et al. (1989) reported that there was an increase in neuroleptic action and toxicity of haloperidol in the brain of mice for PEO-*b*-Poly(propylene oxide)-*b*-PEO micelles (Pluronic P-85) with murine polyclonal antibodies.

Another approach to achieving active targeting is to introduce a polymer sensitive to variation in temperature (Cammas et al., 1997; Chung et al., 1998) or pH (Meyer et al., 1998; Taillefer et al., 2000). The development of thermo and/or pH sensitive polymeric core-shell nanoparticles has been pursued to enhance cellular interaction as well as release in specific sites.

Many pathological processes in various tissues and organs are accompanied with local temperature increase (Helmlinger et al., 1997; Tannock and Rotin, 1989). Therefore thermo-response may be utilised to enhance drug release and/or vascular transport. An *in vitro* study on DOX-loaded PNIPAAm-*b*-poly(butylmethacrylate) (PBMA) micelles showed that below the LCST (33^{o}C), the release of DOX from the micelles remained under 20% and the micelles formulation exhibited lower cytotoxicity than free DOX towards bovine aorta endothelial cells. However, at temperatures above the LCST, the activity of the micelles was greater than that of free DOX. Also, the release of DOX from the micelles reached 80% after 15 hours at 37 and 40^{o}C (Jones and Leroux, 1999).

The pH-sensitive core-shell nanoparticles could serve for the delivery of drugs to tumours, inflamed tissues or endosomal compartments since they are all associated with a lower pH value than normal tissues (Helmlinger et al., 1997; Tannock and Rotin, 1989). They can disintegrate in such areas, and release the incorporated drug (Pratten and Lloyd, 1985).

2.11 Research objective

The main objective of this study is to investigate the potential application of two types of core-shell nanoparticles made from cholesteryl end-capped poly(*N*-isopropylacrylamide-*co*-*N,N*-dimethylacrylamide) [P(NIPAAm-*co*-DMAAm)] and poly(*N*-isopropylacrylamide-*co*-*N,N*-dimethylacrylamide-*co*-oleic acid) [P(NIPAAm-*co*-DMAAm-*co*-OA)], respectively. Specifically,

1. To investigate the possibility of using thermally responsive cholesteryl end-capped P(NIPAAm-*co*-DMAAm), and pH as well as thermally responsive P(NIPAAm-*co*-DMAAm-*co*-OA) amphiphilic polymers for the entrapment of hydrophobic drugs, such as cyclosporin A (CyA) and indomethacin (IMC).

2. To explore the influence of temperature, polymer structure and concentration, and drug molecular size as well as initial drug loading level on the encapsulation efficiency of drugs.

3. To study the effect of temperature/pH or other possible parameters on *in vitro* release behaviours of drugs from the core-shell nanoparticles.

CHAPTER 3 MATERIALS AND METHODS

3.1 Materials

Unless stated otherwise, all reagents and solvents were of commercial grade, and used as received. Cholesteryl end-capped poly(*N*-isopropylacrylamide-*co*-*N,N*-dimethylacrylamide) [P(NIPAAm-*co*-DMAAm)] and poly(*N*-isopropylacrylamide-*co*-*N,N*-dimethylacrylamide-*co*-oleic acid) [P(NIPAAm-*co*-DMAAm-*co*-OA)] were kindly provided by Dr. Liu Xue-Ming and Ms Wang Li-Shan, respectively. Indomethacin (IMC, Mw 358), cyclosporin A (CyA, Mw 1202), bovine serum albumin (BSA), and pyrene were purchased from Sigma, USA. Fetal bovine serum (FBS) was supplied from Invitrogen Corporation, UK. *N*,*N*-Dimethylformamide (DMF) was purchased from J.T. Baker (NJ, USA). Water was purified with Milli-Q® Ultrapure Water Purification Systems (Gradient system, Millipore, Millipore Singapore Pte. Ltd., Millipore, SG).

3.2 Methods

3.2.1 Characterisation of polymers

3.2.1.1 Determination of composition

The composition of polymers was determined by 400 Hz ^{1}H NMR spectrometer (Bruker AVANCE 400). $CDCl_3$ was used as the solvent. Chemical shifts were expressed in parts per million (δ) using residual protons in the indicated solvent as the internal standard.

3.2.1.2 Determination of polymer molecular weight

The molecular weight of polymers and their polydispersity were measured by a gel permeation chromatography (GPC) system consisting of a Waters 2690 separation module and a 410 RI detector (Waters, Milford, MA, USA) with HR 1E and HR 2E columns (Waters, Milford, MA, USA). Tetrahydrofuran (THF) (J.T. Baker, USA) was used as the mobile phase at a flow rate of 1.0 mL/min and polystyrenes (Polymer Laboratories Ltd, Amherst, MA 01002, USA) with various molecular weights were employed as calibration standards. About 10 mg of polymer was dissolved in 2 mL of THF and the solution was then filtered. Weight average molecular weights were calculated from a calibration curve using a series of polystyrene standards (Polymer Laboratories Inc., MA, USA) with molecular weights ranging from 1350 to 151700.

3.2.1.3 Thermal degradation study

Thermal degradation study of P(NIPAAm-*co*-DMAAm-*co*-OA) polymer was performed using a thermogravimetric analyser (TGA) (Perkin-Elmer TGA 7, USA) under nitrogen flow at 20 mL/min. The sample weight was around 4-5 mg, and it was heated from 50 to 800^{o}C with a heating rate of 40^{o}C/min. The temperature at 5 w % of polymer loss was considered to be the onset of polymer degradation. The temperature for maximum degradation rate was determined at the minimum peak of the derivative weight curve.

3.2.2 Characterisation of drugs

3.2.2.1 Thermal degradation study

Thermal degradation study of IMC and CyA was performed using TGA as described above.

3.2.2.2 Determination of IMC solubility

The solubility of IMC was determined as described by Příborský et al. (1998). An excess amount of IMC was added to the phosphate buffer solution (PBS, pH 7.4), pH 6 and pH 9 buffers, respectively. The solution was then vortexed and kept at certain temperatures for few hours. The solution was then centrifuged (5417R, Eppendorf, Germany) at 14000 rpm for 3 minutes, and filtered through a filter of 0.45 μm pore size to remove non-dissolved IMC. The concentration of IMC was determined by a UV-VIS microplate spectrophotometer (PowerWave$_X$, BIO-TEK Instruments, USA) at 318 nm.

3.2.3 Preparation of pH buffer solutions

The buffer solutions of varying pH values were prepared according to buffer solutions reference (Dean, 1999). The ionic strength of the buffer solutions was adjusted to the ionic strength of PBS (0.18 M, pH 7.4) using sodium chloride (NaCl). The pH of the solution was measured at room temperature using a pH meter (744, Metrohm, Switzerland). Prior to the measurements, the pH meter was calibrated with proper standard buffer solutions.

3.2.4 Determination of LCST and phase transition pH

The lower critical solution temperature (LCST) of the polymer solutions was determined by monitoring the optical transmittance as a function of temperature. Sample solutions of 5 mg/mL were determined at 500 nm using a Shimadzu UV-VIS spectrophotometer (Shimadzu UV-2501, Shimadzu, Japan). Sample cells were thermostated with a temperature controlled circular system (TCC-Controller, Shimadzu, Japan). The temperature was gradually increased with 0.3^{o}C/min and 0.1^{o}C/min heating rate for cholesteryl end-capped P(NIPAAm-*co*-DMAAm) and P(NIPAAm-*co*-DMAAm-*co*-OA) polymers, respectively. The LCST of polymer solutions was determined at the temperature indicating 50% optical transmittance. The effects of pH and salts on the LCST were also investigated. The phase transition pH was further determined by observing the transmittance change of 5 mg/mL polymer solution as a function of pH at 31^{o}C. The phase transition pH was determined at the pH showing an optical transmittance of 50%.

3.2.5 Determination of CAC and polarity of the surroundings of pyrene by fluorescent probe techniques

The critical association concentration (CAC) and the polarity of the nanoparticles core were determined by monitoring the changes in the fluorescence excitation and emission spectra of pyrene in polymer solutions (Chung et al., 2000). Fluorescence spectra were recorded using a LS50B Luminescence Spectrometer (Perkin Elmer, USA) as a function of polymer concentration and temperature (heating and cooling rate:

1°C/min). The temperature of samples was controlled with a thermostated circulating bath. Pyrene was used as a hydrophobic fluorescent probe for all measurements.

The CAC values of the polymer in pH 4.0, 7.4 and 10.0 buffer solutions, as well as ultra pure water were determined. Pyrene solution in acetone (1.54×10^{-5} M, 400 μl) was added to 30 mL containers and the acetone was allowed to evaporate overnight. Hereafter, 10 mL of aqueous polymer solutions at a concentration ranging from 0.0005 to 1.0 g/L were then added into the above containers containing the pyrene residue. All the aqueous polymer solutions contained final pyrene concentration of 6.17×10^{-7} M. The solutions were then allowed to equilibrate for 24 hours at 20°C. Both emission and excitation spectra were recorded.

For cholesteryl end-capped P(NIPAAm-*co*-DMAAm) polymer, the emission spectra were recorded from 350 to 500 nm with an excitation wavelength of 340 nm. The excitation and emission bandwidths were set at 4.5 nm. The intensity (peak height) ratio (I_1/I_3) of the first band (374nm, I_1) to the third band (391nm, I_3) from the emission spectra was analysed as a function of polymer concentration. The CAC value was taken from the midpoint of the plot for I_1/I_3 changes.

On the other hand, for P(NIPAAm-*co*-DMAAm-*co*-OA) polymer, the emission spectra were recorded from 360 to 420 nm with an excitation wavelength of 339 nm. As for the excitation spectra, the emission was carried out at 395 nm, and the excitation spectra were recorded from 300 to 360 nm. The excitation and emission bandwidths were set at 3 nm. The intensity ratio of peaks at 338 nm to those at 333 nm from the excitation spectra was plotted against the logarithm of polymer concentration. The

CAC values were obtained from the intersection of the extrapolations of the rapidly varying part of the plot and the nearly horizontal part at low polymer concentrations. To ascertain the polarity of the surroundings of pyrene, the intensity ratio of the first band to the third band (I_1/I_3) from pyrene emission spectra was analysed as a function of temperature.

3.2.6 Preparation of core-shell nanoparticles

Core-shell nanoparticles were prepared using the dialysis method. A total of 15 mg of polymer was dissolved in 5 mL of DMF. The polymer solutions were dialysed for 24 hours against 500 mL of ultra pure water at different temperatures using cellulose dialysis membrane with the molecular weight cut-off of 2000 and 12000-14000 (Sigma, USA) for cholesteryl end-capped P(NIPAAm-*co*-DMAAm) and P(NIPAAm-*co*-DMAAm-*co*-OA) polymers, respectively. The water was replaced hourly for the first 7 hours. After dialysis, the solution remaining in the dialysis membrane was collected and centrifuged (5417R, Eppendorf, Germany) at 14000 rpm for 3 minutes to remove the aggregated nanoparticles. The supernatant, containing the core-shell nanoparticles, was filtered through a syringe filter of 0.45 μm pore size, and lyophilised by a freeze dryer (Labconco, USA) for 2 days to obtain dried nanoparticles.

3.2.7 Incorporation of drug into core-shell nanoparticles

CyA and IMC were loaded into the core-shell nanoparticles using a membrane dialysis method. Briefly, cholesteryl end-capped (0.5-3.0 mg/mL) P(NIPAAm-*co*-DMAAm) or P(NIPAAm-*co*-DMAAm-*co*-OA) (15.0 mg/mL) was dissolved in 5 mL of DMF,

followed by the addition of CyA (0.5-6.0 mg) or IMC (5-30 mg). The solutions were dialysed against ultra pure water at various temperatures (5, 10, 15 and 20^{o}C) for 24 hours. The water was replaced hourly for the first 7 hours. The solution was filtered using a filter of 0.45 μm pore size, and then analysed or lyophilised for 24 hours for further examination. In addition, P(NIPAAm-*co*-DMAAm-*co*-OA) solution was also dialysed against 0.02 M hydrochloride acid and 0.02 M sodium hydroxide solutions.

3.2.8 Recovery of nanoparticles

The lyophilised nanoparticles were weighed, and the nanoparticles recovery was calculated using the following equation.

$$Nanoparticles\ recovery\ (w/w\,\%) = \frac{Mass\ of\ nanoparticles\ recovered}{Mass\ of\ polymer\ and\ drug\ fed}\ x\ 100\% \qquad (3.1)$$

3.2.9 Drug loading level and encapsulation efficiency

3.2.9.1 CyA-loaded nanoparticles

A fixed amount of CyA-loaded core-shell nanoparticles was first dissolved in 1 mL of chloroform, and 2mL of ether was then added drop-wise to precipitate the polymer. The suspension was centrifuged at 10000 rpm for 5 minutes. The supernatant was removed and dried. The sample was then reconstituted with an appropriate amount of mobile phase and analysed for CyA levels using high-performance liquid chromatography (HPLC). The HPLC system consisted of a Waters 2690 separation module and Waters 996 PDA detector (Waters Corporation, USA). A Waters

SymmetryShield^{TM} C_8 4.6 x 15.0 cm column fitted with C_8 pre-column was used. The mobile phase consisted of water and acetonitrile (15:85 in volume) with column and sample temperatures set at 50^{o}C and 15^{o}C, respectively. The detection wavelength was set at 210 nm. The retention time was 3.2 ± 0.1 min. A calibration curve was constructed to determine CyA concentration in the range from 1 to 20 ppm and the r^2 value was at least 0.999.

The loading level and encapsulation efficiency were calculated from the following equations.

$$Loading\ level\ (w/w\ \%) = \frac{Mass\ of\ drug\ encapsulated}{Mass\ of\ nanoparticles\ recovered}\ x\ 100\% \qquad (3.2)$$

$$Encapsulation\ efficiency\ (\%) = \frac{Mass\ of\ drug\ encapsulated}{Mass\ of\ drug\ loaded}\ x\ 100\% \qquad (3.3)$$

3.2.9.2 IMC-loaded nanoparticles

The amount of IMC loaded in the nanoparticles was investigated using a UV-VIS microplate spectrophotometer (PowerWave$_X$, BIO-TEK Instruments, USA). To evaluate the loading amount of drugs, 1 mg of freeze-dried IMC-loaded nanoparticles was dissolved in 2 mL of methanol, and vigorously vortexed for an hour. The amount of IMC entrapped was determined by measuring the UV absorbance at 318 nm. Prior to this analysis, a calibration curve was constructed to determine the IMC concentration in the range from 2.5 to 70 ppm and the r^2 value was at least 0.999.

The loading level and encapsulation efficiency were calculated from equations (3.2) and (3.3).

3.2.10 Determination of DMF removal rate during the dialysis process

The removal of DMF from the dialysis bag into the external aqueous phase was monitored at various temperatures (e.g. 5, 10, 15 and 20ºC). To simulate the fabrication process of drug-loaded core-shell nanoparticles, 5 mL of DMF was placed in a dialysis bag with a molecular weight cut-off of 2000 and immersed in 500 mL of ultra pure water at a fixed temperature. The external water was replaced hourly for the first 7 hours. At fixed time intervals, the solution in the dialysis bag was collected and analysed for DMF level by gas chromatography (GC, Perkin Elmer AutoSystem XL, Perkin Elmer, USA). The GC system was equipped with a flame ionisation detector (FID), and connected to an automatic liquid sample injector (Perkin Elmer Autosampler, Perkin Elmer, USA). A data processor (Turbochrom Navigator Version 4.1) was employed for data acquisition and analysis of DMF levels. A 30 m long HP-1 capillary GC column (J & W Scientific, USA, 0.25 mm in inner diameter and 0.25 μm in film thickness) was used. The injection port and detector were heated at 160^{o}C and 180^{o}C, respectively. Helium, a carrier gas, was allowed to flow at a rate of 20 mL/min (90 psi). The supply of hydrogen gas and air to the detector was at 45 mL/min (60 psi) and 450 mL/min (60 psi), respectively. The sample was introduced to the column in a split mode with a ratio of 50:1 (He carrier gas and analyte). The column temperature was kept at 95^{o}C for 5 minutes. The calibration curve was constructed using a series of DMF standards in a concentration ranging from 20 to 100% in volume (DMF/H_2O) and the linearity was at least 0.99 ($r^2 = 0.995$).

3.2.11 Characterisation of core-shell nanoparticles

3.2.11.1 Morphology

The surface morphology of the nanoparticles fabricated at different temperatures and pH was observed at 300 kV using a transmission electron microscope (TEM) (Philips CM300, Holland). A drop of the resultant nanoparticles solution containing 0.01 w/v % of phosphotungstic acid was placed on a copper grid coated with carbon film and dried at room temperature for overnight.

3.2.11.2 Size analysis

Average size and size distribution of nanoparticles were analysed by dynamic light scattering (DLS) (Coulter N4Plus, Coulter Corporation, UK) equipped with He-Ne laser beam at a wavelength of 633 nm. The intensity of the scattered light was detected at 90^{o} to the incident beam. Measurements were obtained for nanoparticles fabricated under different conditions. The lyophilised nanoparticles were redispersed in water and vortexed for a few minutes. The samples were then filtered through a filter of 0.45 μm pore size and kept for 30 minutes at 20^{o}C before measurements.

In addition, changes in size of nanoparticles upon temperature cycles through the LCST were examined to investigate their thermo-responsive reversibility. For instance, after the first measurement at 20^{o}C, the solution was heated to 40^{o}C and incubated for 30 minutes. Then, the solution was cooled back to 20^{o}C. This heating and cooling were repeated for few cycles.

The size of nanoparticles was also measured as a function of temperature. Prior to the measurements, the solution was kept for 30 minutes at each temperature. The mean diameter ± S.D. of five determinations were obtained from unimodal analysis.

3.2.11.3 Surface charge

The zeta potential of P(NIPAAm-*co*-DMAAm-*co*-OA) nanoparticles was determined using a Zetasizer® 3000HS$_A$ (Malvern Instruments Ltd., Malvern, UK). The measurements of nanoparticles in ultra pure water were performed at different temperatures, ranging from 5 to 40^{o}C. For each temperature, the mean value ± S.D. of five determinations was established.

3.2.12 Fourier transformation infrared (FTIR) spectroscopy

A FTIR spectrophotometer (Perkin Elmer Spectrum 2000, Perkin Elmer, USA) was employed to explore the nature of driving force for the formation of core-shell nanoparticles. A small amount of polymer or blank nanoparticles was mixed with potassium bromide (KBr) and pressed into disc for FTIR analysis.

3.2.13 Determination of glass transition temperature (T_g)

The glass transition temperatures of the polymer and core-shell nanoparticles were determined by modulated differential scanning calorimetry (MDSC) (TA 2920, Research Instruments Pte Ltd., USA) (Yamamoto et al., 2002; Zhang et al., 1996b) under nitrogen flow. About 5-6 mg of the samples were weighed into the aluminium

sample pans and then heated to 200°C at 10°C/min heating rate. The linear portion of the glass transition on the thermogram was extrapolated to the above and below glass transition, and the T_g was determined from the midpoint. The T_g values of polymers and nanoparticles were determined from the second heating run.

3.2.14 Determination of melting temperatures (T_m)

The melting temperatures of pure IMC and CyA, and those encapsulated in the nanoparticles were measured with MDSC (Jeong et al., 1998). The measurements were carried out using MDSC at temperatures ranging from 20 to 200°C with a heating rate of 5°C/min.

3.2.15 *In vitro* drug release studies

3.2.15.1 CyA-loaded nanoparticles

The release of CyA from the cholesteryl end-capped P(NIPAAm-*co*-DMAAm) and P(NIPAAm-*co*-DMAAm-*co*-OA) core-shell nanoparticles was determined by the dialysis method (Kim et al., 1998; Kim et al., 2000b; Kim et al., 2000c; La et al., 1996). About 5 mg of CyA-loaded nanoparticles was introduced into 1 mL of 0.18 M phosphate buffer solution (PBS, pH 7.4) in the cellulose dialysis membrane (molecular weight cut-off: 12000-14000, Sigma, USA). The membrane was then placed in 50 mL of PBS, which was incubated at 10, 20 and 40°C, respectively. At specific time intervals, the entire medium was removed and replaced with the same amount of fresh PBS. Subsequently, extraction of CyA was carried out by adding 5 mL of dichloromethane (DCM) into the collected medium. The mixture was then vigorously

vortexed for 3 minutes and left for phase separation. The extraction efficiency was determined to be more than 97%. The aqueous phase was drawn out carefully and the remaining organic phase was left to evaporate overnight. The dried sample was reconstituted with 2 mL of acetonitrile:water (85:15). The amount of CyA released into the medium was analysed with HPLC as described above. Release behaviours of CyA from P(NIPAAm-*co*-DMAAm-*co*-OA) core-shell nanoparticles were investigated at 31^{o}C at pH 6 and 9.

3.2.15.2 IMC-loaded nanoparticles

Similarly, the release of IMC from the P(NIPAAm-*co*-DMAAm-*co*-OA) core-shell nanoparticles was performed in PBS using the dialysis method (Kim et al., 2000b; Kim et al., 2000c; La et al., 1996; Kim et al., 1998). About 5 mg of IMC-loaded nanoparticles was introduced into 1 mL of PBS in cellulose dialysis membrane (molecular weight cut-off: 12000-14000, Sigma, USA). The membrane was then placed in 50 mL of the release medium, which was incubated at 20^{o}C and 37^{o}C. At predetermined time intervals, 1 mL aliquot of solution was withdrawn from the release medium. The samples were assayed using the UV-VIS microplate spectrophotometer at 318 nm. The solution taken as the sample was replaced with fresh medium. Release behaviours of IMC from the core-shell nanoparticles were also investigated at 31^{o}C at pH 6 and 9.

3.2.16 Evaluation of nanoparticles stability

Besides the CAC and nanoparticles size, high *in vivo* stability of nanoparticles can also be weighed in terms of the interactions of core-shell nanoparticles with plasma components (serum proteins) (Chilkoti et al., 2002; Kwon et al., 1995; Lavasanifar et al., 2002). It is an important consideration especially for soluble thermosensitive carrier such as PNIPAAm, because such interactions can alter the LCST of the polymer, as well as promote recognition and uptake by the mononuclear phagocyte system (MPS). The interaction of P(NIPAAm-*co*-DMAAm-*co*-OA) core-shell nanoparticles with serum proteins was studied by measuring the LCST (Meyer et al., 2001) and size changes in the presence of bovine serum albumin (BSA) and fetal bovine serum (FBS). Prior to the LCST measurement, 0.5 mg/mL of polymer in different pH buffer solutions were incubated in 10 w/v % of BSA and 10 w/v % of FBS for 5 minutes, respectively. The optical transmittance was determined at 500 nm using the UV-VIS spectrophotometer. For the particle size analysis, the core-shell nanoparticles were suspended in 10 w/v % of BSA and 10 w/v % of FBS, respectively. The size distribution of core-shell nanoparticles was determined by DLS. The measurements were performed at 20^{o}C by applying multimodal analysis.

CHAPTER 4 RESULTS AND DISCUSSION

4.1 Temperature-sensitive core-shell nanoparticles

A thermally responsive cholesteryl end-capped poly (*N*-isopropylacrylamide-*co*-*N,N*-dimethylacrylamide) [P(NIPAAm-*co*-DMAAm)] amphiphilic polymer (Figure 4.1) was designed and utilised to encapsulate hydrophobic drug within core-shell nanoparticles. Cholesterol was chosen as the hydrophobic segment because of its potential interaction with cholesterol receptors on cell surfaces (Alberts et al., 1989) and its well-known ability to drive the self-assembly of cholesteryl-containing materials (Goodby, 1998). The CAC and LCST values of core-shell nanoparticles were measured in various media, and the effects of salts and proteins were investigated. Model drug such as cyclosporin A (CyA) was encapsulated into the core-shell nanoparticles by a membrane dialysis method. The influence of temperature, polymer concentration, and initial drug loading level on the encapsulation efficiency of drugs was explored. The *in vitro* release of drug-loaded core-shell nanoparticles was also studied at different temperatures.

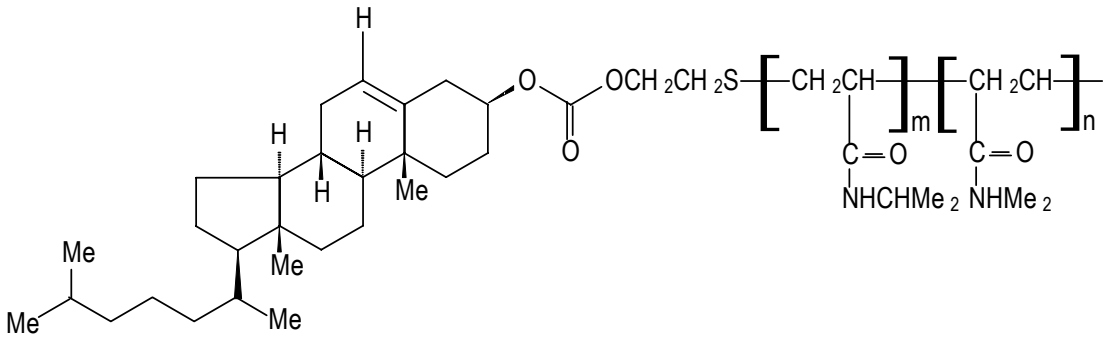

Figure 4.1 Chemical structure of cholesteryl end-capped P(NIPAAm-*co*-DMAAm)

4.1.1 Thermal analysis

The FTIR spectra of the polymer and blank nanoparticles were compared (results not shown). No obvious differences were observed between the polymer and nanoparticles, indicating that the self-assembly of the core-shell nanoparticles was caused by physical interactions (e.g. hydrophobic interactions) of cholesterol segments, and there were no chemical interactions involved. This was further confirmed with DSC measurements. The T_g value of cholesteryl end-capped P(NIPAAm-*co*-DMAAm) was 128.5^{o}C whereas its nanoparticles yielded a T_g value of 137.5^{o}C. This increase is due to the formation of a more orderly structure stabilised by intermolecular hydrophobic interactions, which required more energy to break down.

4.1.2 LCST, CAC and their factors

Figure 4.2 shows optical transmittance of core-shell nanoparticles made from cholesteryl end-capped P(NIPAAm-*co*-DMAAm) at various temperatures in different media. The LCST of the polymer in water was higher than that of PNIPAAm because of the hydrophilic contribution of DMAAm segments. The incorporation of hydrophilic segments shifts the phase transition point by increasing the water solubility of the polymer (Dong and Winnik, 1984). This phenomenon was consistent with what Chung et al. (2000) reported.

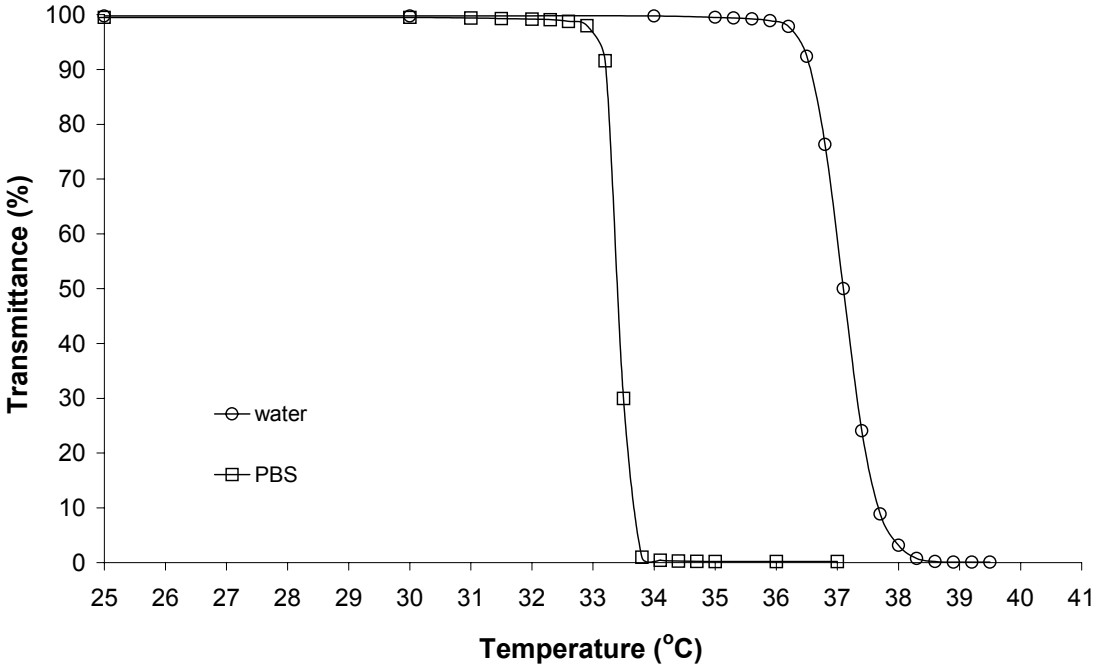

Figure 4.2 Optical transmittance of cholesteryl end-capped P(NIPAAm-*co*-DMAAm) aqueous solution at various temperatures (polymer concentration: 5000 mg/L; 500 nm)

PBS contains a large amount of salts including sodium chloride, which have a strong affinity with water molecules, reducing the number of free water molecules for polymer solubilisation. Thus, the phase transition was accelerated, and the LCST was reduced in the presence of salts. For instance, the LCST of cholesteryl end-capped P(NIPAAm-*co*-DMAAm) nanoparticles in PBS was 33.4°C but 37.0°C in water (Table 4.1). Hydrophilic proteins like BSA also compete with the polymer chains for water molecules. Therefore, the presence of BSA or FBS (consisting of approximately 10% bovine albumin) further reduced the LCST. As protein concentration increased, LCST was further decreased (Table 4.1). For instance, the LCST of the nanoparticles in PBS/10% FBS, PBS/10% BSA and water/10% BSA was 33.4, 30.9 and 36.4°C, respectively.

Table 4.1 The LCST values of cholesteryl end-capped P(NIPAAm-*co*-DMAAm) in various media (polymer concentration: 5000 mg/L, heating rate: 0.3°C/min)

	LCST[a] (°C)		
Medium	**Medium**	**Medium + 10% BSA[b]**	**Medium + 10% FBS[c]**
PBS (pH 7.4)	33.4	30.9	33.4
Water	37.0	36.4	-

[a] Determined at 500 nm.
[b] Bovine serum albumin.
[c] Fetal bovine serum.

The CAC is an important parameter to characterise the behaviour of amphiphilic polymer in aqueous solutions. Above the CAC, amphiphilic polymer molecules can self-assemble into an ordered structure, in which a hydrophobic core is surrounded with a hydrophilic shell. The hydrophobic microenvironment of cholesteryl end-capped P(NIPAAm-*co*-DMAAm) nanoparticles in aqueous solutions was investigated by fluorescence spectroscopy using pyrene as a probe. The ratio of I_1 to I_3 was monitored as a function of polymer concentration. Figure 4.3 shows a typical plot of I_1/I_3 for cholesteryl end-capped P(NIPAAm-*co*-DMAAm) polymer. A lower ratio is obtained when pyrene exists in more hydrophobic environment (Dong and Winnik, 1984). This property of pyrene can be utilised to study core-shell nanoparticles formation and deformation. The CAC value was determined to be approximately 20 mg/L for cholesteryl end-capped P(NIPAAm-*co*-DMAAm). The CAC value of the polymer in PBS (pH 7.4) was about 12 mg/L, which was lower than that in water. This is probably because the relative hydrophilicity of the polymer is lower in PBS.

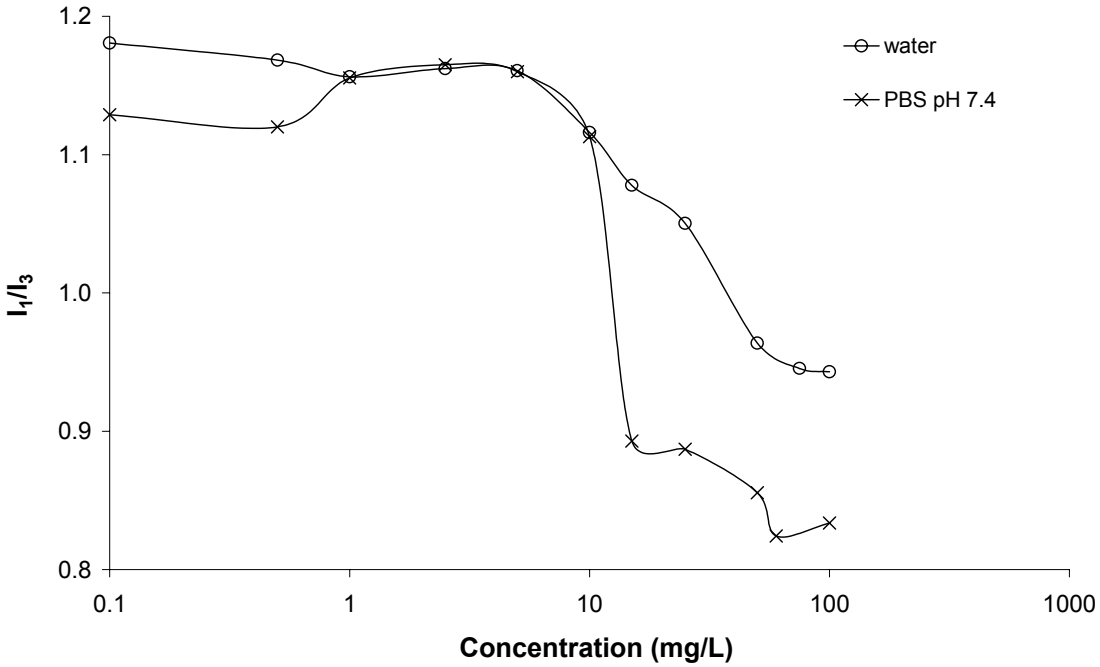

Figure 4.3 I_1/I_3 changes as a function of cholesteryl end-capped P(NIPAAm-*co*-DMAAm) polymer concentration

4.1.3 Morphology and size distribution of the blank and drug-loaded core-shell nanoparticles

The size and morphology are important for evaluating the possibility of using core-shell nanoparticles as a carrier for targeted drug delivery. Figure 4.4 shows TEM pictures of the blank and drug-loaded core-shell nanoparticles. Generally, the core-shell nanoparticles formed were spherical in nature under the current fabrication conditions (e.g. polymer concentration: 0.3 w/v %, temperature: 10°C). The mean diameter of blank nanoparticles was about 50 nm. After loading with CyA, the mean diameter increased to more than 100 nm.

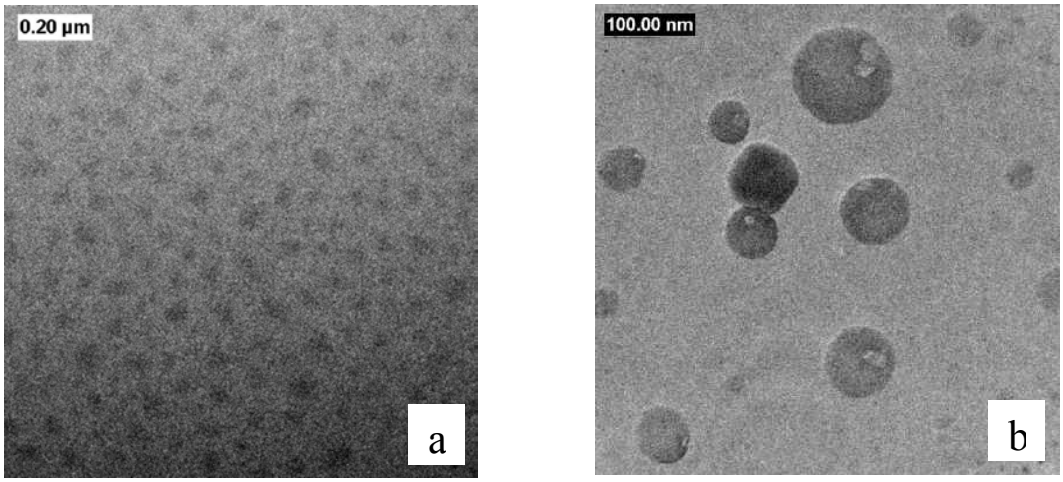

Figure 4.4 TEM pictures of (a) blank and (b) CyA-loaded core-shell nanoparticles (fabrication temperature: 10°C, polymer concentration: 0.3 w/v %)

Meanwhile, it was observed that upon heating of the nanoparticles solution to a temperature around the LCST, the size increased because of secondary aggregation (Figure 4.5). However, the aggregates re-dispersed and the size reduced to the original level upon cooling.

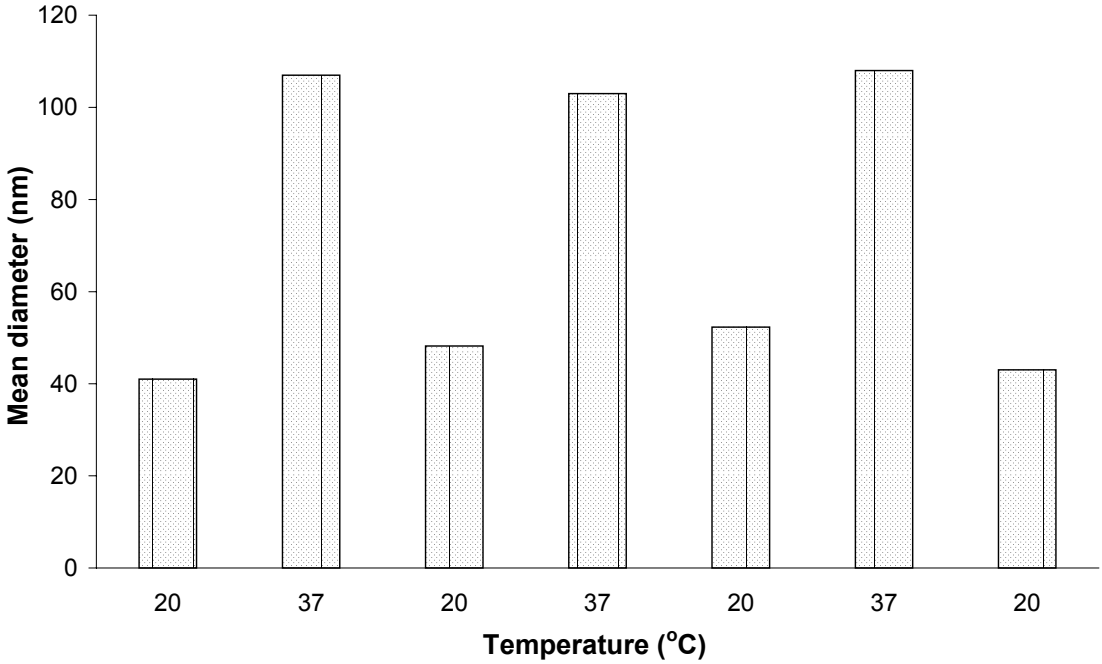

Figure 4.5 Particle size changes when temperature cycles through the LCST (polymer concentration: 0.3 w/v %)

4.1.4 Drug encapsulation efficiency

Figure 4.6 shows encapsulation efficiency of CyA-loaded cholesteryl end-capped P(NIPAAm-*co*-DMAAm) nanoparticles at different fabrication temperatures. The encapsulation efficiency and actual loading level of CyA were very low at room temperature. However, a reduced fabrication temperature yielded much greater encapsulation efficiency and loading level as well as bigger nanoparticles. For instance, the encapsulation efficiency of CyA at 5 and 20°C was 55 and 6.7%, respectively, and the actual loading level of CyA was 15.6 and 1.9 w/w %, respectively. The mean diameter of nanoparticles fabricated at 5 and 20°C was 193 and 41 nm, respectively. There were two possible factors that influenced drug encapsulation efficiency, including dissolution of CyA into the continuous phase during the dialysis process and precipitation of CyA upon solvent removal. CyA is a cyclic undecapeptide that exhibits unusual solubilisation behaviour in response to changes in temperature. The intramolecular H-bonds of CyA are strong at high temperatures. Thus, CyA adopts a conformation corresponding to an individual rather than solvated molecules. However, this conformation becomes weak as temperature decreases, resulting in higher water solubility (Loosli et al., 1985; Ismailos et al., 1991). For instance, the solubility of CyA in water increased approximately 15-fold when temperature was reduced from 37 to 5^{o}C (7.3 mg/L *versus* 101.5 mg/L). A study of CyA diffusion through the dialysis membrane with a molecular weight cut-off of 2000 was performed using a 40.0 ppm CyA aqueous solution at 10°C. The release rate of CyA from the dialysis bag was very low, which was less than 5% per hour. This is consistent with the finding of other researchers (Yang and Elmquist, 1996). The dissolution loss of CyA was hindered by the dialysis membrane barrier.

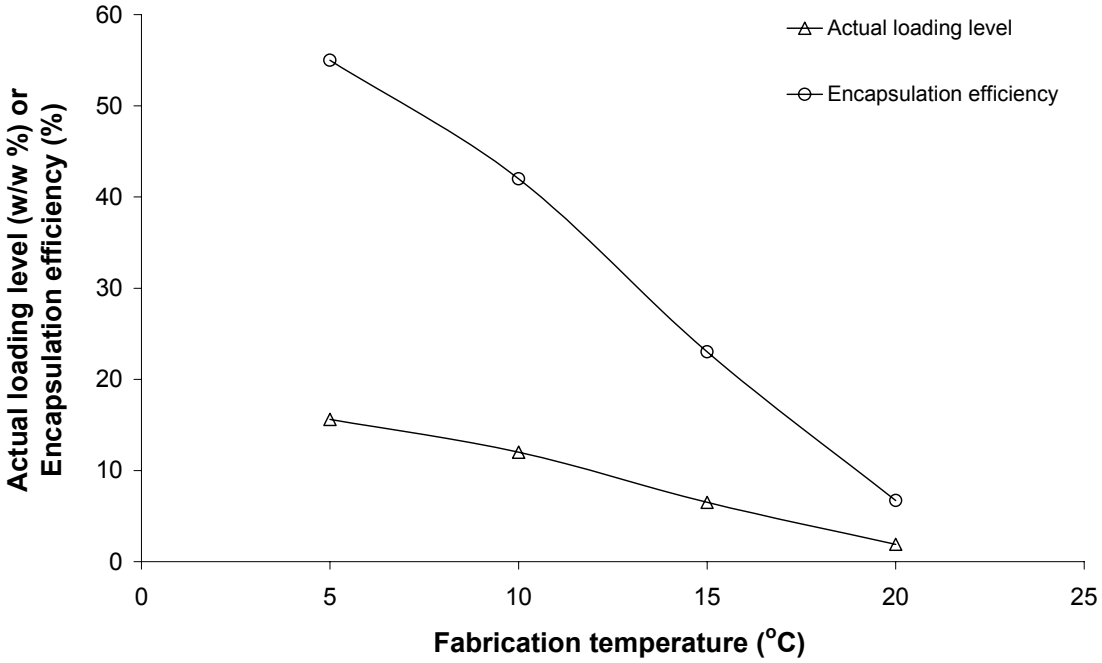

Figure 4.6 Effect of temperature on encapsulation efficiency of CyA-loaded cholesteryl end-capped P(NIPAAm-*co*-DMAAm) core-shell nanoparticles (polymer concentration: 0.3 w/v %; initial CyA loading: 28.5 w/w %)

On the other hand, the solvent DMF, having much smaller molecular size, can diffuse through the dialysis membrane easily. An increased temperature yielded faster DMF removal as shown in Figure 4.7. This led to rapid precipitation of CyA before being entrapped into the core of nanoparticles. As observed during the experiments, the turbidity occurred at Hour 1 with the fabrication temperature of 15°C, but the solution was clear at 5°C during the whole dialysis process. During the dialysis process, core-shell nanoparticles were formed as the solvent was removed and water content increased. Kohori et al. (2002) reported that the size of nanoparticles increased with increasing water content at the initial stage, but the nanoparticles shrank after reaching a maximum size value. It is believed that before the nascent nanoparticles started shrinking, there should be a liquid-state core, providing great flexibility for assembly of CyA molecules with the hydrophobic segments of polymer. With the progression of solvent removal, the core solidified, leading to difficulty in drug incorporation. Finally,

strong hydrophobic interactions between hydrophobic segments of the nanoparticles and hydrophobic segments of CyA molecules resulted in a relatively stable structure within the solid-state core, and the incorporation of drug molecules stopped. The occurrence of shrinking suppressed drug incorporation. A reduced temperature yielded longer swollen time so that drug molecules had enough time to assemble into the core before precipitation. Therefore, fabrication temperature had dual effects on CyA encapsulation efficiency. A reduced fabrication temperature led to greater dissolution loss of the drug but less drug precipitation. From the fact that a reduced temperature yielded better CyA entrapment, precipitation of CyA upon rapid DMF removal at high temperatures was a dominant factor.

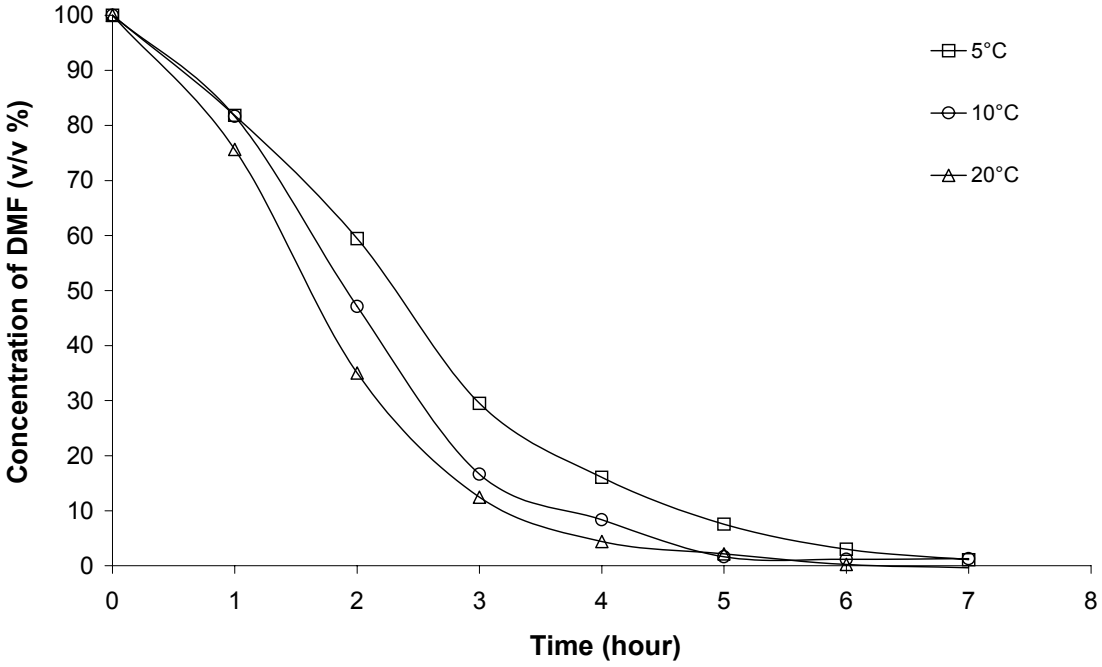

Figure 4.7 Effect of fabrication temperature on DMF removal

The effects of polymer concentration and initial drug loading on CyA encapsulation efficiency were also investigated. An increase in polymer concentration yielded higher encapsulation efficiency and drug loading level (Figure 4.8). As reported by Liu et al.

(2003), higher polymer concentrations produced bigger nanoparticles. The number of polymer molecules in each nanoparticle was thus increased, providing a larger hydrophobic microdomain for the incorporation of drug molecules.

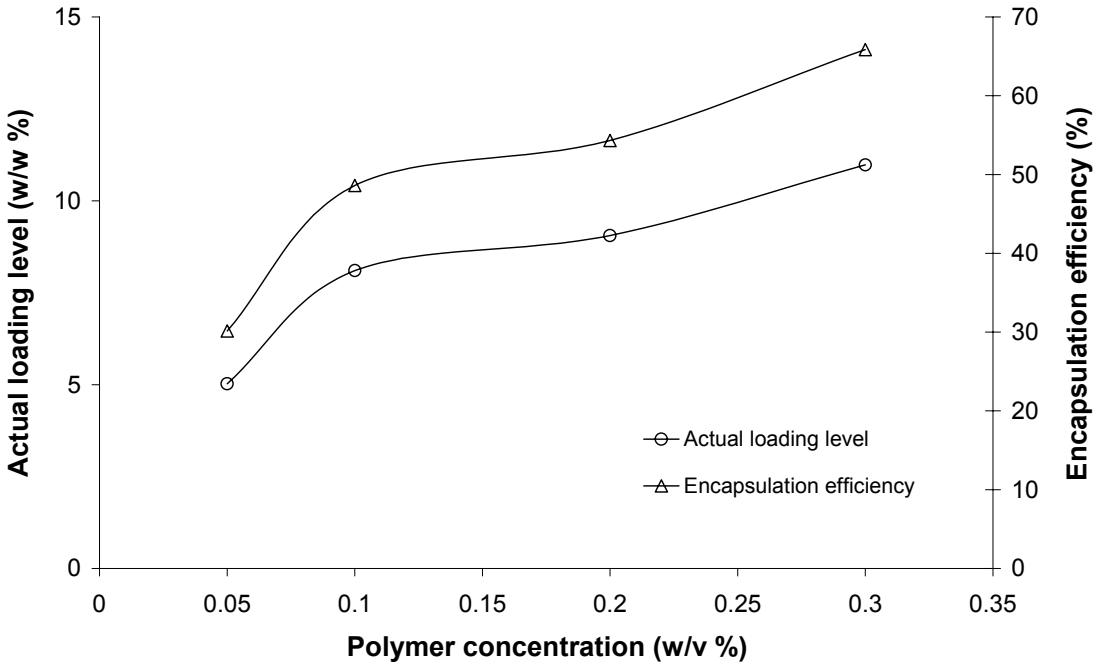

Figure 4.8 Effect of polymer concentration on encapsulation efficiency of CyA-loaded cholesteryl end-capped P(NIPAAm-*co*-DMAAm) core-shell nanoparticles (initial CyA loading: 16.7 w/w %, temperature: 10°C)

Table 4.2 shows the effect of initial drug loading at different temperatures. An increase in initial drug loading yielded lower encapsulation efficiency. The solvent removal might be promoted at higher drug contents because the interactions between the drug molecules and hydrophobic segments might lead to more free solvent molecules. Thus, the formation of solid-state core might be earlier at high drug contents, resulting in poor incorporation of drug molecules. Another possible reason is the precipitation of drug at high initial drug contents. At the initial stage of dialysis process, CyA was well dissolved in DMF. As water molecules penetrated into the dialysis membrane and DMF diffused into the external aqueous phase, the solubility of CyA was reduced in

the DMF-water mixture. After the core of nascent nanoparticles solidified, the residual CyA molecules that were not incorporated in the core-shell nanoparticles precipitated if the amount of residual CyA was greater than its solubility. As observed at 15°C, at the initial drug loading of 28.5 w/w %, the solution in the dialysis membrane appeared to be turbid during the first hour. However, at the initial loading of 16.7 w/w %, turbidity of the solution occurred after 4 hours dialysis and the extent of turbidity was much lower compared to that fabricated with the initial CyA loading of 28.5 w/w %. The similar phenomena were also observed for the core-shell nanoparticles fabricated at 10°C.

Table 4.2 The effect of initial CyA loading on its encapsulation efficiency at various fabrication temperatures

Dialysis temperature (^{o}C)	**Polymer concentration (w/v %)**	**Initial loading (w/w %)**	**Actual loading (w/w %)**	**Encapsulation efficiency (%)**	**Turbidity**
15	0.3	28.5	6.5	23	+++
15	0.3	16.7	6.5	39	+
10	0.3	28.5	12.0	42	++
10	0.3	25.0	11.2	45	++
10	0.3	16.7	11.0	66	+
5	0.3	28.5	15.6	55	-
5	0.3	10.2	6.3	62	-

4.1.5 *In vitro* release studies

Figure 4.9 shows the *in vitro* release profiles of CyA from the cholesteryl end-capped P(NIPAAm-*co*-DMAAm) core-shell nanoparticles at temperatures below and above the LCST. The physically entrapped CyA was gradually released over 24 hours, demonstrating a slow and sustained release characteristic. Higher amounts of CyA were released at 10 and 20^{o}C than at 40^{o}C, indicating that CyA release was faster at temperatures below the LCST. One possible explanation could be that when the

temperature was raised above the LCST, there was a conformational change in the outer shell of the nanoparticles, in which the expanded form of the PNIPAAm was changed into a compact form. Hence, the diffusion of CyA from the core was restricted by the shrunken structure. This finding was consistent with the results of other researchers (Kim et al., 2000b; Kim et al., 2000c). The lower release rate of CyA at higher temperature could be also attributed to the unusual solubility behaviour of CyA in aqueous media, which was found to be inversely proportional to the temperature (Ismailos et al., 1991; Augustijns et al. 2000). Moreover, the tendency of CyA binding to the dialysis membrane further decreased CyA release rate (Yang and Elmquist, 1996).

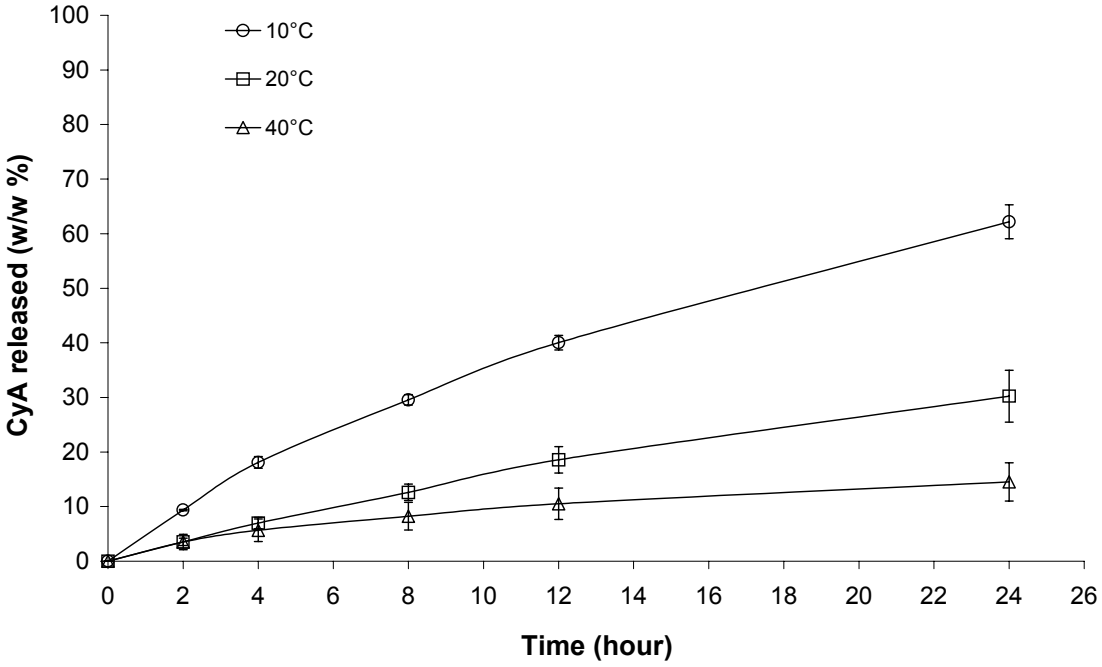

Figure 4.9 Release of CyA from cholesteryl end-capped P(NIPAAm-*co*-DMAAm) core-shell nanoparticles in PBS (pH 7.4) at different temperatures (CyA loading level: 11.2 w/w %)

4.2 Temperature/pH-sensitive core-shell nanoparticles

As introduced in Chapter 2, drug delivery systems capable of releasing active compounds in response to pH have been the most comprehensively studied due to the possible applications in targeted drug delivery. However, most of them are based on lipids. Very few studies have been reported for both temperature and pH-responsive core-shell nanoparticles (Taillefer et al., 2000).

In this chapter, poly(*N*-isopropylacrylamide-*co*-*N,N*-dimethylacrylamide-*co*-oleic acid) [P(NIPAAm-*co*-DMAAm-*co*-OA)] (Figure 4.10) was designed and utilised to form core-shell nanoparticles. In an aqueous medium, this polymer should form a core-shell structure, in which a pH-responsive hydrophobic core (oleic acid segment) is surrounded by the temperature-responsive outer shell [poly(NIPAAM-*co*-DMAAm)]. While maintaining the passive targeting ability, these temperature- and pH-sensitive nanoparticles possess a potential for active targeting by their reversible stimuli responsive character. The core-shell nanoparticles were characterised by size, CAC, LCST at different pH and morphology. The stability of the nanoparticles was examined in the presence of serum.

Indomethacin (IMC) and cyclosporin A (CyA) are chosen as the model drugs. IMC, which is practically insoluble in water, is one of the most potent nonsteroidal anti-inflammatory drugs for the treatment of conditions such as rheumatoid arthritis, ankylosing spondylitis, osteoarthritis and acute gouty arthritis (Figure 4.11). Its side effect, such as disturbance, ulceration and bleeding within the GI tract, are always found by oral administration. To avoid these adverse actions of IMC, administration by

injection has been extensively studied. CyA (Figure 4.12) is a cyclic undecapeptide and has been extensively used to prevent transplanted organ rejection and for the treatment of various autoimmune diseases. It is usually administered *via* oral and intravenous routes. Its major drawbacks are the broad toxicity profile including nephrotoxicity and hepatoxicity, and the low oral bioavailability because it is unstable and has a poor solubility in aqueous solution. The CyA or IMC-loaded P(NIPAAm-*co*-DMAAm-*co*-OA) core-shell nanoparticles were fabricated by the dialysis membrane method. The effect of pH, temperature and initial drug loading on drug encapsulation efficiency was investigated. The release kinetics of drug was studied at different pH and temperatures.

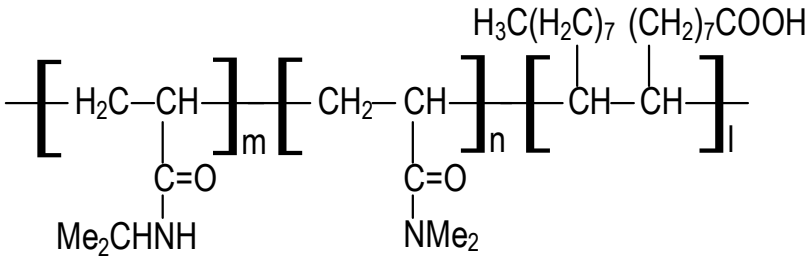

Figure 4.10 Chemical structure of P(NIPAAm-*co*-DMAAm-*co*-OA)

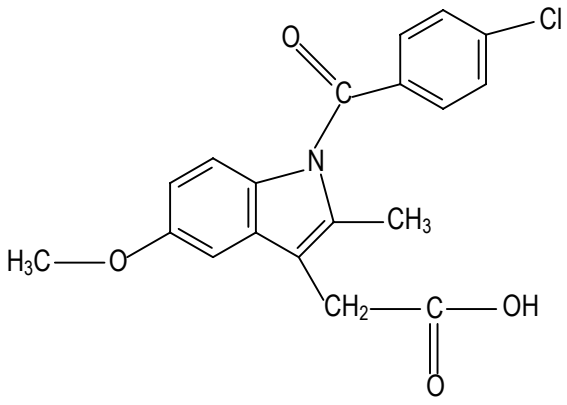

Figure 4.11 Chemical structure of indomethacin (IMC)

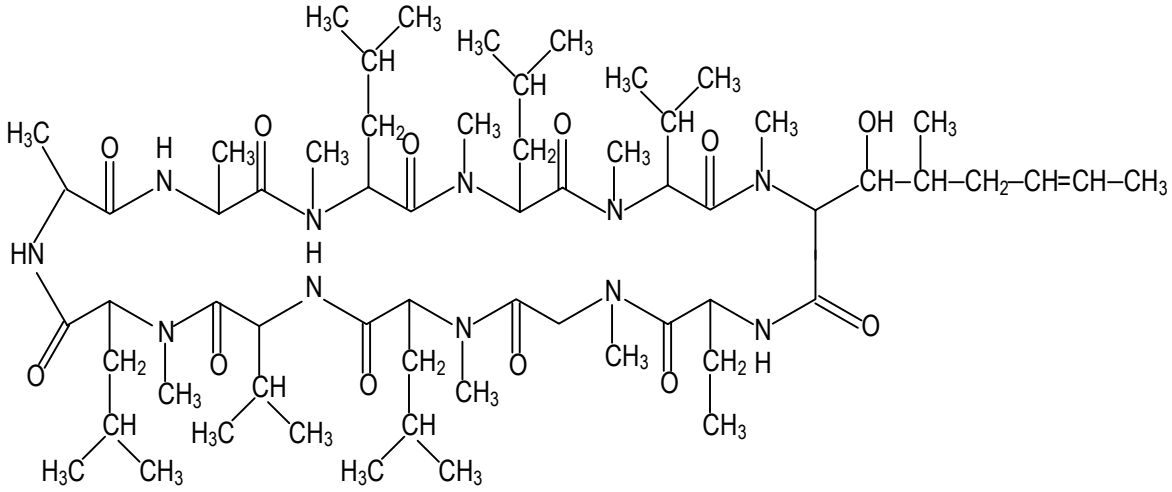

Figure 4.12 Chemical structure of cyclosporin A (CyA)

4.2.1 Characterisation of P(NIPAAm-*co*-DMAAm-*co*-OA)

The compositions of P(NIPAAm-*co*-DMAAm-*co*-OA) were determined with ^{1}H NMR spectrometer using $CDCl_3$ as the solvent. Figure 4.13 shows the ^{1}H NMR spectrum of the polymer. Signal **a** with two peaks overlapped was from C*H*$_2$CHCONHCHMe$_2$ in the NIPAAm moieties or C*H*$_2$CHCONMe$_2$ in the DMAAm moieties. Signals **b**, **d**, **e** and **f** were from CH$_2$C*H*CONHCHMe$_2$, CH$_2$CHCON*H*CHMe$_2$, CH$_2$CHCONHC*H*Me$_2$ and CH$_2$CHCONHCH*Me*$_2$ in the NIPAAm moieties, respectively. Signals **c** and **g** were from CH$_2$C*H*CONMe$_2$ and CH$_2$CHCON*Me*$_2$ in the DMAAm moieties, respectively. Signal **h** was from the terminal Me group of oleic acid segment. From the integration ratio of the signals **c** and **g** to the signal **e**, the NIPAAm/DMAAm ratio was estimated to be 6:1. On the other hand, the NIPAAm/oleic acid ratio was estimated to be 6:0.2 from the integration ratio of the signal **e** to the signal **h**.

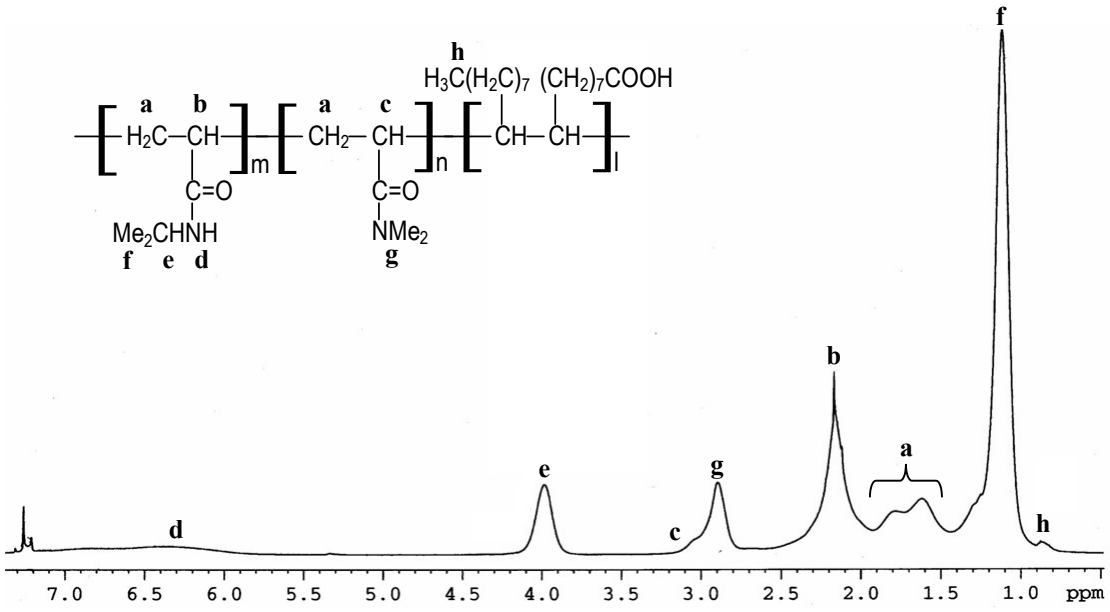

Figure 4.13 ^{1}H NMR spectrum of P(NIPAAm-*co*-DMAAm-*co*-OA) in $CDCl_3$

The molecular weights and polydispersity of the polymer were determined by GPC (relative to polystyrene standards). The weight average molecular weight of the polymer was 12.1k Da (Table 4.3).

Table 4.3 Composition and weight average molecular weight of P(NIPAAm-*co*-DMAAm-*co*-OA)

M_w[a]	$(M_w/M_n$[b]$)$[c]	Molar composition[d]		
		NIPAAm	**DMAAm**	**Oleic acid**
12.1k	1.8	6.0	1.0	0.2

[a] Weight-averaged molecular weight.
[b] Number-averaged molecular weight.
[c] Polydispersity of the polymer.
[d] The molar ratios of monomers were determined by NMR integration.

The thermal properties of P(NIPAAm-*co*-DMAAm-*co*-OA) were examined by TGA measurements. Figure 4.14 shows the TGA thermogram of the polymer over the temperature range from 50 to 800^{o}C. The thermogram under nitrogen flow shows a single mass loss with the onset degradation temperature of 330.5^{o}C. The polymer

rapidly degraded at 457.8°C. Therefore, this polymer is stable for storage and transportation.

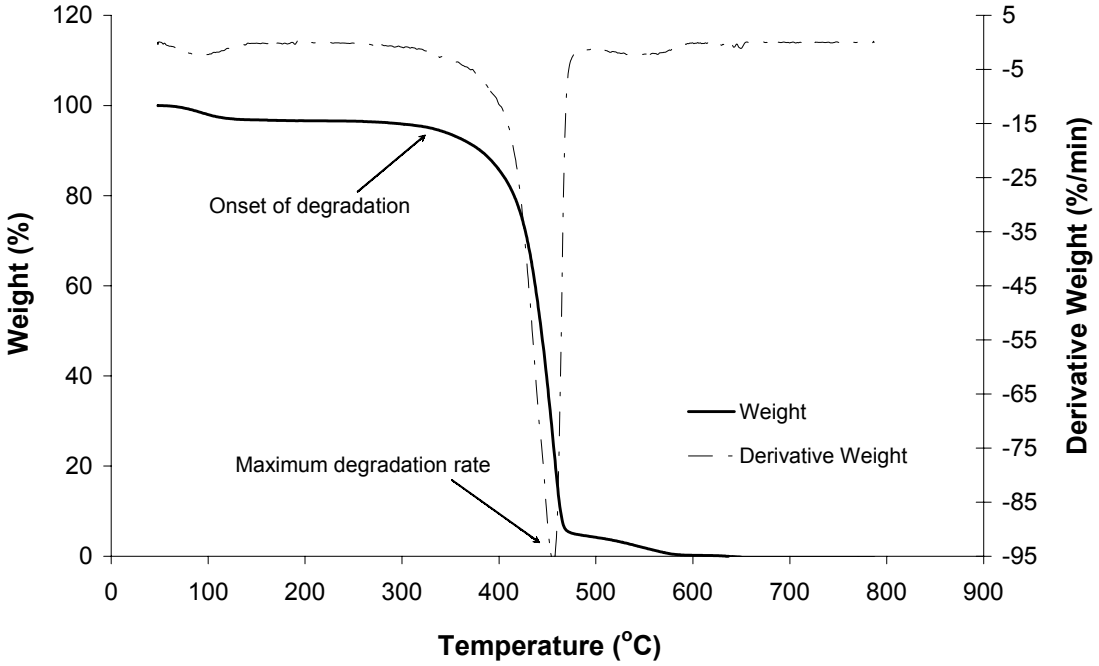

Figure 4.14 TGA thermogram of P(NIPAAm-*co*-DMAAm-*co*-OA) in N_2 atmosphere

4.2.2 Characterisation of drugs

4.2.2.1 Thermal stability

Figures 4.15 and 4.16 illustrate the thermogravimetric analysis (TGA) profiles of IMC and CyA, respectively. The thermograms for both IMC and CyA also show a single mass loss. The onset degradation temperature for IMC was 274.8°C. The degradation accelerated to a maximum rate when the temperature was raised to 340.9°C. CyA was stable up to 321.0°C and then rapidly degraded at around 404.0°C. By comparing the onset degradation temperature for both drugs, thermal stability of CyA was higher than that of IMC. This could be due to the larger structure of CyA and its higher molecular weight.

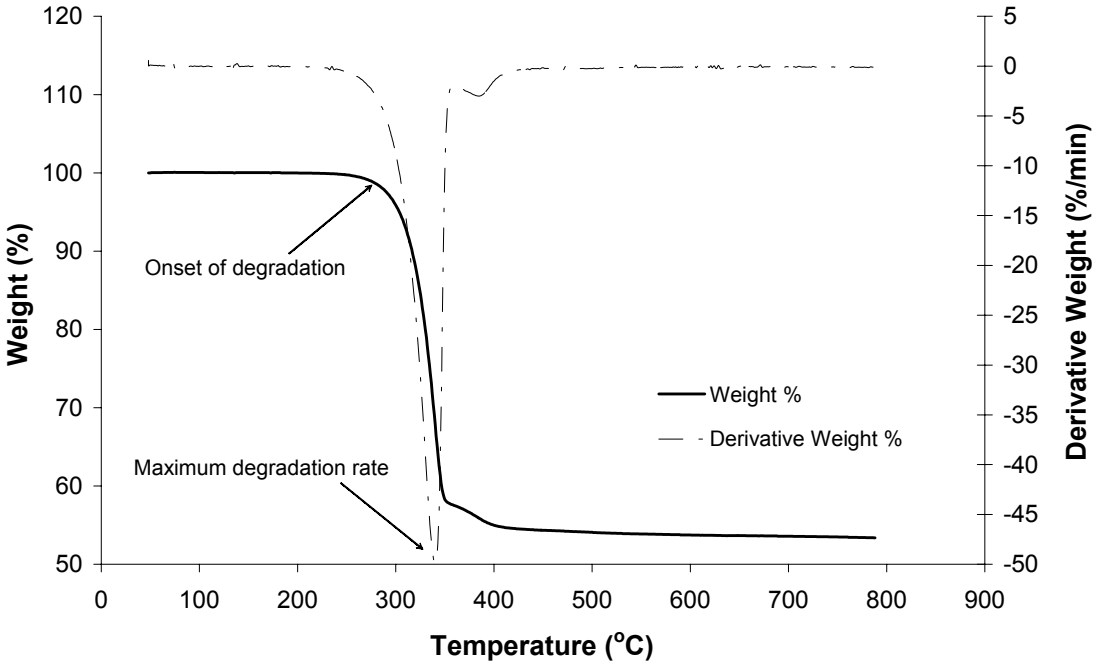

Figure 4.15 TGA thermogram of IMC in N_2 atmosphere

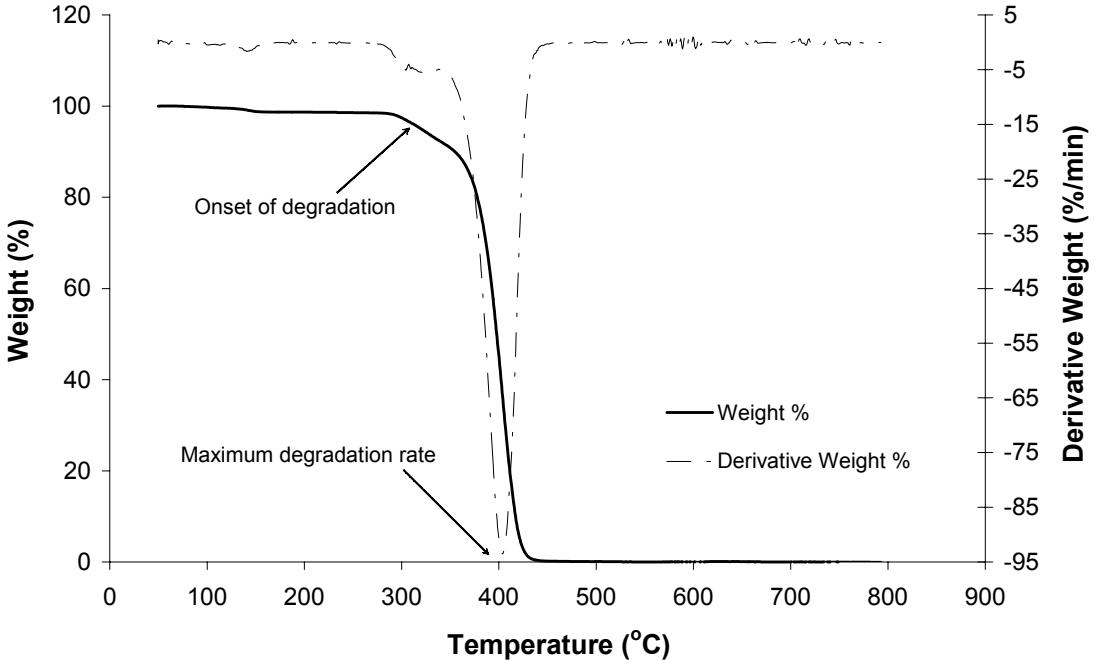

Figure 4.16 TGA thermogram of CyA in N_2 atmosphere

4.2.2.2 IMC solubility

The aqueous solubility of a drug is important in determining its bioavailability. To elucidate the solubility of IMC in a range of isotonic pH buffer solutions, further experiments were carried out by adding excessive IMC into pH 6 to pH 9 buffer solutions, incubated at different temperatures. The solubility measurements are reported in Table 4.4.

As expected, at a fixed incubation temperature (31^{o}C), the solubility of IMC was higher at pH 9 than that at pH 6. IMC solubility showed a 5-fold increase at pH 9 compared to pH 6. The improved solubility of IMC (pK_a = 4.5) was influenced by the ionisation degree of the drug. Under alkaline condition, the carboxylic acid group of IMC was ionised, resulting in an increase of hydrogen bonding between the drug and water. Consequently, IMC solubilised to a greater extent in a basic medium. On the contrary, the low ionisation degree of IMC in pH 6 (> pK_a) was expected to produce low drug dissolution.

In addition, the solubility of IMC was determined in PBS (pH 7.4) at 20 and 37^{o}C. An increase in the incubation temperature resulted in a corresponding increase in the solubility of IMC. From Table 4.4, IMC solubility at 37^{o}C was estimated to be nearly 2-fold greater than that at 20^{o}C. This was attributed to the changes in the relative strengths of solvent-solvent, solvent-solute, and solute-solute interactions, in which the hydrogen bonding was a predominant factor.

Table 4.4 The solubility of IMC determined in different isotonic pH buffers

pH buffer[a]	Temperature (°C)	Solubility[b] (ppm)
9.0	31	2217.5 ± 4.4
6.0	31	441.7 ± 6.4
7.4	37	967.0 ± 6.8
7.4	20	539.5 ± 5.5

[a] Ionic strength is 0.18 M.
[b] Mean ± S.D. of three determinations.

4.2.3 LCST and phase transition pH of nanoparticles

PNIPAAm is a thermoresponsive polymer that exhibits a lower critical solution temperature (LCST) of ca. 32°C (Ringsdorf et al., 1991). At temperatures below the LCST, the polymer is water-soluble but it precipitates when the temperature is raised above the LCST. To ascertain whether P(NIPAAm-*co*-DMAAm-*co*-OA) polymer exhibits a thermal response similar to the PNIPAAm homopolymer, the LCST transition of the polymer in water was characterised by monitoring the solution turbidity as a function of temperature. The LCST was determined by the temperature showing 50% transmittance at 500 nm. Figure 4.17 shows the optical transmittance of the aqueous solution of P(NIPAAm-*co*-DMAAm-*co*-OA) at various temperatures.

The drop in transmittance as a function of temperature was quite broad. The LCST of the polymer in water was estimated to be 32.8°C, which was higher than that of PNIPAAm. Incorporation of DMAAm, which was a hydrophilic group, into the PNIPAAm chains strengthened the interactions between the polymer chains and water. Concurrently, there was an increase in enthalpy of hydrogen bonding between the polymer and water, thus stabilised the polymer dissolution. As a result, the phase transition phenomenon was slowed down, which subsequently raised the LCST.

In fact, incorporation of a terminal hydrophobic group had a reverse effect on the LCST. However, the thermoresponsive behaviour of core-shell nanoparticles resembled the shell of P(NIPAAM-*co*-DMAAm).

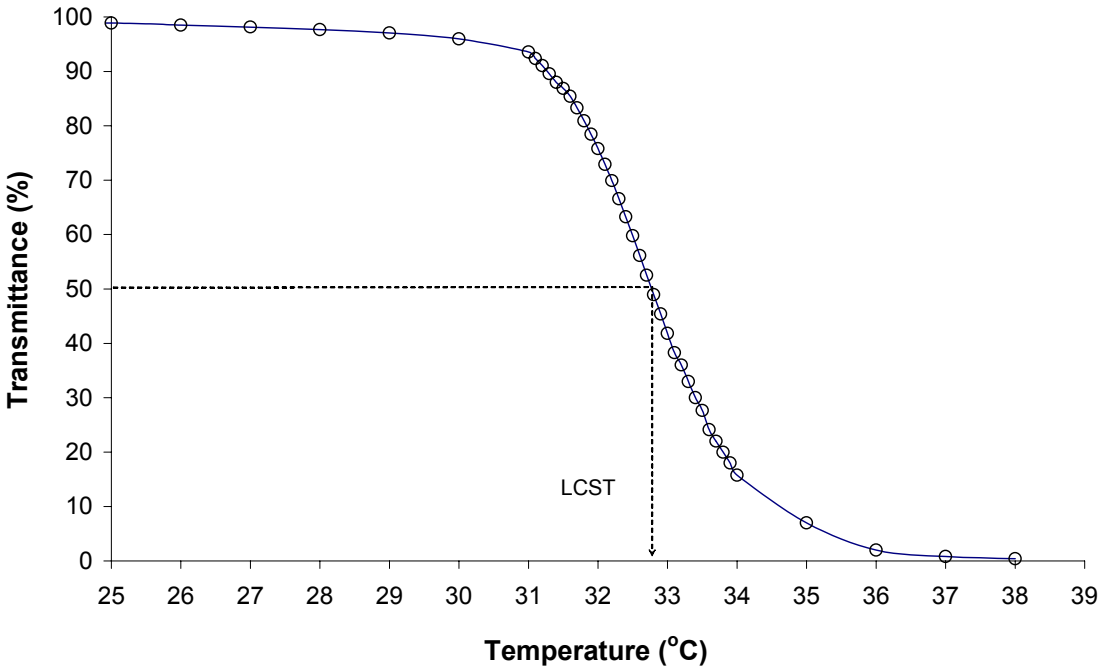

Figure 4.17 Transmittance changes as a function of temperature for solution of P(NIPAAm-*co*-DMAAm-*co*-OA) in water (polymer concentration: 5 mg/mL, absorbance at 500 nm)

To elucidate the influence of pH on the LCST, the optical transmittance was measured for polymer in different pH buffer solutions at 500 nm, against temperatures. The polymer was soluble in aqueous buffers at room temperature, except for pH 4. Hence, prior to the measurements, the polymer solution that was prepared in pH 4, was filtered through a filter of 0.45 µm pore size. However, the solutions became turbid upon heating, indicating precipitation of the polymer. A series of plots of changes in turbidity of polymer solutions ranging from pH 4.0 to 11.0 are illustrated in Figure 4.18.

The drop in transmittance as a function of temperature was very sharp for solutions at higher pH values. It can be obviously seen that the LCST of the polymer was greatly influenced by the changes in pH. In an acidic buffer (pH 4.0 and pH 6.0), the LCST was determined to be 27.2 and 28.8^{o}C, respectively. The LCST rose to 32.0^{o}C at physiological pH. As the pH of the polymer solution was increased to 9, 10 and 11, the LCST of the polymer further increased to 33.5, 33.7 and 35.2^{o}C, respectively. In solutions with pH value greater than pK_a of 4.5, the carboxylic acid group of oleic acid segments was ionised, causing the polymer chains to interact more favourably with water. Increasing pH then promoted the ionisation degree of the carboxylic acid group. As a result, the enthalpy of hydrogen bonding between the polymer and water was increased, thereby increasing the LCST of the polymer.

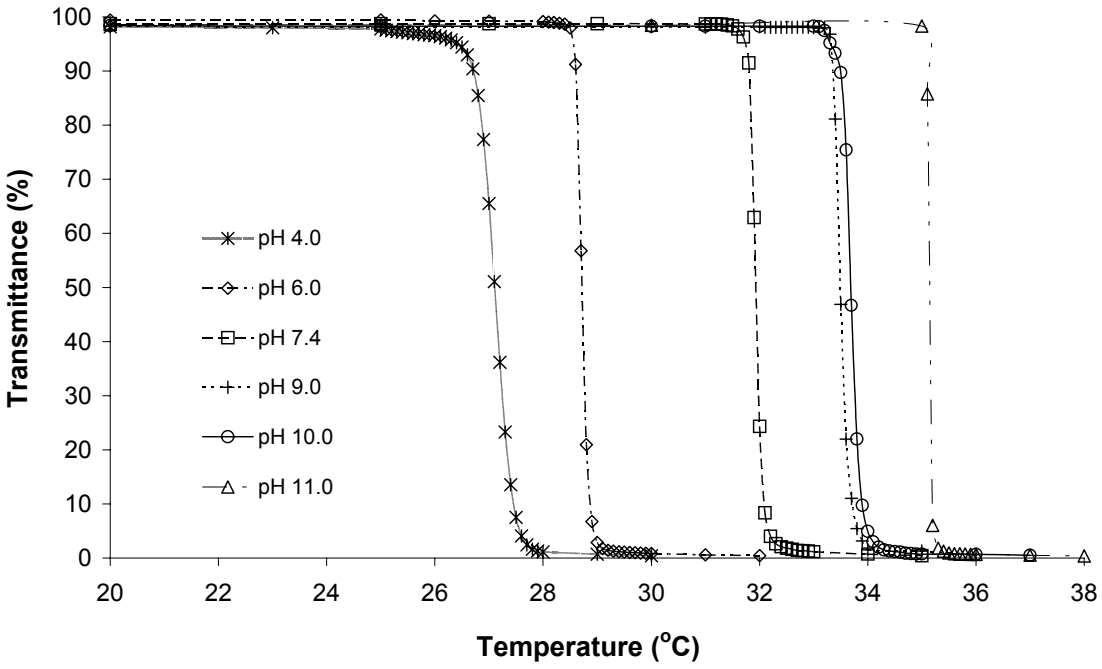

Figure 4.18 Transmittance changes as a function of temperature for solutions of P(NIPAAm-*co*-DMAAm-*co*-OA) in various pH buffer solutions (polymer concentration: 5 mg/mL, absorbance at 500 nm)

The phase transition pH of the nanoparticles was further determined by monitoring the transmittance change of the aqueous polymer solution as a function of pH at 500 nm. The pH showing an optical transmittance of 50% was estimated to be the pH of phase transition. Figure 4.19 shows the pH at which the phase transition occurred at 31^{o}C in different isotonic aqueous buffers. The nanoparticles showed a phase transition around pH 6.25. The nanoparticles were water-soluble above the phase transition pH but precipitated when the pH was below the phase transition pH. The acidity of the P(NIPAAm-*co*-DMAAm-*co*-OA) was due to the carboxylic acid group in the hydrophobic segment. At low pH, the carboxylic acid groups were protonated, thus the nanoparticles were insoluble in aqueous solution. However, as the pH of the polymer solution increased, the carboxylic acid groups were progressively deprotonated. This phenomenon will prolong until the polymer was fully ionised and subsequently soluble in aqueous solution.

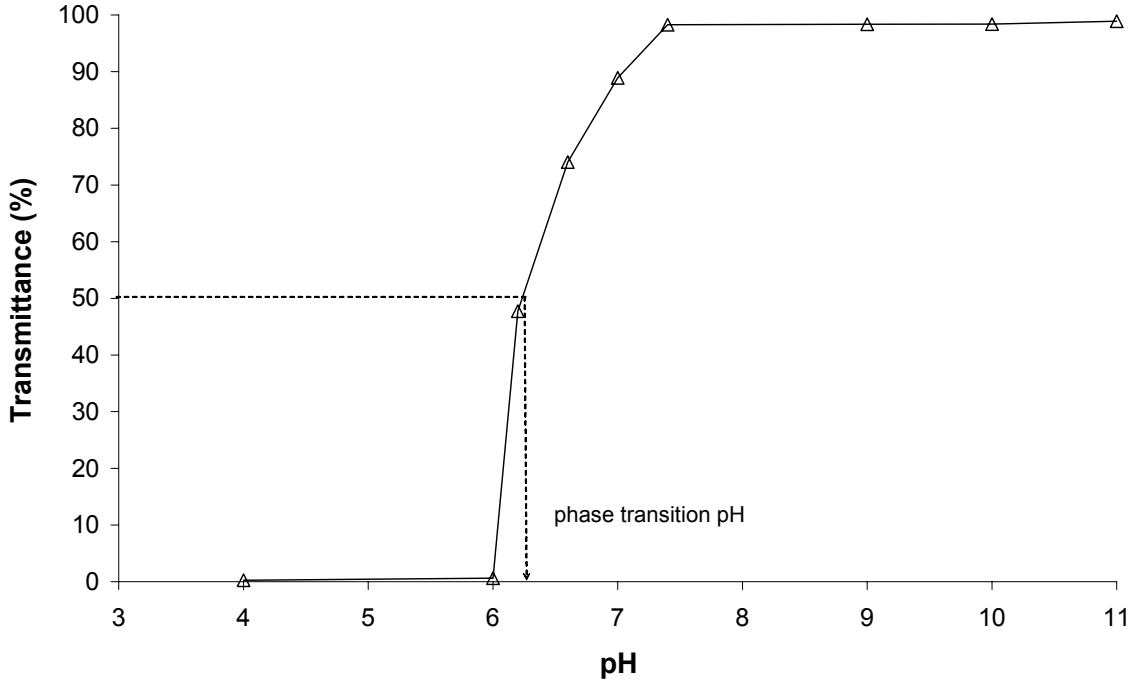

Figure 4.19 Transmittance changes as a function of pH for solutions of P(NIPAAm-*co*-DMAAm-*co*-OA) at 31^{o}C (polymer concentration: 5 mg/mL, absorbance at 500 nm)

4.2.4 Formation of core-shell nanoparticles

The formation of core-shell nanoparticles from the polymer was verified by the detection of critical association concentration (CAC) using a fluorescence technique. Fluorescence is a very sensitive technique and can detect the location of pyrene (e.g. in hydrophobic domains or in the aqueous solution). Pyrene was chosen as a fluorescent probe because its vibrational structure is sensitive to polarity and it produces distinct excimer fluorescence under conditions of sufficiently high concentration and mobility (Kalyanasundaram and Thomas, 1977). It is strongly hydrophobic and its solubility in water is very low. In the presence of core-shell nanoparticles, pyrene is solubilised into the inner core of the particles. As a result, significant changes in the spectroscopic properties are observed upon transfer of the pyrene from the aqueous environment to the non-polar environment of the inner core. Such changes can be observed from the emission and excitation spectra of pyrene.

Both emission and excitation fluorescence spectra of pyrene are shown to depend on the nature of the solvent (Nakajima, 1971). However, the patterns of emission and excitation spectra recorded for pyrene in the aqueous solution of P(NIPAAm-*co*-DMAAm-*co*-OA) were similar regardless of the solvent used. Figure 4.20 shows the emission spectra of pyrene, at fixed excitation wavelength of 339 nm, at various polymer concentrations. The fluorescence emission spectra of pyrene were affected by the polarity of its environment. An increase in the total fluorescence intensity and a change in the vibrational structure of monomer fluorescence were observed with increasing polymer concentrations, indicating the formation of core-shell nanoparticles. The excitation spectra of pyrene in the presence of P(NIPAAm-*co*-DMAAm-*co*-OA)

polymer at a fixed emission wavelength of 395 nm are shown in Figure 4.21. At low polymer concentrations, changes in the total fluorescence intensity and the shift of the (0, 0) band at 333 nm were insignificant. As the concentration of the polymer was increased, however, an increase in the total fluorescence intensity and a red shift of the (0, 0) band were clearly observed. Specifically, the (0, 0) band for pyrene, which is at 333 nm in water, has been shown to shift to 338 nm upon addition of P(NIPAAm-*co*-DMAAm-*co*-OA) polymer. The shift of the excitation peak demonstrated that the pyrene molecules gradually transferred to less polar microdomains of the interior of core-shell nanoparticles.

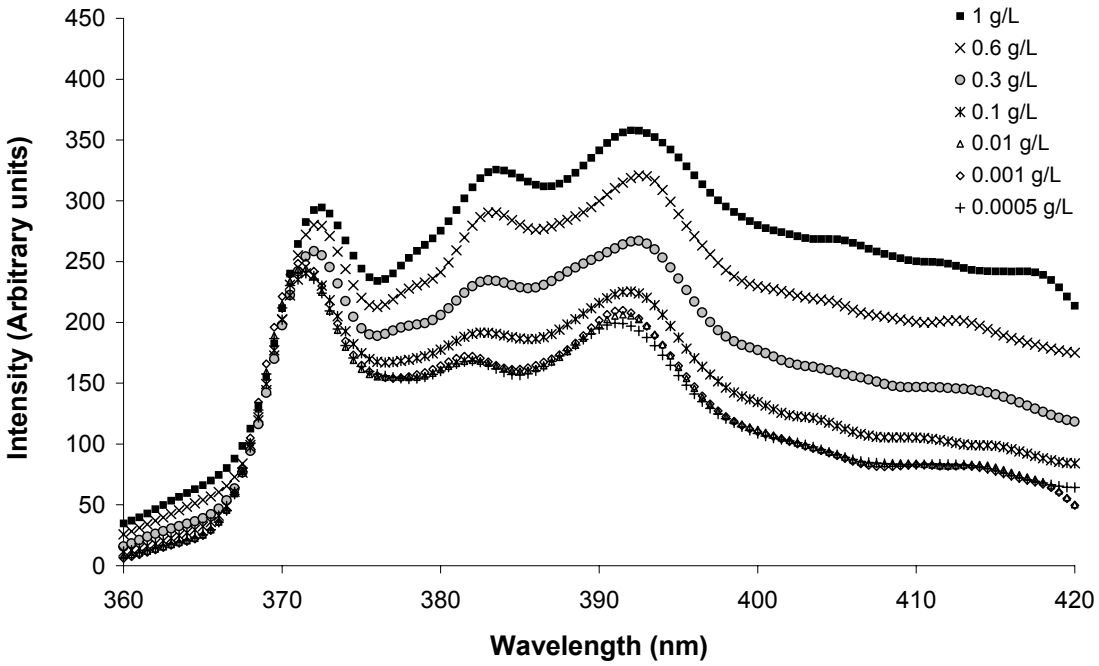

Figure 4.20 Emission spectra of pyrene (6.17×10^{-7} M) at pH 10 in the presence of P(NIPAAm-*co*-DMAAm-*co*-OA) (excitation wavelength: 339 nm)

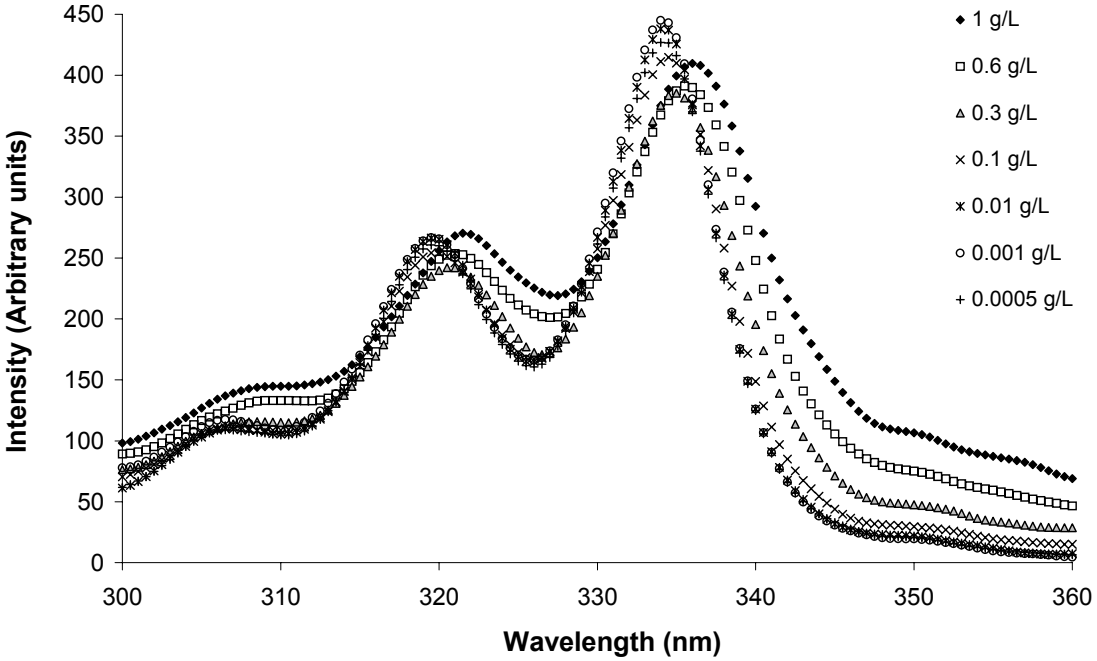

Figure 4.21 Excitation spectra of pyrene (6.17×10^{-7} M) at pH 10 in the presence of P(NIPAAm-*co*-DMAAm-*co*-OA) (emission wavelength: 395 nm)

The CAC, which is the threshold concentration of self-assembly formation by intra- and/or intermolecular association, was determined from the change of the intensity ratio (I_{338}/I_{333}) of the pyrene in the presence of amphiphilic polymer. Figure 4.22 illustrates the plot of the intensity ratio (I_{338}/I_{333}) from pyrene excitation spectra against the log C of P(NIPAAm-*co*-DMAAm-*co*-OA) polymer. CAC value was taken from the intersection of the tangent to the curve at the inflection with the horizontal tangent through the points at low polymer concentrations, as shown in Figure 4.22 (a). Below the CAC, the pyrene fluorescence spectrum exhibits a low value and mild slope of I_{338}/I_{333}. However, at the CAC, the curve shows a sharp increase in the I_{338}/I_{333} ratio. From Figure 4.22 (a), the CAC in water was estimated to be 64.0 mg/L. Although the CAC of the P(NIPAAm-*co*-DMAAm-*co*-OA) in water was higher than that of the poly(ethylene oxide)-poly(*β*-benzyl L-aspartate) copolymer micelles (5.0-10.0 mg/L) (Kwon et al., 1993a), it was much lower than that of oligo(methyl methacrylate)-*b*-poly(acrylic acid) copolymer micelles (100.0 mg/L) (Inoue et al., 1998).

To study the effect of pH on the CAC, the change of the intensity ratio (I_{338}/I_{333}) of pyrene in the presence of amphiphilic polymer, under acidic, physiological and basic conditions was evaluated [Figure 4.22 (b)]. The intensity ratio was relatively constant at low concentrations, and rapidly increased at high concentrations. The estimated CAC in pH 4.0, 7.4 and 10.0 was ca. 46.0, 64.0 and 81.0 mg/L, respectively. The core-shell nanoparticles were formed at a higher concentration in basic environment, and with a lower CAC in acidic environment. The higher CAC value was attributed to the increase of hydrophilicity of the inner core. Increasing pH (> 4.5) promoted the ionisation of the carboxylic acid group. This inhibited the hydrophobic interactions, and thus a higher polymer concentration was required to form the hydrophobic core (Na et al., 2000). The results are similar to those reported by Han et al. (2003). The CAC of poly(L-lactide)/poly(ethylene glycol)-poly(sulfadimethoxine) increased with decreasing hydrophobic portion.

In addition, the results obtained from this study also showed that the CAC was not affected by the presence of salts. It remained the same in both water and PBS (ca. 40 mg/L). Zhang et al. (1996b) reported that the CAC of methoxy-poly(ethylene oxide)-*b*-poly(D,L-lactide acid) was similar in water, 0.9% saline solution, and 5% dextrose solution. This is not surprising considering the non-ionic nature of the polymer. Another study also demonstrated that the CAC for poly(*N*-isopropylacrylamide-*co*-methacrylic acid-*co*-octadecyl acrylate) in water and PBS was similar (Taillefer et al., 2000). In the case of poly(*N*-isopropylacrylamide-*co*-methacrylic acid-*co*-octadecyl acrylate) and P(NIPAAm-*co*-DMAAm-*co*-OA) polymers, increased ionisation of the polymer in PBS should enable the formation of core-shell nanoparticles at higher polymer concentrations. On the other hand, the presence of salt decreased the ability of

water as a solvent for polyelectrolytes, resulting in a lower CAC (Astafieva et al., 1995). As a result, the effect of salt on CAC for these polymers in PBS was negligible.

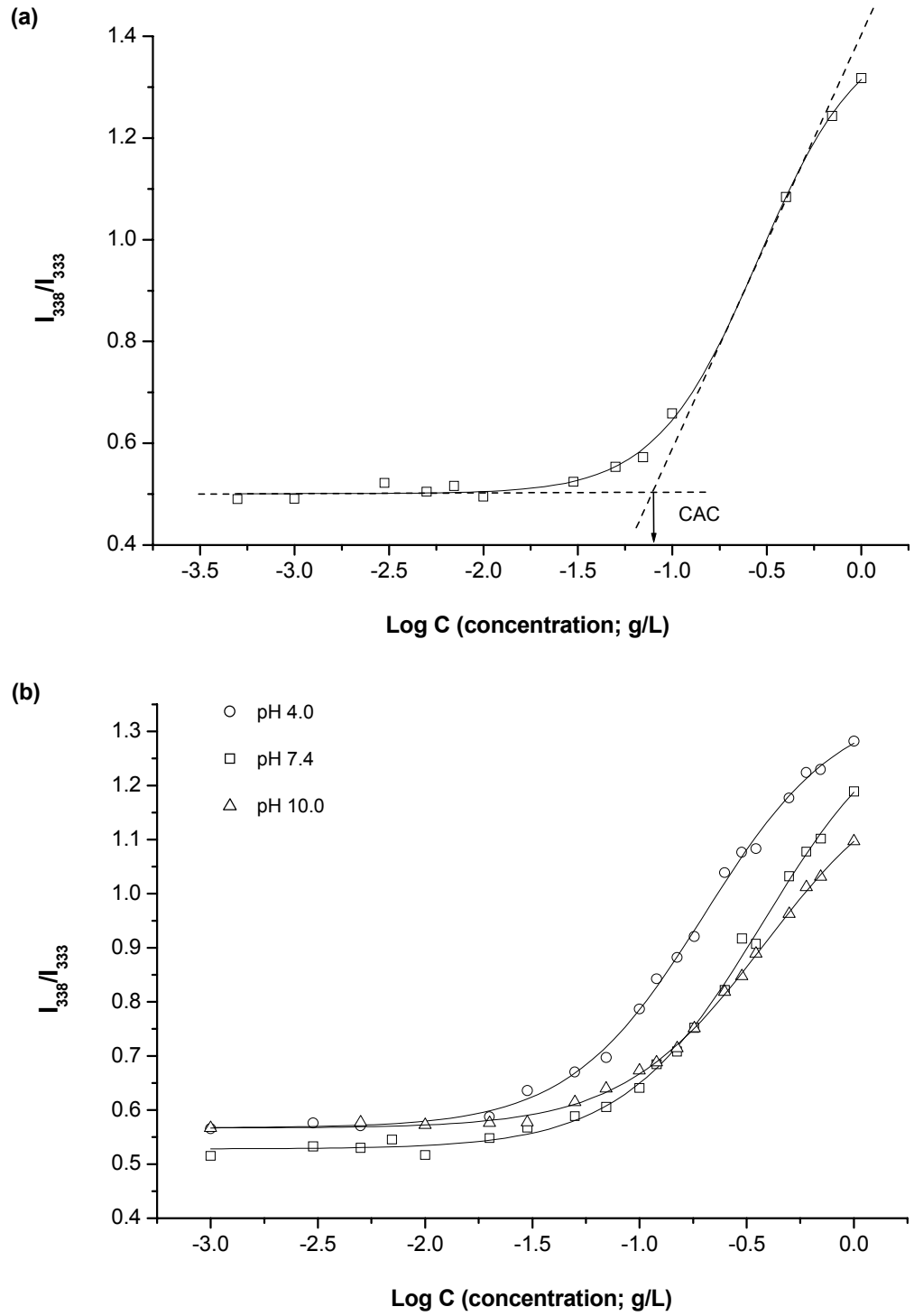

Figure 4.22 Plot of intensity ratio I_{338}/I_{333} from excitation spectra *versus* log C of P(NIPAAm-*co*-DMAAm-*co*-OA)in (a) ultra pure water and (b) different isotonic pH buffers

The change in the polarity of microenvironment of pyrene can be estimated from the specific intensity ratio of the (0, 0) band, I, to the (0, 2) band, III, in the fluorescence spectra of pyrene, which is known as the pyrene scale (Dong and Winnik, 1984). The ratio of the intensity of the I_1/I_3 is correlated to the dipolar and the dielectric constants of the solvent (Kalyanasundaram and Thomas, 1977). I_1/I_3 ratios were normally used to ascertain the location of pyrene. As reported by Gautier et al. (1999), a high I_1/I_3 ratio indicated either that the hydrophobic character of the solubilisation regions is less pronounced (e.g. that they are less dense, or they are infiltrated with more water molecules), or pyrene partitioned towards the hydrophilic phase (e.g. expulsion from microdomains due to the structural deformation). This ratio is not preferentially used as a CAC determination procedure because it depends on the wavelength of excitation. When the excitation wavelength is 339 nm, the plot of the I_1/I_3 ratio is shifted in favour of pyrene in a hydrophobic environment. However, when the excitation wavelength is 333 nm, it is strongly weighted toward pyrene in an aqueous medium. Figure 4.23 shows micropolarity changes, as measured using polarity-sensitive pyrene, as a function of P(NIPAAm-*co*-DMAAm-*co*-OA) concentration. At low concentrations, the I_1/I_3 ratios were as high as ca. 1.45-1.55. As the polymer concentration increased, a sharp decrease in I_1/I_3 was observed. This indicates the partitioning of the hydrophobic pyrene probe into the hydrophobic microdomains, because of the formation of core-shell nanoparticles.

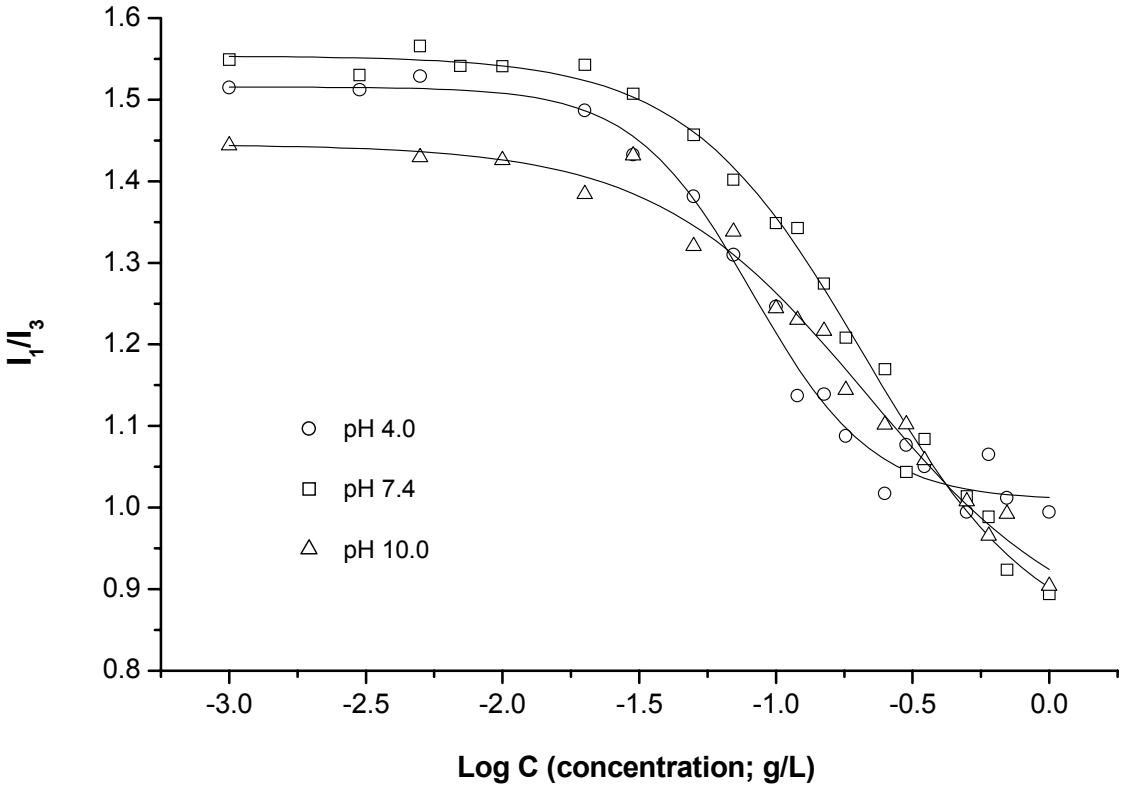

Figure 4.23 Plot of intensity ratio I_1/I_3 from emission spectra *versus* log C of P(NIPAAm-*co*-DMAAm-*co*-OA) in different isotonic pH buffers

4.2.5 Morphology of nanoparticles

The morphology of P(NIPAAm-*co*-DMAAm-*co*-OA) and drug-loaded P(NIPAAm-*co*-DMAAm-*co*-OA) core-shell nanoparticles was investigated at different temperatures and pH buffers with a transmission electron microscopes (TEM). The TEM images clearly indicated the presence of nanoparticles with nanoscopic dimensions as in a dehydrated state (Figure 4.24). The nanoparticles were spherical and discrete.

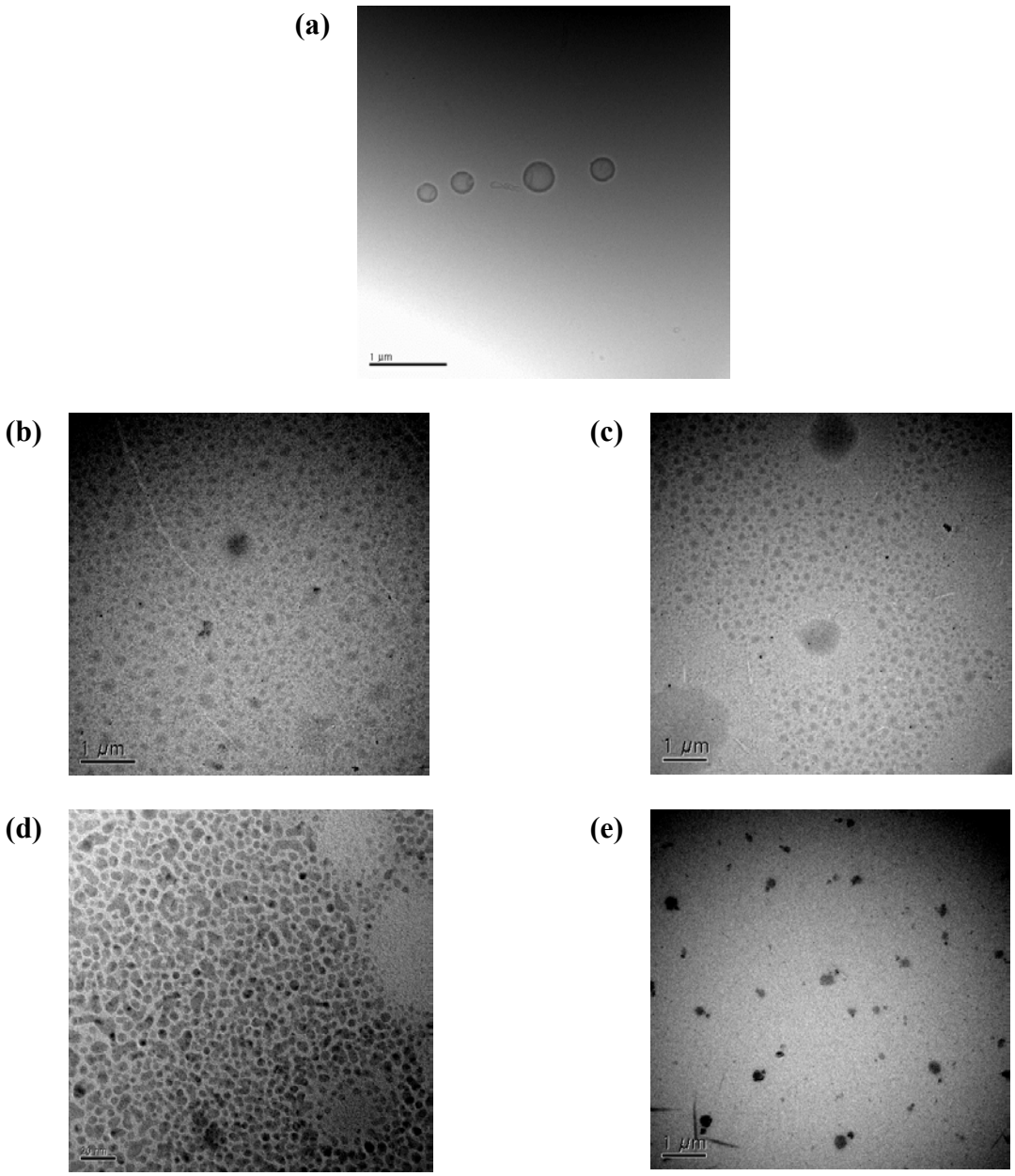

Figure 4.24 Transmission electron microscopes (TEM) photographs of (a) loaded nanoparticles (25.0 w/w % of IMC, water, 10^{o}C); and unloaded nanoparticles at (b) 10^{o}C (water), (c) 20^{o}C (water), (d) pH 4.0 (10^{o}C) and (e) pH 9.0 (10^{o}C)

4.2.6 Size and size distribution of nanoparticles

The size of the nanoparticles is one of the major parameters that can affect their interactions with cells and distribution in the organs during their application as drug carriers (Kabanov et al., 1992). The size and size distribution of the unloaded

nanoparticles prepared from the dialysis method were measured by a dynamic light scattering (DLS) equipped with He-Ne laser. Prior to the measurements, the lyophilised nanoparticles were redispersed in water, vortexed and then filtered through a filter of 0.45 μm pore size. Figure 4.25 illustrates the typical size distribution of P(NIPAAm-*co*-DMAAm-*co*-OA) core-shell nanoparticles. It shows a bimodal pattern, a small portion at ca. 10 nm and a large portion at ca. 170-180 nm. Therefore, they are considered to be an efficient drug carrier without scavenging by RES. The small particles should be due to drug and/or small polymer aggregates, which can be removed by filtration.

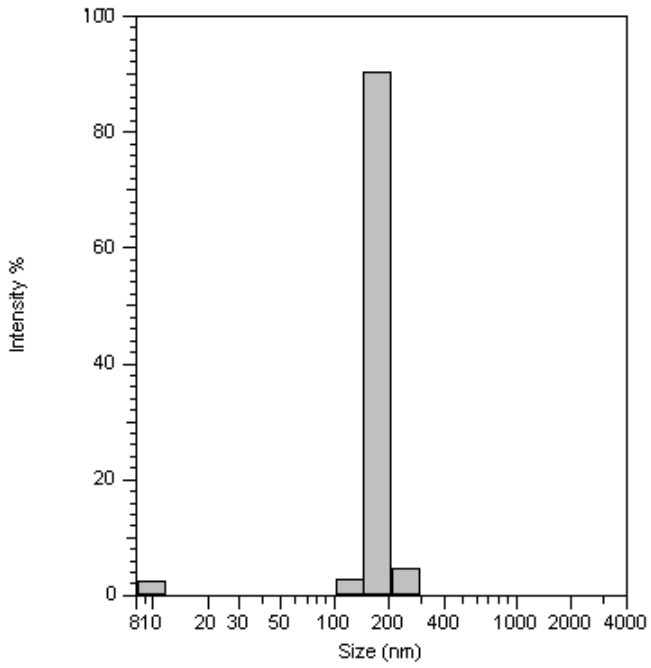

Figure 4.25 Typical size distribution profile of P(NIPAAm-*co*-DMAAm-*co*-OA) core-shell nanoparticles analysed by dynamic light scattering at 20^{o}C

Prior to getting the in-depth understandings of the influence of temperature and pH on the particle size, the effect of fabrication temperature was investigated. Unloaded nanoparticles were prepared using the dialysis method at 10 and 20^{o}C, respectively.

From Figure 4.26, it can be concluded that the particle size was independent on the fabrication temperature.

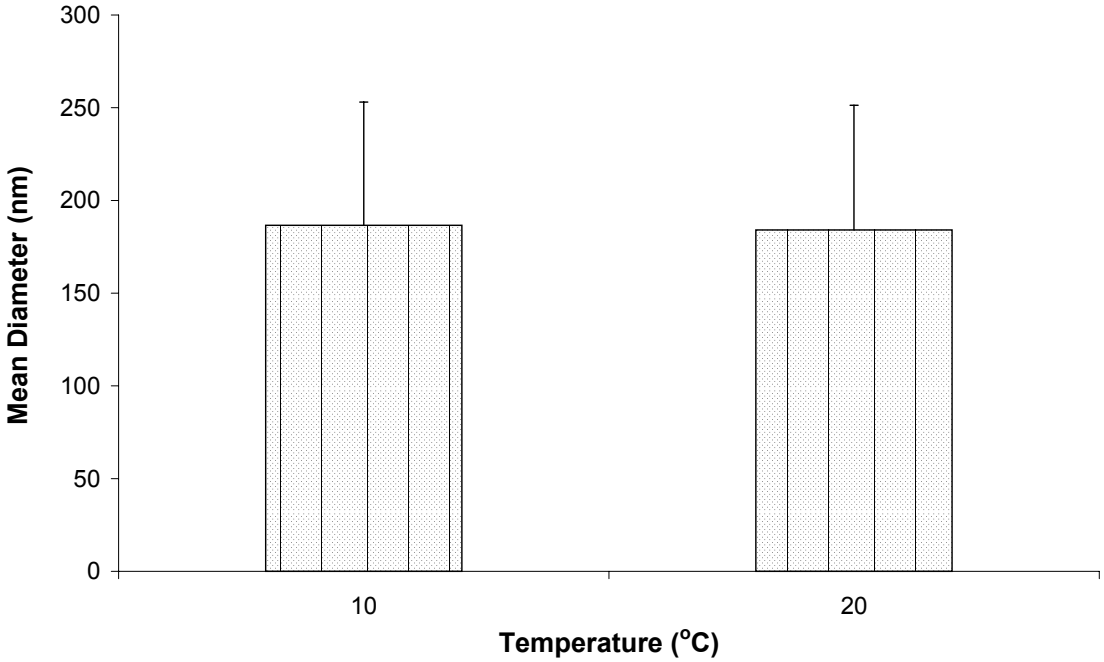

Figure 4.26 Mean diameter of P(NIPAAm-*co*-DMAAm-*co*-OA) core-shell nanoparticles prepared at different temperatures

The thermal response behaviour of P(NIPAAm-*co*-DMAAm-*co*-OA) nanoparticles was further determined by studying the size change of the nanoparticles as a function of temperature. As shown in Figure 4.27, below 25°C, the particles showed a nearly constant size (ca. 170 nm). However, as the temperature was raised to 35°C, which was close to the LCST of nanoparticles in water, the size increased insignificantly. Further heating to 40°C (above the LCST) caused a markedly increase in size (Jeong et al., 1999). The hydrodynamic size of the particles was speculated to remain constant while the aggregation number increased with temperature as a result of dehydration of the PNIPAAm chains in the outer shell. The increase in size was contributed by the aggregation at the temperature higher than the LCST.

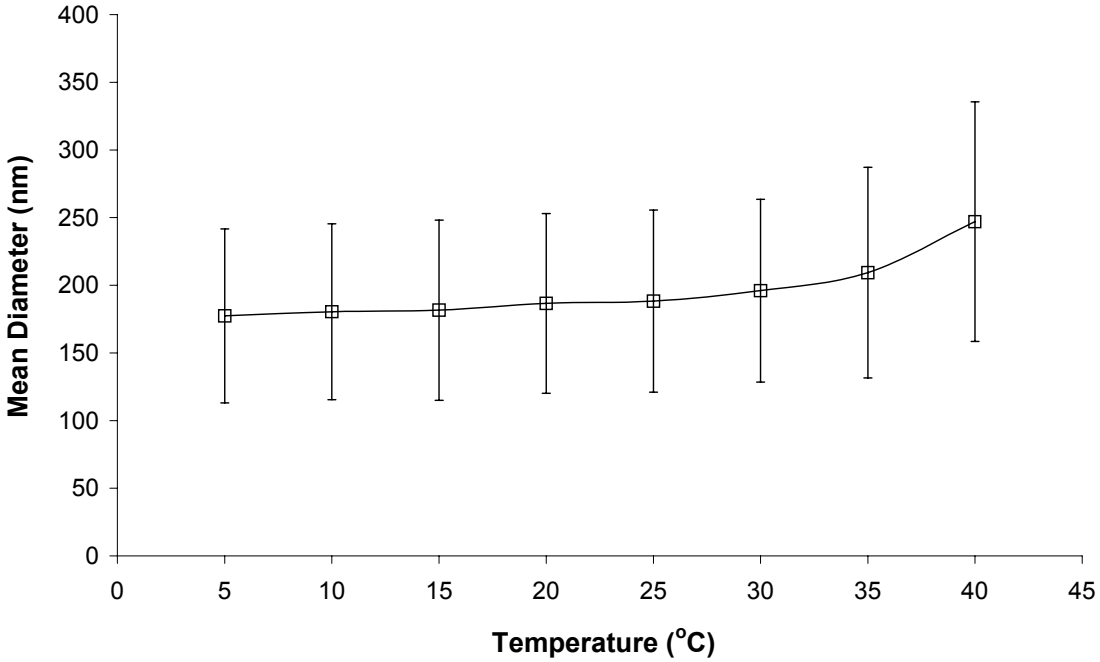

Figure 4.27 Effect of temperature on the size of P(NIPAAm-*co*-DMAAm-*co*-OA) core-shell nanoparticles

On the other hand, the thermoresponsive reversibility of P(NIPAAm-*co*-DMAAm-*co*-OA) nanoparticles was evaluated in a repetitive heating and cooling cycle. In a hydrated state, the particle size was reversibly changed by temperature fluctuation from 20 to 40°C, as demonstrated in Figure 4.28. This might be caused by the thermal sensitivity of PNIPAAm in the outer shell of the nanoparticles. The aggregates formed upon heating redispersed to their initial structure upon cooling to the temperature below the LCST. However, the particles showed a smaller average diameter after each heating cycle. The possible reason is that some of large aggregates did not have ample time to redisperse to their hydrated structure, resulting in a lower polymer concentration. Therefore, smaller particles were obtained when the polymer self-assembled again.

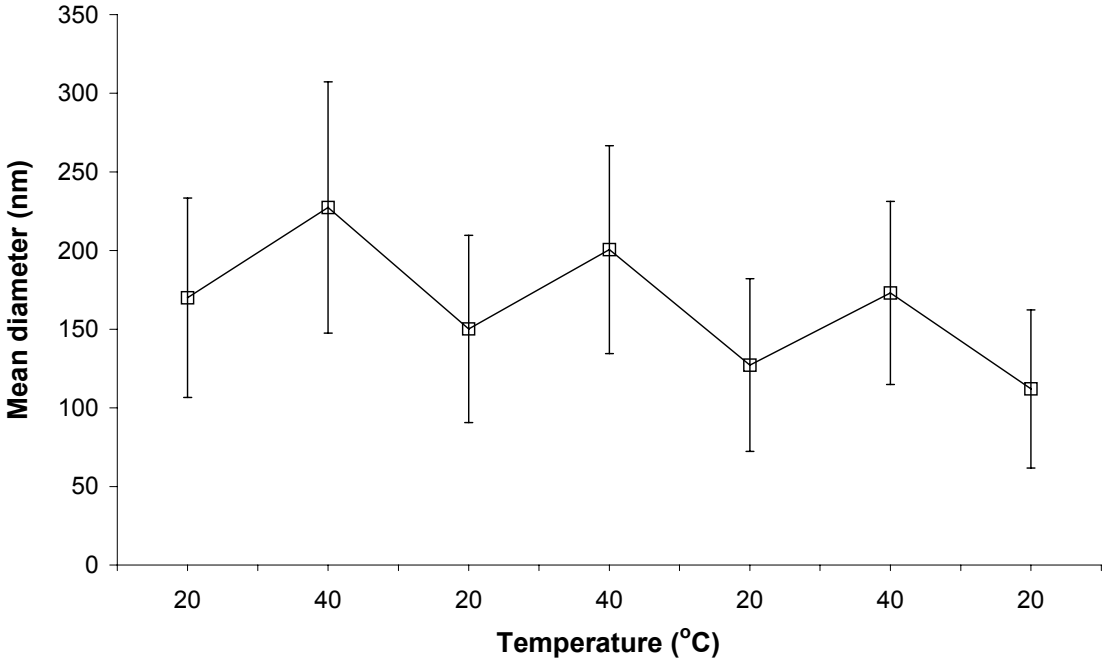

Figure 4.28 Reversible temperature-responsive size change of P(NIPAAm-*co*-DMAAm-*co*-OA) core-shell nanoparticles

In addition to that, the pH-dependent behaviour of the polymeric nanoparticles prepared at 10°C was also examined by measuring the particle size as a function of pH. As shown in Figure 4.29, the mean diameter of the nanoparticles was about 40 nm at the pH where all carboxylic acid groups (pK_a = 4.5) were in the acid form. However, with increasing pH to 9, the particles grew to ca. 130 nm because of a higher ionisation of the carboxylic acid group of oleic acid. The degree of ionisation of the carboxylic acid group controlled the balance between the repulsive and attractive intra- or inter-molecular interactions (Gautier et al., 1999). Hence, a higher pH caused a decrease in the hydrophobicity of the core, leading to the swelling of the core.

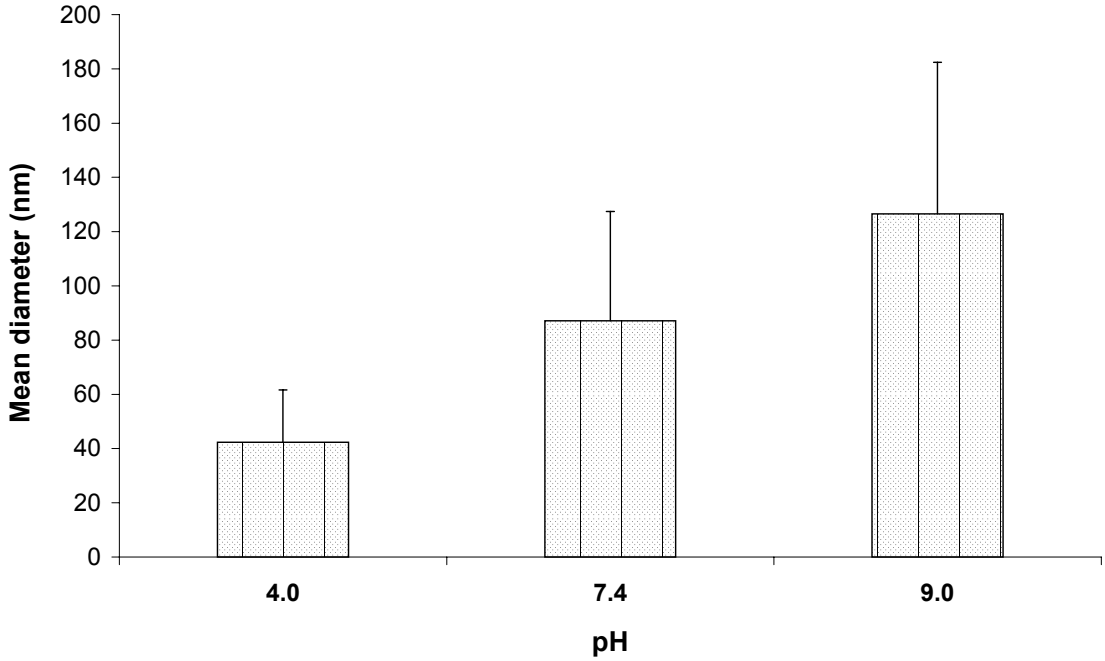

Figure 4.29 Mean diameter of P(NIPAAm-*co*-DMAAm-*co*-OA) core-shell nanoparticles as a function of pH

4.2.7 Zeta potential of core-shell nanoparticles

The surface charge of the nanoparticles was evaluated in water as a function of temperature by the zeta potential measurements. The zeta potential of the nanoparticles was -4 mV at 5^{o}C and decreased in negativity to -20 mV at 40^{o}C (Figure 4.30). Most of the carboxylic acid groups should be deprotonated in water. Therefore, the low surface negativity of the nanoparticles was due to the presence of ionised carboxylic acid groups of the oleic acid chains (Govender et al., 2000; Riley et al., 1999; Stolnik et al., 1995; Yamamoto et al, 1999). As the temperature was increased to be above the LCST, the collapsed PNIPAAm chains of the outer shell induced aggregation. Consequently, the particles presented higher negative charge on the surface at the temperature higher than the LCST because of the formation of larger particles.

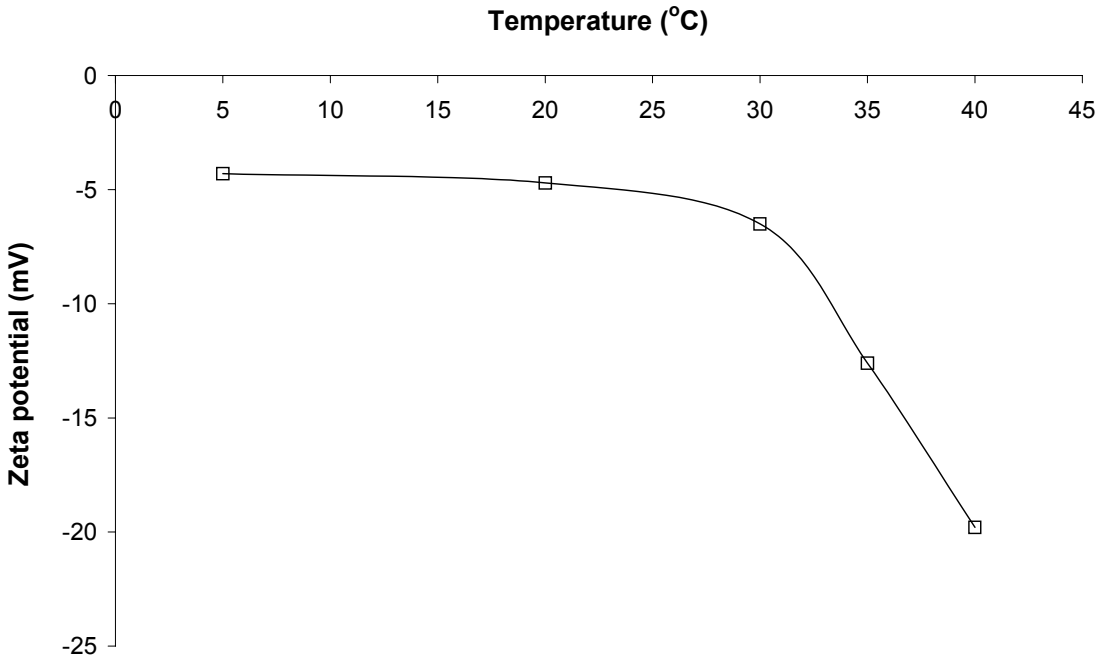

Figure 4.30 Zeta potential of P(NIPAAm-*co*-DMAAm-*co*-OA) core-shell nanoparticles in water as a function of temperature

4.2.8 Drug incorporation into core-shell nanoparticles

The possible application of P(NIPAAm-*co*-DMAAm-*co*-OA) core-shell nanoparticles for drug delivery was evaluated by encapsulating hydrophobic drugs using the dialysis method. During this process, in the gradual decrease of organic solvent (DMF) in the dialysis bag, spontaneous hydrophobic association of oleic acid segments both with themselves and with hydrophobic drugs drive the formation of core-shell nanoparticles and drug incorporation. These interactions were significantly affected by the nature of drugs, fabrication temperature (Chung et al., 1999), dialysis medium (Yu et al., 1998), polymer concentration (Chung et al., 1999), initial drug loading (Allen et al., 2000; Chung et al., 1999; Kim et al., 1998; Kim et al., 1999; Kohori et al., 2002; Riley et al., 1999; Shin et al., 1998; Yokoyama et al., 1998a), solvent exchange speed, organic solvent (Chung et al., 1999; Shin et al., 1998; Yokoyama et al., 1998a), and copolymer

composition (Govender et al., 2000; Kim et al., 1998; Nah et al., 1998; Yokoyama et al., 1998a).

The incorporation of indomethacin (IMC) and cyclosporin A (CyA), respectively into the core-shell nanoparticles was carried out at 10^{o}C. As shown in Table 4.5, the amount of CyA encapsulated was nearly 2-fold higher than that of IMC. The encapsulation efficiency of drug is dependent on the compatibility of drug and polymer, as well as the water-solubility of drug. Compared to IMC, both CyA and oleic acid molecules are more flexible. It might be easier for CyA and oleic acid segments self-assemble into a compact core structure, resulting in higher encapsulation efficiency. On the other hand, IMC is more water soluble than CyA. During the fabrication process, dissolution loss of IMC might be higher than that of CyA, leading to lower encapsulation efficiency.

The fabrication of core-shell nanoparticles was also performed at 20^{o}C in order to investigate the effect of dialysis temperature. Similar trend for loading level and encapsulation efficiency was observed, in which 2-fold amount of CyA was encapsulated compared to IMC. However, it should be noted that higher incorporation was achieved at 10^{o}C, for both IMC and CyA. As shown in Figure 4.7, at lower temperatures, the solvent exchange rate was lower, providing more time for the drug to be solubilised into the core of nanoparticles. In contrast, due to the rapid removal of solvent at higher temperatures, the hydrophobic drug precipitated out rather than being incorporated into the nanoparticles.

Table 4.5 Loading level and encapsulation efficiency of indomethacin or cyclosporin A-loaded P(NIPAAm-*co*-DMAAm-*co*-OA) core-shell nanoparticles at 10 and 20°C

Model Drug	**Temperature (°C)**	**Polymer concentration[a] (w/v %)**	**Initial loading (w/w %)**	**Actual loading[b] (w/w %)**	**Encapsulation efficiency[c] (%)**
IMC	10	0.3	25.0	6.1	24.2
	20	0.3	25.0	3.7	14.7
CyA	10	0.3	25.0	11.2	44.8
	20	0.3	25.0	7.3	29.2

[a] 1w/v % = (1 g/100 ml) x 100%.
[b] Calculated using equation (3.2).
[c] Calculated using equation (3.3).

To elucidate the effect of pH on drug incorporation, the dialysis was performed in 0.02 M hydrochloride acid (HCl) and 0.02 M sodium hydroxide (NaOH) solutions, respectively at 10°C. The solubilisation of IMC and CyA occurred during self-assembly of P(NIPAAm-*co*-DMAAm-*co*-OA) core-shell nanoparticles as the alkaline or acidic aqueous solution replaced DMF. As expected, higher loading level and encapsulation efficiency were acquired as the pH of the dialysis medium decreased. This correlation is demonstrated in Figure 4.31. In highly basic environment, the carboxylic acid group of oleic acid was fully ionised. Hence, the increase of hydrophilicity of the oleic acid segment enhanced the solubility of the amphiphilic polymer in NaOH solution. As a result, only a small amount of core-shell nanoparticles was formed, leading to a drastic drop in drug incorporation. Nonetheless, the effect was more crucial when IMC was chosen as the model drug. The amount of IMC encapsulated decreased by ca. 96% when dialysed in NaOH solution. However, the incorporated CyA was only decreased by ca. 57% under similar conditions. This difference was due to the ionisation of the carboxylic acid group of IMC. Hence, a large quantity of IMC dissolved in NaOH solution rather than solubilised into the hydrophobic core of the nanoparticles.

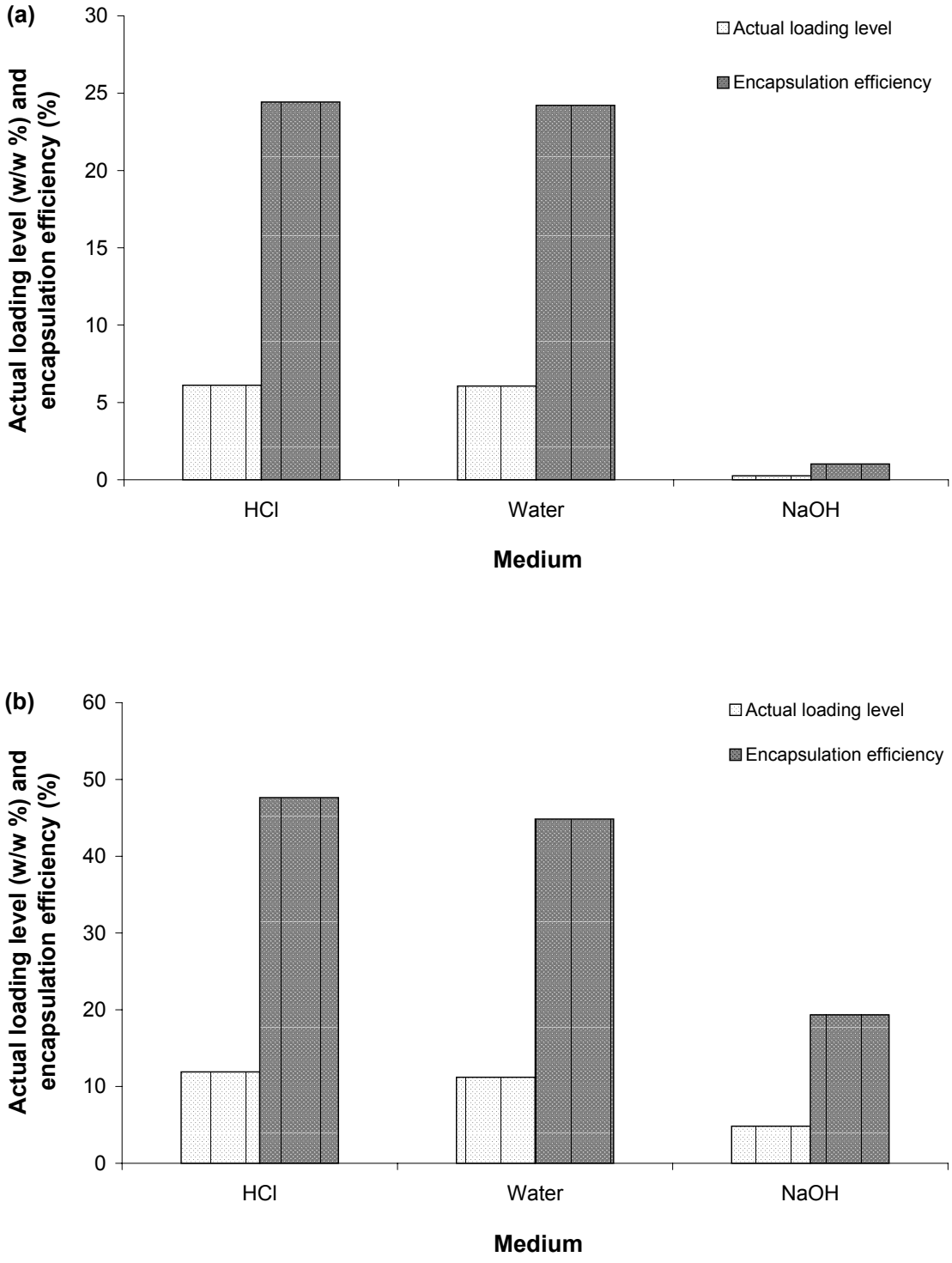

Figure 4.31 Actual loading level and encapsulation efficiency of (a) indomethacin and (b) cyclosporin A in P(NIPAAm-*co*-DMAAm-*co*-OA) core-shell nanoparticles at different dialysis medium (fabrication temperature: 10^{o}C)

4.2.9 Influence of initial drug loading on drug encapsulation

The influence of initial loading of indomethacin on drug encapsulation was studied at 10^{o}C. Drug incorporation was performed by varying the amount of IMC fed. As demonstrated in Figure 4.32, an increase in initial loading from 25 to 67 w/w % led to an increase in encapsulation efficiency until a maximum value was reached. At higher initial loadings, there were a greater number of drug molecules available for entrapment into the nanoparticles. The entrapment of drug molecules made the core more flexible, resulting in greater encapsulation efficiency. However, there was only a small variation of encapsulation efficiency with wide range of initial drug loadings (ca. 25 to 50 w/w %). This could be attributed to the decrease in nanoparticle recovery (ca. 35.5 to 20 w/w %), which would lead to drug loss. When initial drug loading was increased to 57 w/w %, the encapsulation efficiency started to show a decreasing value. This indicated that there was a higher amount of IMC not incorporated into the nanoparticles (high drug wastage of ca. 70%) during the preparation process. Besides having a limited hydrophobic core, another reason for the decreasing drug entrapment with increasing initial drug loadings could be the low yield of nanoparticles. The nanoparticles recovery decreased sharply to 6-7 w/w % as the initial loading increased beyond 50 w/w %. A similar phenomenon was also observed by Kohori et al. (2002) for loading of adriamycin into poly(*N*-isopropylacrylamide-*co*-dimethylacrylamide)-*b*-poly(D,L-lactide) nanoparticles.

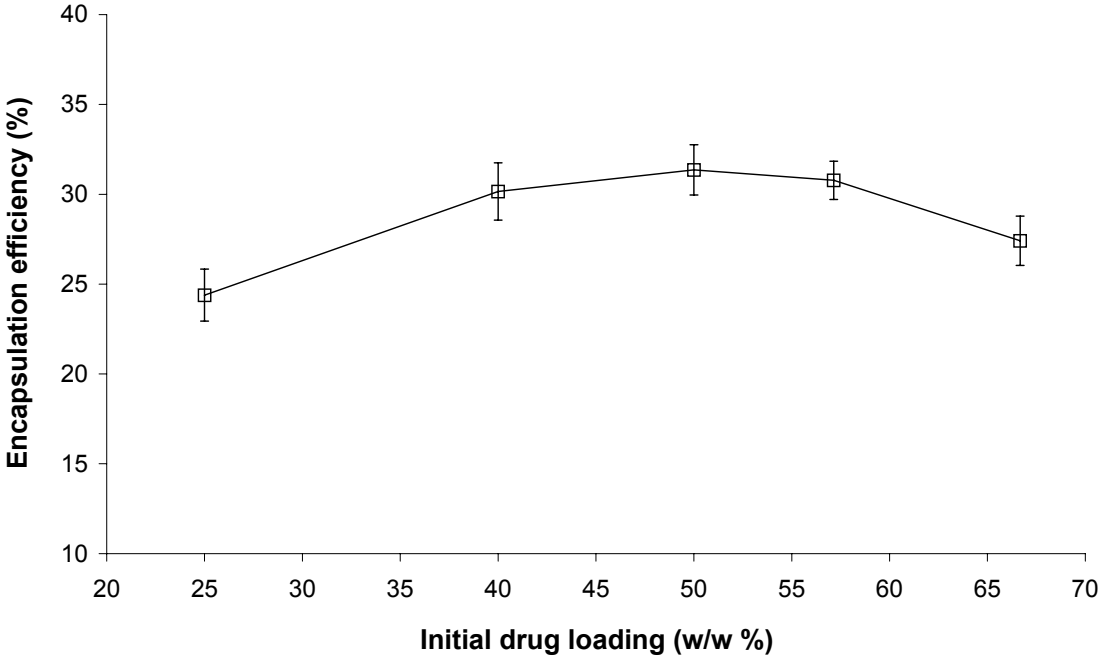

Figure 4.32 Encapsulation efficiency of IMC in P(NIPAAm-*co*-DMAAm-*co*-OA) core-shell nanoparticles at different initial drug loadings (fabrication temperature: 10^{o}C)

4.2.10 Thermo-responsive inner core deformation

Fluorescence spectroscopy using pyrene as a fluorescence probe was used to investigate the changes in the polarity and rigidity of the hydrophobic microdomains of core-shell nanoparticles. The intensity ratio (I_1/I_3) from pyrene emission spectra was monitored as a function of temperature above the critical association concentration (CAC). As described in previous paragraphs, a larger ratio indicates the higher polarity microenvironment around the pyrene probe. Pure PNIPAAm solutions showed an abrupt decrease in polarity when the temperature was raised through its LCST, indicating the transfer of pyrene into the precipitated polymer-rich phase (Chung et al., 1997). In contrast, P(NIPAAm-*co*-DMAAm-*co*-OA) nanoparticles demonstrated an increase in polarity when heated above the LCST, as shown in Figure 4.33. The changes in polarity were also observed in various pH buffer solutions. Figure 4.34 (a), (b), (c) and (d) illustrates micropolarity changes as a function of temperature for

P(NIPAAm-*co*-DMAAm-*co*-OA) in pH 4.0, 6.0, 7.4 and 9.0 buffers, respectively. The nanoparticles showed a low and constant micropolarity below the LCST, regardless of the solvent used. Around the LCST, there was only a slight increase in polarity due to the collapse of shell. However, continuously heating to temperatures above the LCST caused a great rise in polarity around pyrene. Aggregation of collapsed PNIPAAm outer shells induced structural deformation of nanoparticles. This allowed pyrene to be exposed to the aqueous phase, resulting in an increase of pyrene polarity.

In addition, the reversibility of the thermo-responsive nanoparticles was also examined by heating and cooling the solutions through the LCST (Figures 4.33 and 4.34). The pyrene polarity reduced to its initial level when the solutions were cooled to temperatures below the LCST, inferring that the deformed structure recovered back to the original structure upon rehydration of PNIPAAm chains. However, there was a small hysteresis around the LCST, which could be attributed to the delayed hydration of PNIPAAm chains upon cooling (Chung et al., 1997; Chung et al., 1999).

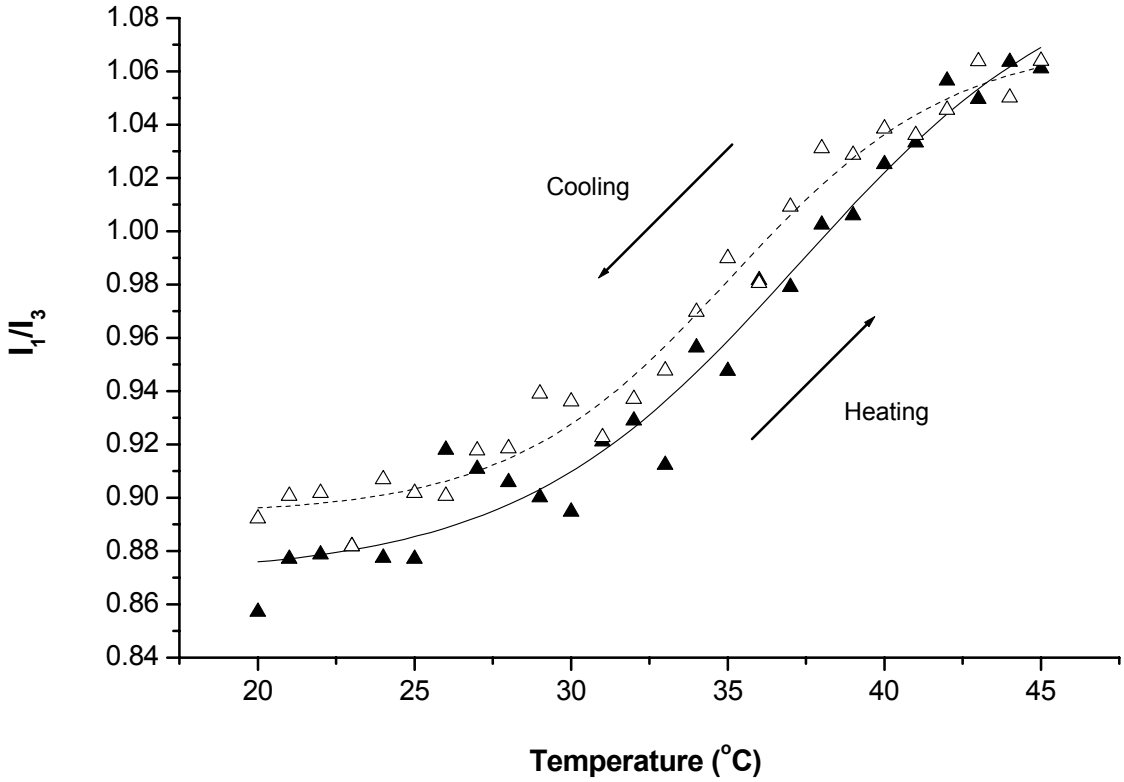

Figure 4.33 Plots of the ratio of intensities (I_1/I_3) of the vibrational bands in the pyrene fluorescence spectrum as a function of temperature for P(NIPAAm-*co*-DMAAm-*co*-OA) in water, λ_{ex} = 339 nm, [pyrene] = 6.17 x 10^{-7} M, 1°C/min, [polymer] = 1 g/L

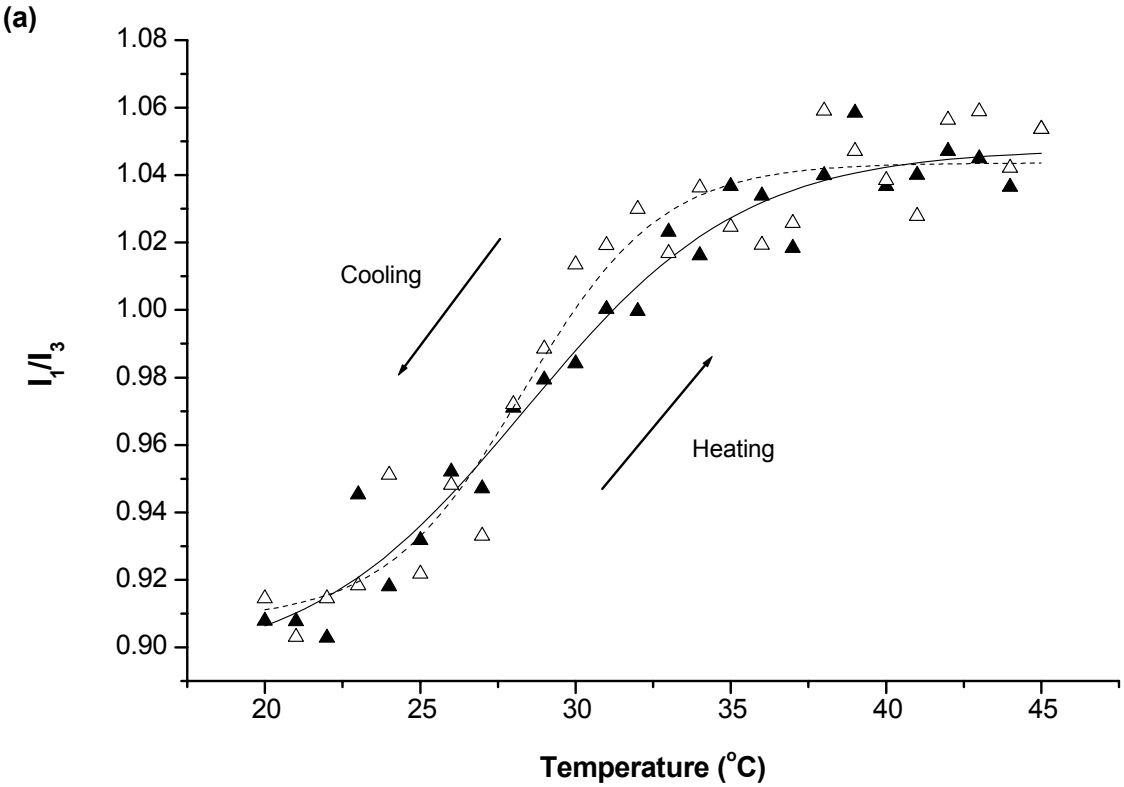

(b)

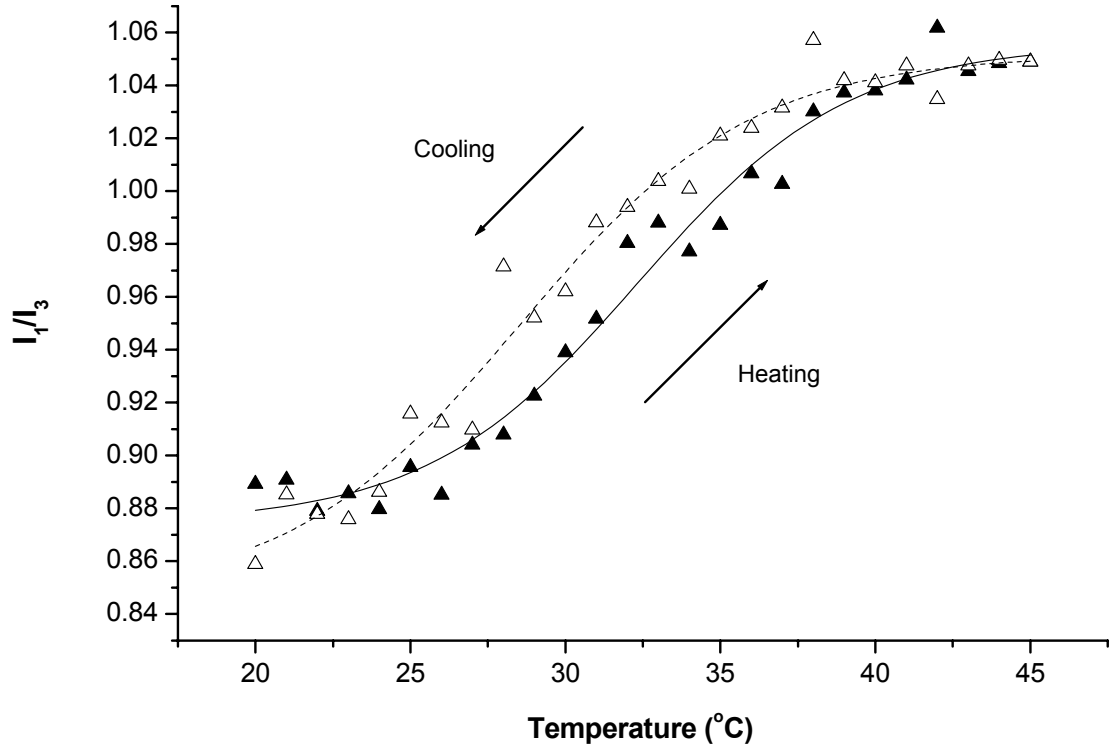
1.06
1.04
1.02
1.00
0.98
0.96
0.94
0.92
0.90
0.88
0.86
0.84
I_1/I_3
Cooling
Heating
20
25
30
35
40
45
Temperature (°C)

(c)

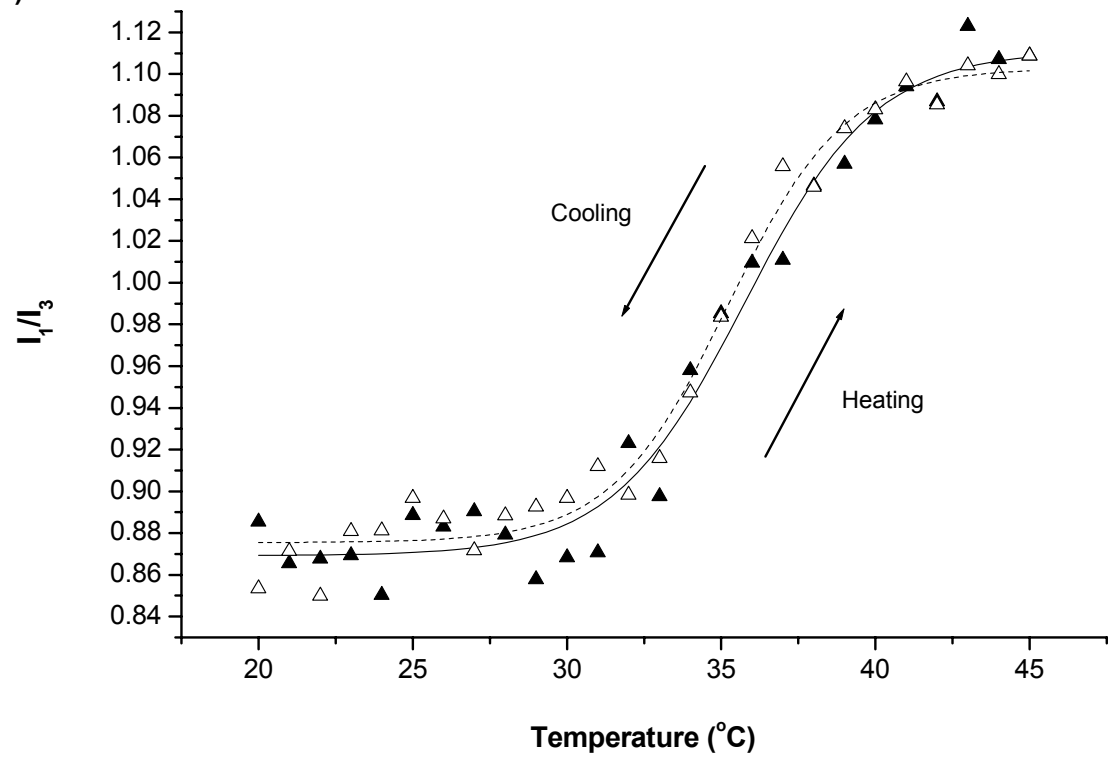
1.12
1.10
1.08
1.06
1.04
1.02
1.00
0.98
0.96
0.94
0.92
0.90
0.88
0.86
0.84
I_1/I_3
Cooling
Heating
20
25
30
35
40
45
Temperature (°C)

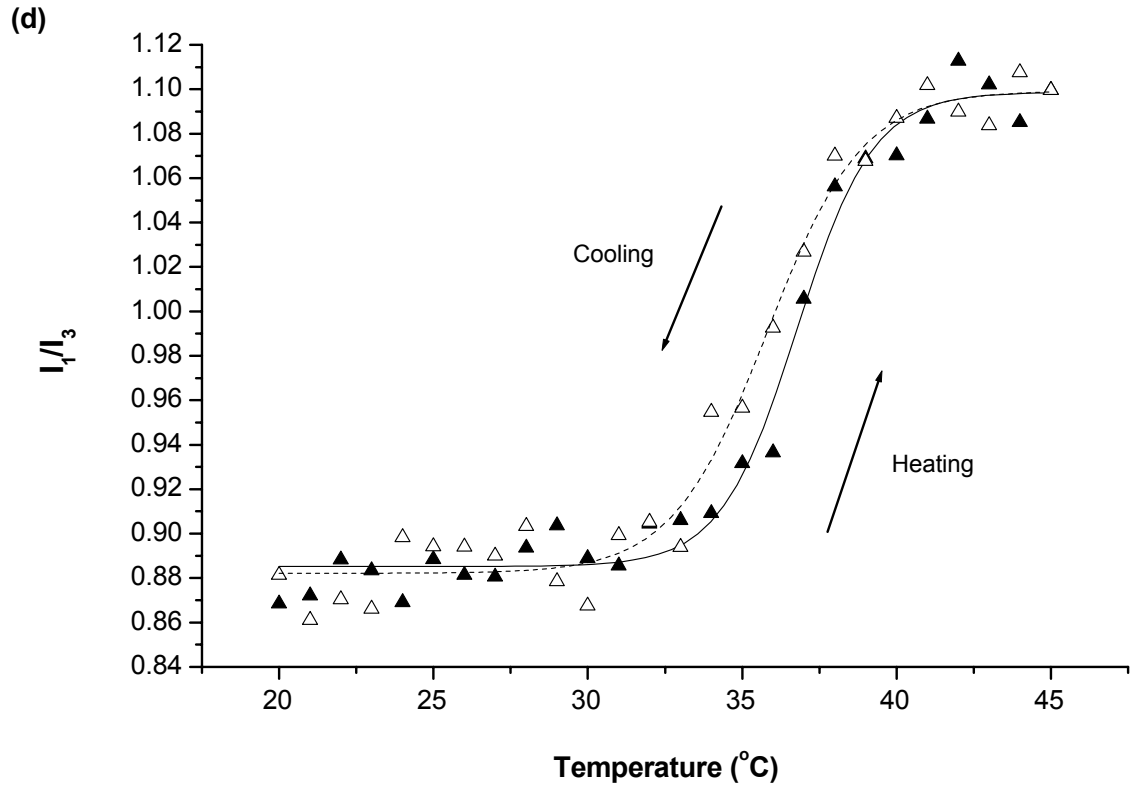

Figure 4.34 Plots of the ratio of intensities (I_1/I_3) of the vibrational bands in the pyrene fluorescence spectrum as a function of temperature for P(NIPAAm-*co*-DMAAm-*co*-OA) in (a) pH 4.0 (b) pH 6.0 (c) pH 7.4 and (d) pH 9.0 buffers, λ_{ex} = 339 nm, [pyrene] = 6.17 x 10^{-7} M, 1°C/min, [polymer] = 1 g/L

Changes in the ratio of intensities (I_1/I_3) of the vibrational bands in the pyrene fluorescence spectrum for P(NIPAAm-*co*-DMAAm-*co*-OA) as a function of temperature were plotted in Figure 4.35 for easy comparison. At 31°C, the nanoparticles were stable at pH 7.4 and 9.0 but deformed at pH 4.0 and 6.0. This unique property can be utilised for intracellular drug delivery because the pH is around 5-6 in endosomes.

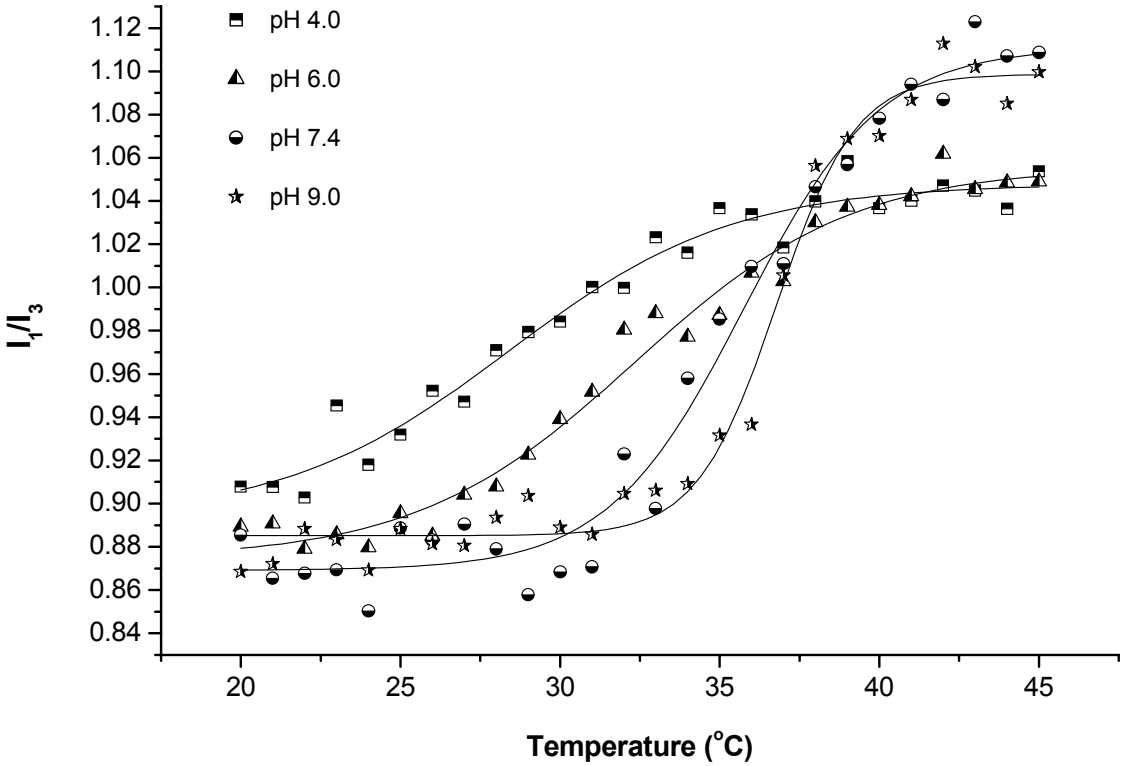

Figure 4.35 Influence of pH on the intensity ratio (I_1/I_3) of the vibrational bands in the pyrene fluorescence spectrum as a function of temperature for P(NIPAAm-*co*-DMAAm-*co*-OA), λ_{ex} = 339 nm, [pyrene] = 6.17 x 10^{-7} M, 1°C/min, [polymer] = 1 g/L

4.2.11 Stability of core-shell nanoparticles in the presence of serum proteins

Nanoparticles for intravenous administration are one of the approaches to the site-specific delivery of drugs. Plasma protein adsorption is regarded as a key factor for the distribution of intravenously administered drug carriers and strongly depends on their surface characteristics (e.g. surface hydrophobicity or charge) (Gessner et al., 2002). Therefore, the aim in this study was to evaluate the stability of P(NIPAAm-*co*-DMAAm-*co*-OA) core-shell nanoparticles in the presence of bovine serum albumin (BSA) and fetal bovine serum (FBS). Ten percent of BSA and FBS were chosen because these are the maximum possible concentration that can be found in the body. Two methods were chosen to determine the stability of the nanoparticles after incubation in BSA and FBS, including the size distribution and LCST measurements.

By using dynamic light scattering, the size distribution of the nanoparticles was measured as a function of time, in the presence of BSA and FBS. As illustrated in Figure 4.36 (i), BSA showed a bimodal size distribution with 78.0% of smaller particles (ca. 10 nm) and 22.0% of larger particles (180-220 nm). The same pattern was observed for the blank nanoparticles. However, the majority of the particles were in the range of 150-200 nm. After one-hour incubation, the size distribution for particles in the presence of BSA demonstrated a bimodal pattern with 78.0% of smaller particles (ca. 10 nm) and 22.0% of larger particles (180-220 nm). The content of larger particles decreased significantly probably because of dissociation of core-shell nanoparticles in the presence of BSA. It continuously decreased as a function of incubation time.

(i)

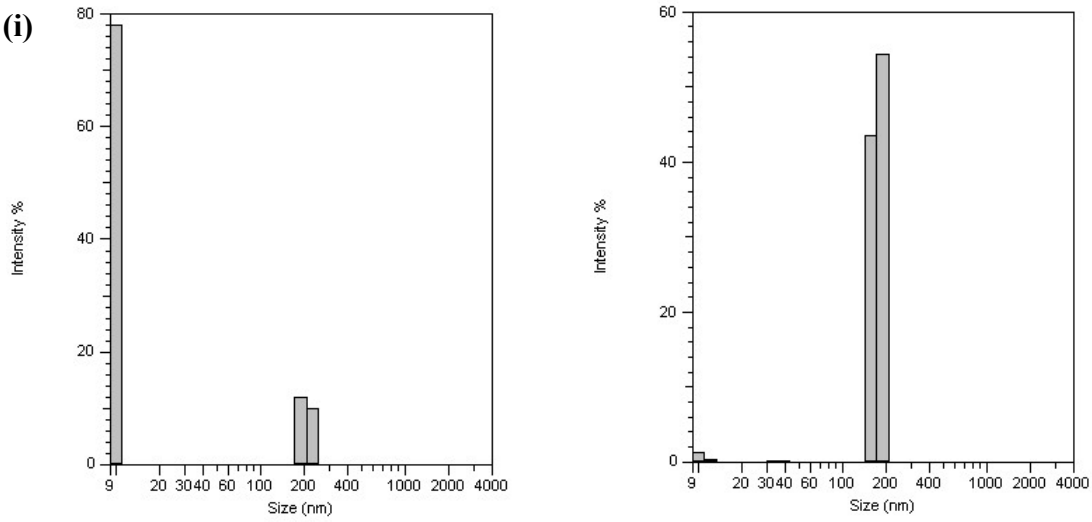

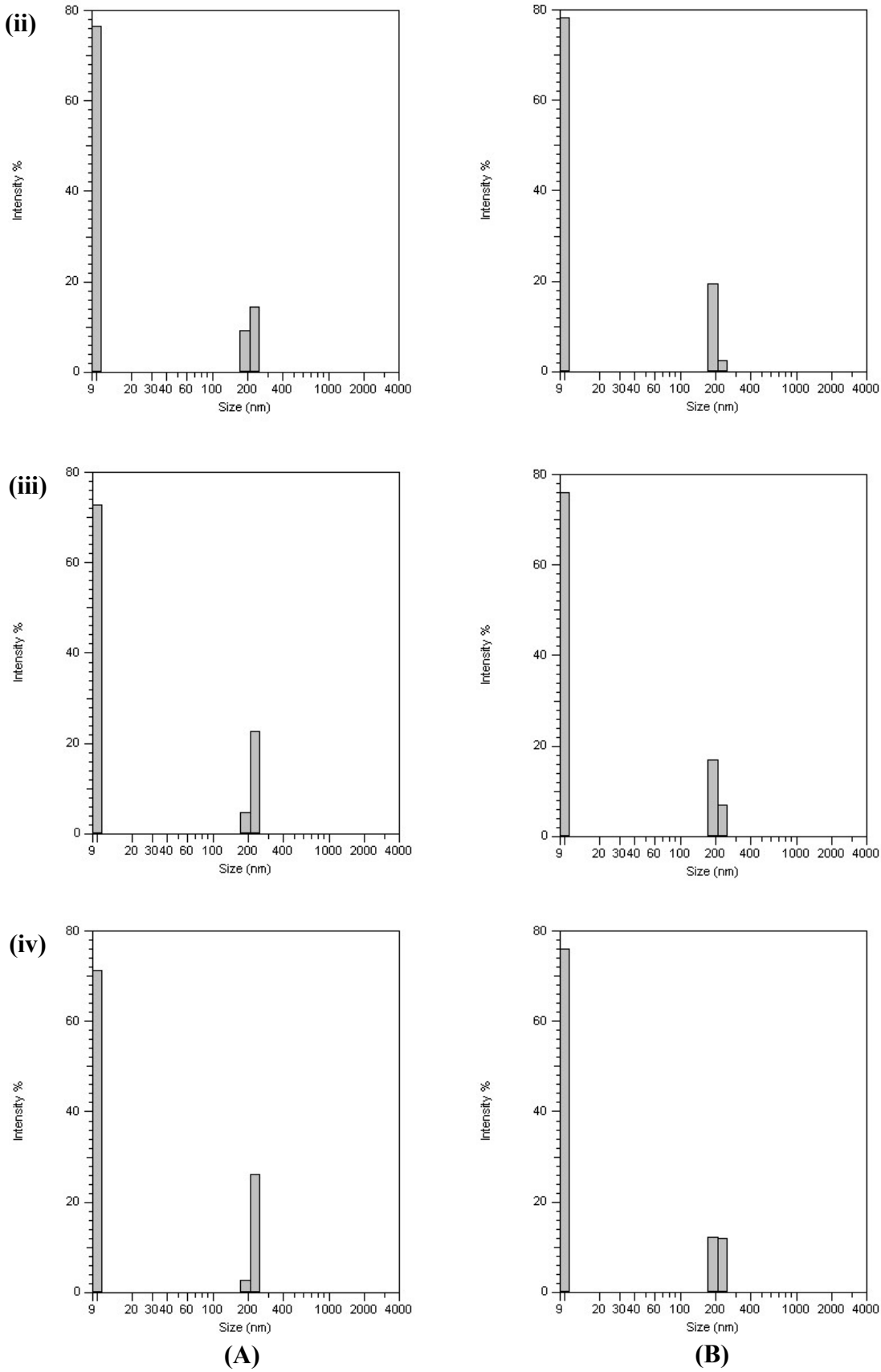

Figure 4.36 Size distribution profiles of (A) bovine serum albumin (BSA) and (B) core-shell nanoparticles in presence of BSA at (i) 0 hr (ii) 1 hr (iii) 6 hrs and (iv) 24 hrs by dynamic light scattering at 20^{o}C

Figure 4.37 demonstrated the size distribution of FBS and the nanoparticles in the presence of FBS. Both FBS and blank nanoparticles showed a unimodal size distribution. FBS was observed to form larger aggregates as the incubation time was prolonged. The aggregates were also found for the nanoparticles in the presence of FBS. Then, because of further aggregation, the mean size increased. However, after six-hour incubation in FBS, although larger aggregates were formed with a longer incubation time, the amount of them decreased significantly (Figure 4.37 (B) (iii and iv)). Smaller particles (ca. 60-100 nm and 400-700 nm) that was not observed previously in the size distribution, started to appear, possibly indicating the dissociation of some of the core-shell nanoparticles.

(i)

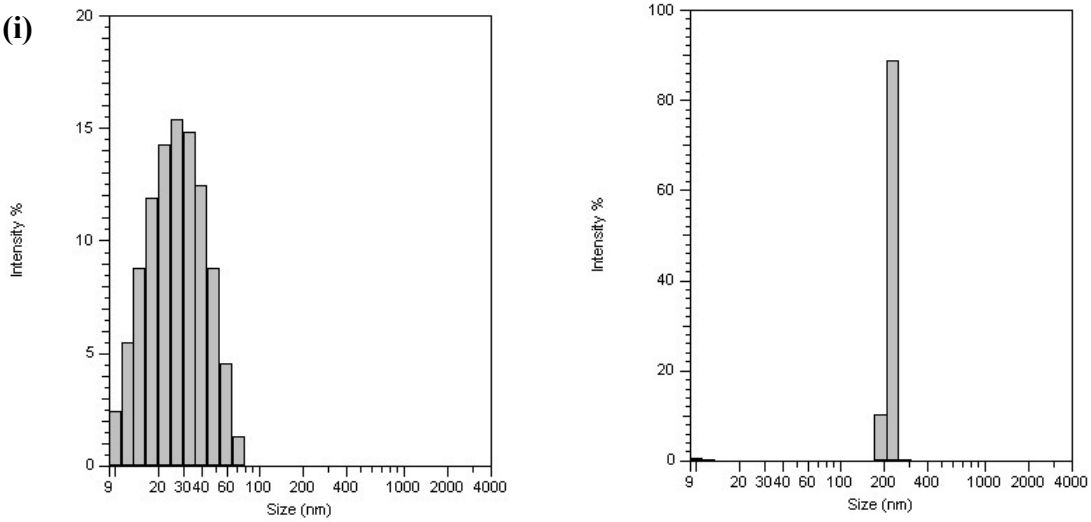

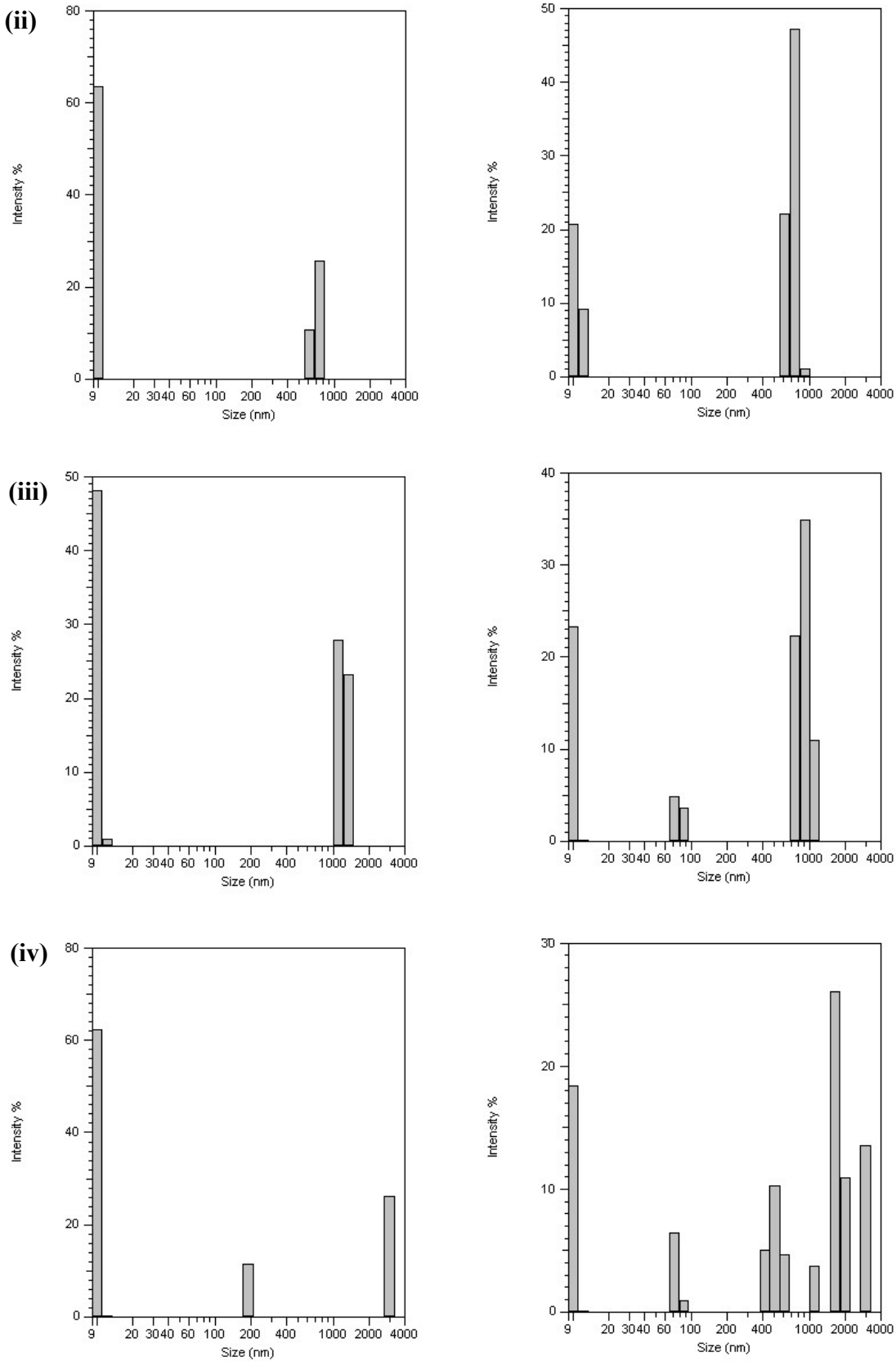

Figure 4.37 Size distribution profiles of (a) fetal bovine serum (FBS) and (b) core-shell nanoparticles in the presence of FBS at (i) 0 hr (ii) 1 hr (iii) 6 hrs and (iv) 24 hrs by dynamic light scattering at 20^{o}C

Based on the above results, it seems that the dynamic light scattering measurement is not a suitable method to determine protein adsorption because both BSA and FBS tend to aggregate. Therefore, the stability of the nanoparticles was further investigated by measuring the LCST in presence of BSA and FBS since such interactions can alter the LCST of the particles. Table 4.6 showed that the LCST was only changed by less than 2^{o}C upon the addition of BSA and FBS, except for pH 11.0. However, under physiological condition (pH 7.4), BSA and FBS only lowered the LCST by 0.8 and 0.2^{o}C, respectively. This insignificant change proved that there were weak interactions between the protein and the particles.

Table 4.6 The LCST values of P(NIPAAm-*co*-DMAAm-*co*-OA) nanoparticles (polymer concentration: 5 g/L, heating rate: 0.1^{o}C/min)

	LCST[b] (^{o}C)		
Medium (pH value)[a]	**Medium**	**Medium + 10% BSA**	**Medium + 10% FBS**
4.0	27.2	25.4	26.6
6.0	28.8	26.9	27.4
7.4	32.0	31.1	31.8
9.0	33.5	32.5	33.0
11.0	35.2	32.3	32.7

[a] Ionic strength is 0.18 M.
[b] Determined at 500 nm.

4.2.12 Physical state of the hydrophobic core and encapsulated drug

The physical state of the hydrophobic core of nanoparticles has a great influence on the rate of drug release (Allen et al., 1999a). The relative fluidity of the core was studied by measuring the glass transition temperature (T_g) of the polymer and nanoparticles using modulated differential scanning calorimetry (MDSC) (Burt et al., 1999). As shown in Figure 4.38, the T_g of polymer and nanoparticles were 130.6 and 128.4^{o}C, respectively, indicating that the nanoparticles were in a glassy state at room

temperature. The lower glass transition temperature of nanoparticles was due to the plasticisation of water molecules in the core. This phenomenon was also observed for the micelles system developed from methoxy-ended PEG-*b*-PDLLA (Yamamoto et al., 2002). Further decrease in T_g was observed when the hydrophobic drugs were incorporated into the nanoparticles (Table 4.7). The molecularly dispersed drug within the core was acting as a plasticiser and thus, lowered the glass transition temperature of the nanoparticles. The higher the drug loading level, the greater was the T_g decrease.

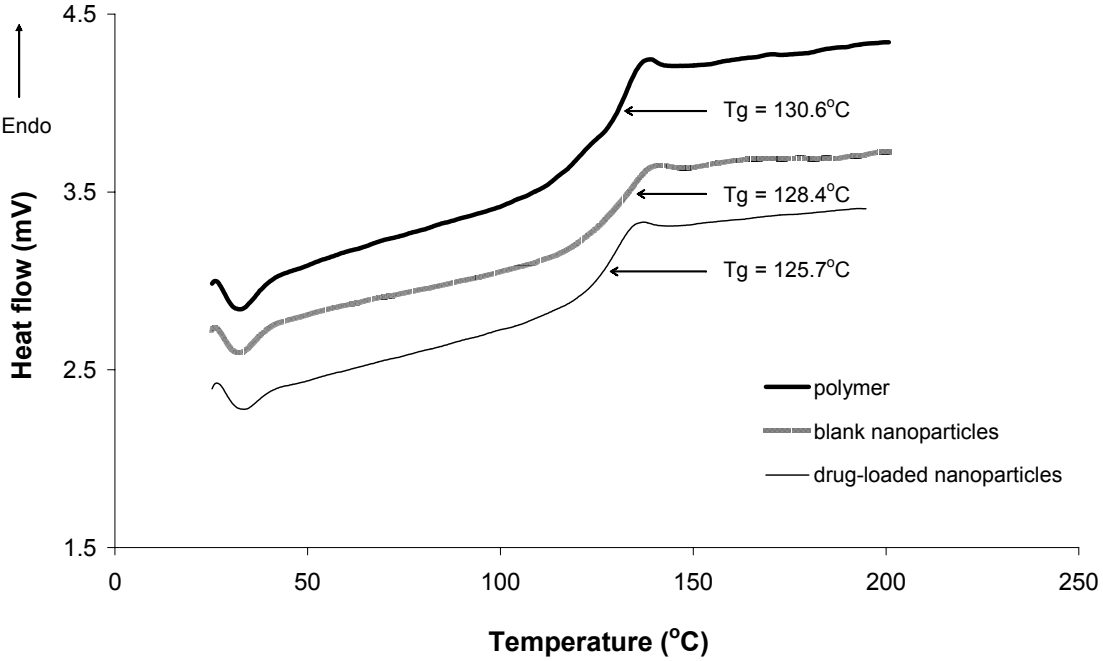

Figure 4.38 DSC thermograms of P(NIPAAm-*co*-DMAAm-*co*-OA) polymer and core-shell nanoparticles

Table 4.7 Effect of loading level on glass transition temperature of P(NIPAAm-*co*-DMAAm-*co*-OA) core-shell nanoparticles containing IMC

Initial loading (w/w %)	**Actual loading level[a] (w/w %)**	**T_g[b] (°C)**
25.0	6.1	125.7
50.0	15.6	117.9
66.7	18.3	118.0

[a] Calculated using equation (3.2).
[b] Glass transition temperature measured by MDSC.

Besides the physical state of the core, the physical state of incorporated drugs can also have a significant effect on the release kinetics since they can either exist as a crystal or disperse molecularly inside the core (Allen et al., 1999a). Figure 4.39 shows a sharp melting peak of indomethacin (IMC) at 161.8^{o}C, signifying that IMC is a crystal at room temperature. However, no melting peak was observed when IMC was incorporated into the nanoparticles. This result indicated that IMC was molecularly dispersed within the core. Similar finding was observed for CyA (Figure 4.40). Naked CyA showed a melting peak at 127.5^{o}C. After incorporated into the nanoparticles, the melting peak disappeared.

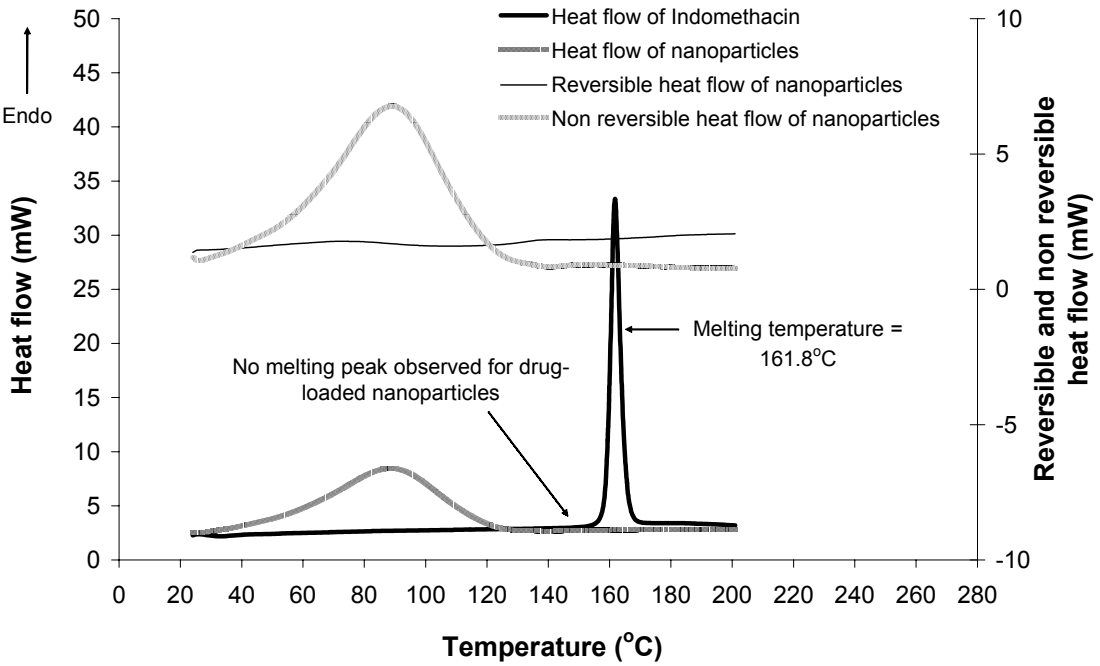

Figure 4.39 DSC thermograms of P(NIPAAm-*co*-DMAAm-*co*-OA) polymer and IMC-loaded P(NIPAAm-*co*-DMAAm-*co*-OA) core-shell nanoparticles (actual drug loading: 6.1 w/w %)

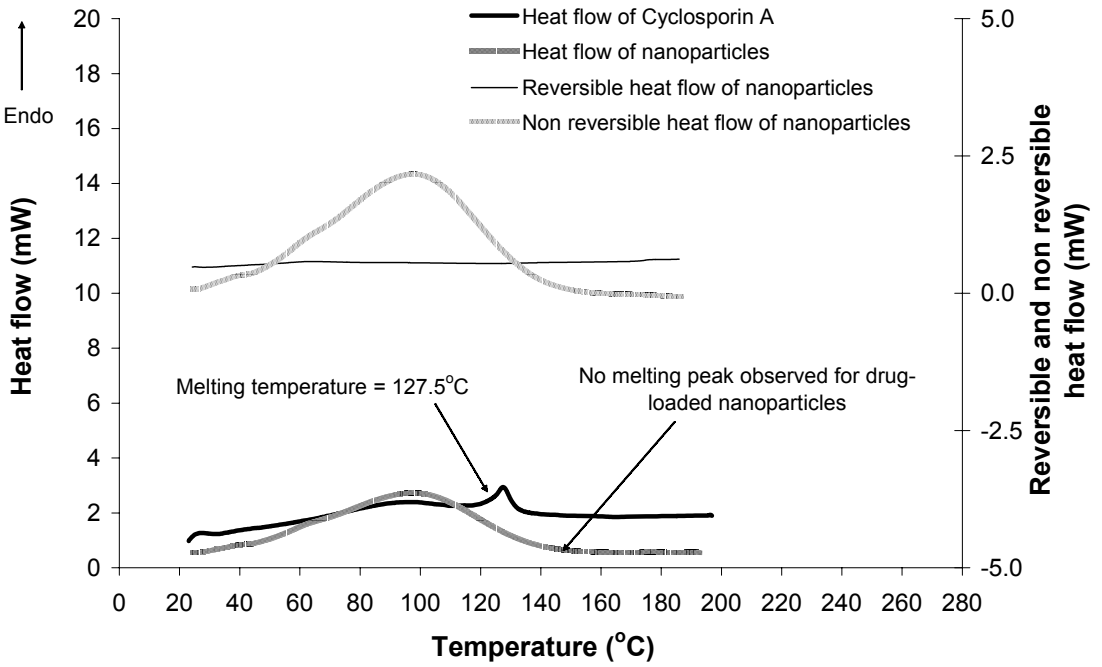

Figure 4.40 DSC thermograms of P(NIPAAm-*co*-DMAAm-*co*-OA) polymer and CyA-loaded P(NIPAAm-*co*-DMAAm-*co*-OA) core-shell nanoparticles (actual drug loading: 11.2 w/w %)

Nonetheless, when the actual loading of IMC was increased to 18.3 w/w %, two crystalline peaks (158.4 and 164.8°C) were observed in the DSC thermogram of nanoparticles (Figure 4.41), indicating the drug existed as crystals in the core. This result was supported by studies done by Gref et al. (1994) and Jeong et al. (1998).

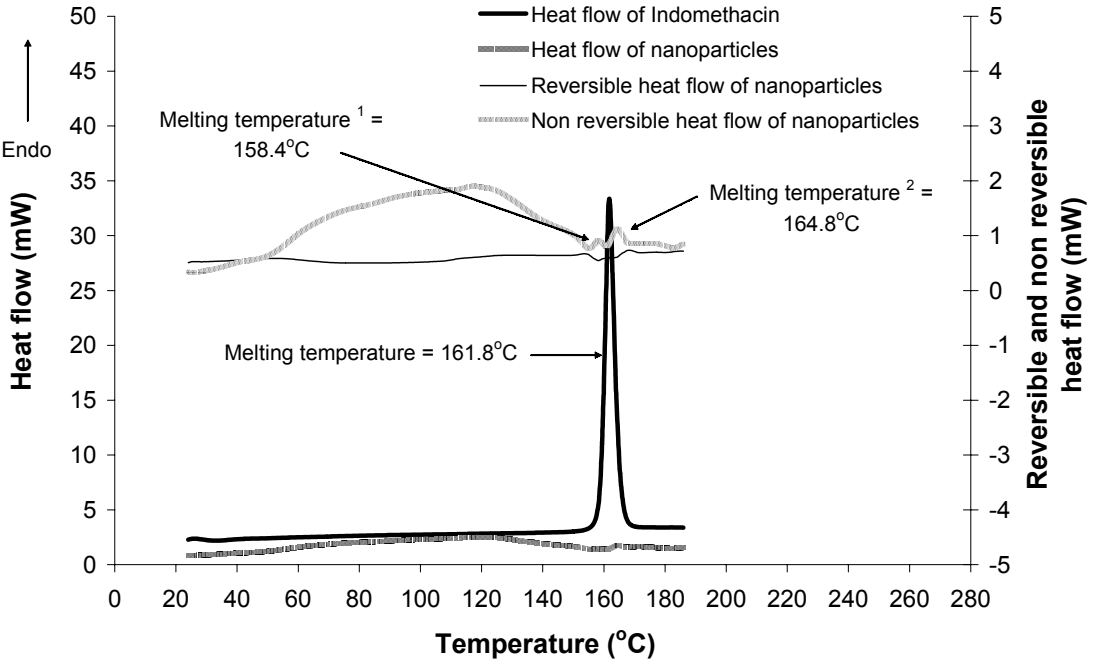

Figure 4.41 DSC thermograms of P(NIPAAm-*co*-DMAAm-*co*-OA) polymer and IMC-loaded core-shell P(NIPAAm-*co*-DMAAm-*co*-OA) nanoparticles (actual drug loading: 18.3 w/w %)

4.2.13 Drug release study

The *in vitro* release kinetics of indomethacin (IMC) and cyclosporin A (CyA) from the nanoparticles was investigated. Figure 4.42 shows the release profiles of IMC at 37 and 20°C. IMC release was accelerated upon heating through the LCST, while the release was suppressed below the LCST. This was demonstrated in the release for the first 10 mins, where the amount of IMC released at 37°C was ca. 40 w/w %, which was 2-fold higher than that at 20°C. The accelerated IMC release was in correlation with temperature-induced inner core structural deformation sensed by pyrene, as reported in previous paragraph. However, despite having a stable structure below the LCST, the particles were shown to exhibit an initial burst (ca. 60 w/w %) after an hour release. This is probably because of high water solubility of IMC in PBS (pH 7.4) and flexible core of nanoparticles.

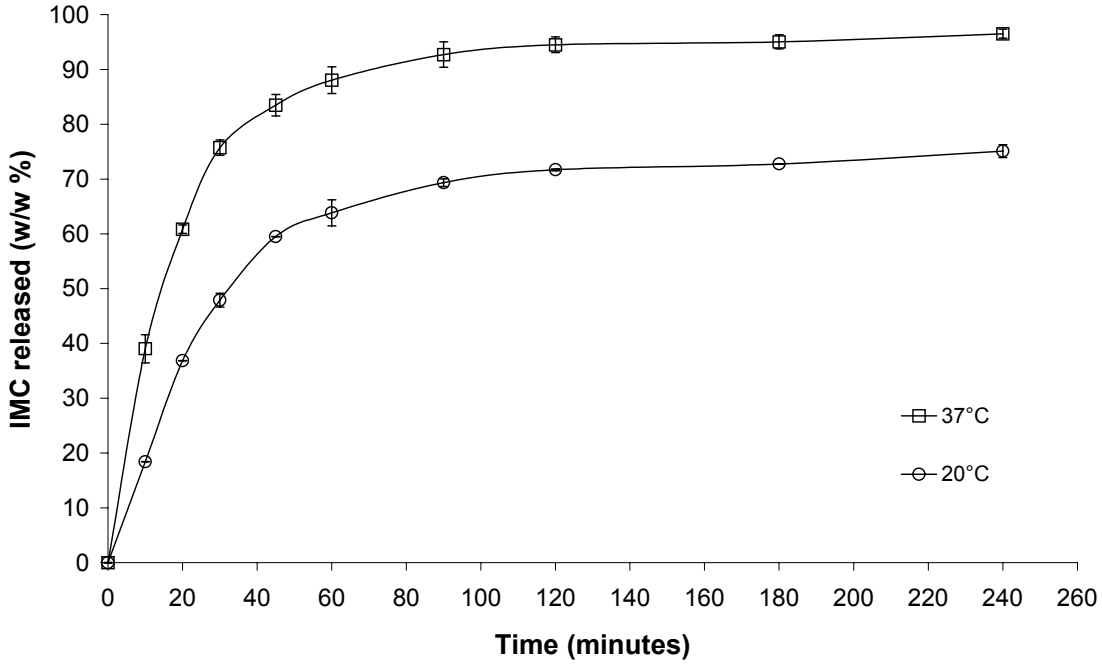

Figure 4.42 Release of IMC from P(NIPAAm-*co*-DMAAm-*co*-OA) core-shell nanoparticles in PBS (pH 7.4) at 37 and 20^{o}C (actual drug loading: 6.1 w/w %)

Figure 4.43 shows the release profiles of CyA from the nanoparticles at 20 and 37^{o}C. Compared to IMC, CyA release was slower and more sustained probably because of its lower water-solubility and more stable core stemming from better compatibility between CyA and the core. A higher amount of CyA was released at 20^{o}C than at 37^{o}C. This could be ascribed to the unusual solubility behaviour of CyA in aqueous media. The solubility of CyA was found to be inversely proportional to temperature (Augustijns et al. 2000; Ismailos et al., 1991; Loosli et al., 1985). The higher the temperature, the lower is the solubility. Hence, at 37^{o}C, upon the burst release of CyA from the deformed nanoparticles, CyA immediately precipitated. On the contrary, at the lower temperature, CyA slowly diffused out from the nanoparticles but only in a small amount because of the stable structure of the core.

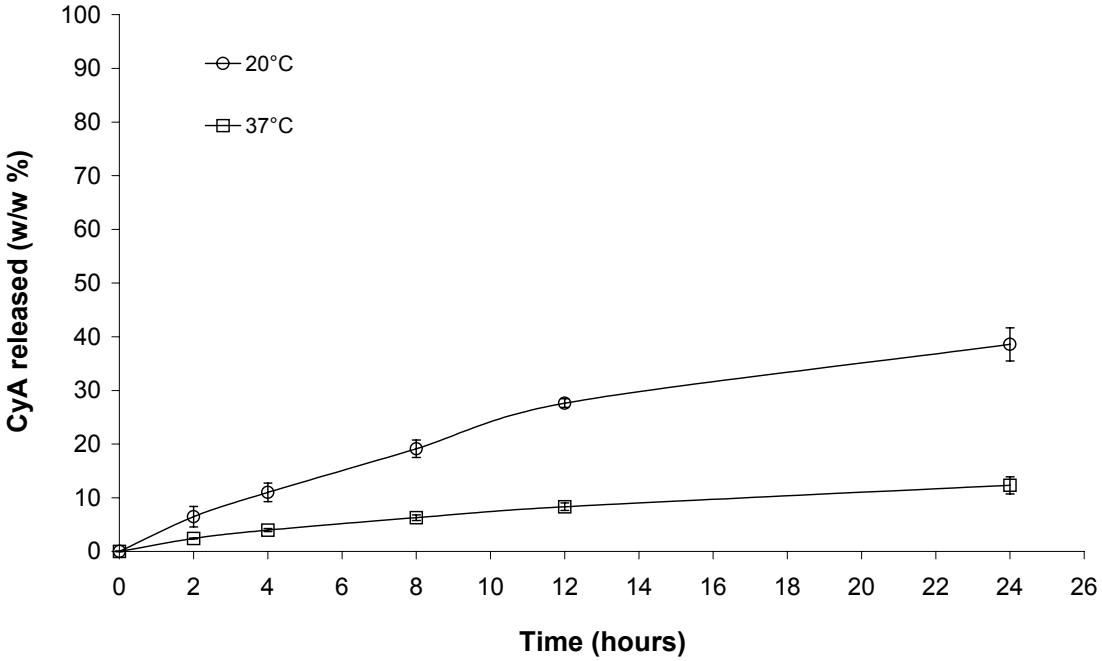

Figure 4.43 Release of CyA from P(NIPAAm-*co*-DMAAm-*co*-OA) core-shell nanoparticles in PBS (pH 7.4) at 37 and 20^{o}C (actual drug loading: 11.2 w/w %)

The release kinetics of IMC and CyA was further studied at different pH. Figure 4.44 illustrates the release profiles of IMC at pH 9 and pH 6. The results revealed that the release of IMC was higher in the basic environment. Similar results were obtained in studies done by La et al. (1996). Under the basic condition (pH 9), the carboxylic acid group (pK_a = 4.5) of IMC and oleic acid core were ionised, causing both of them to interact more favourably with water. As a result, the fluidity of the inner core increased and the hydrophobic interactions between the drug and core was reduced, thus accelerated the diffusion of IMC out of the ionised core. Conversely, the release was lower in acidic condition despite having deformed nanoparticles (Figure 4.44). The low ionisation degree of IMC in pH 6 was expected to produce low drug dissolution, which was 5-fold lower than in pH 9 (Table 4.4). Hence, upon the burst release of IMC from the deformed nanoparticles, a portion of IMC precipitated and the rest diffused out into the release medium.

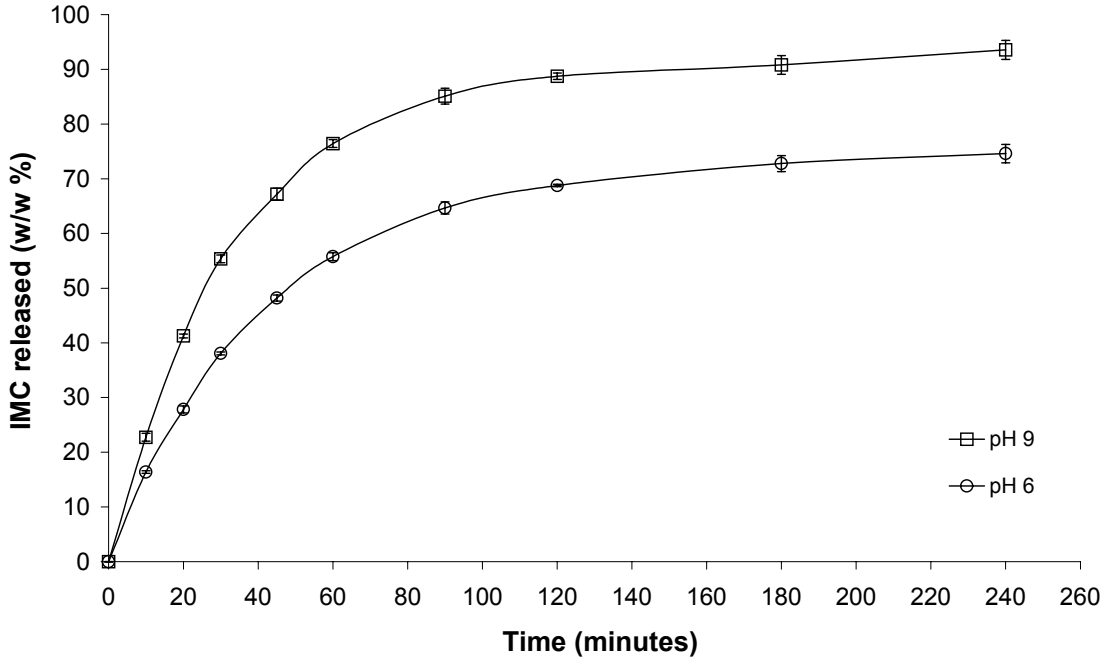

Figure 4.44 Release of IMC from P(NIPAAm-*co*-DMAAm-*co*-OA) core-shell nanoparticles at 31°C at pH 9 and pH 6 (ionic strength: 0.18 M, actual drug loading: 6.1 w/w %)

Ismailos et al. (1991) reported that the solubility of CyA was not affected by pH. As shown in Figure 4.45, the difference in CyA release between 20°C and 37°C was not significant because of the low water solubility of CyA. Since the LCST of the nanoparticles at pH 6 was lower than 31°C, the structure of nanoparticles was deformed upon putting into the *in vitro* medium. Subsequently, it precipitated after released from the core because of its low solubility, promoting aggregation between the nanoparticles and thus reducing surface area for CyA dissolution.

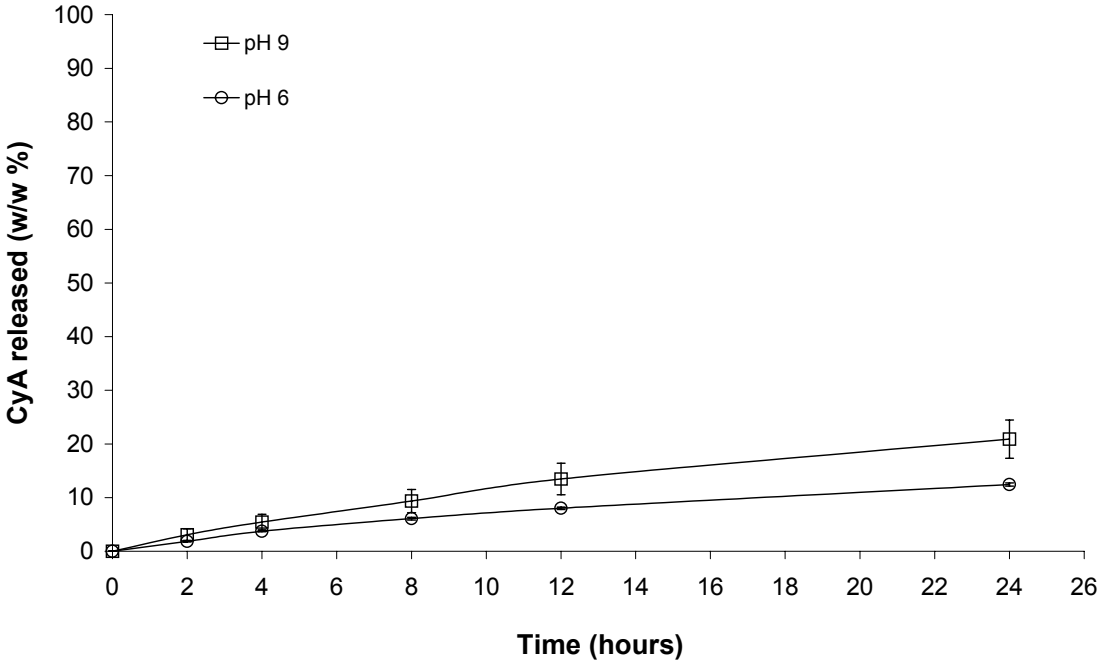

Figure 4.45 Release of CyA from P(NIPAAm-*co*-DMAAm-*co*-OA) core-shell nanoparticles at 31°C at pH 9 and pH 6 (ionic strength: 0.18 M, actual drug loading: 11.2 w/w %)

4.2.14 Influence of drug loading content on release behaviours

The effect of loading content on drug release kinetics was also explored by performing the *in vitro* release of IMC from nanoparticles with actual loading levels of 6.6 w/w % and 18.3 w/w %. As shown in Figure 4.46, an increase in drug loading level resulted in a slower release of IMC. This finding was consistent with the results of other researchers (Na et al., 2000; Gref et al., 1994; Jeong et al., 1998; Kim et al., 1999; Nah et al., 1998; Kim et al., 1998). It is possibly due to the physical state of the drug in the nanoparticles. As reported in previous paragraphs, IMC existed as crystals at the high loading level. The crystalline phase is inaccessible to water, resulting in slower IMC release.

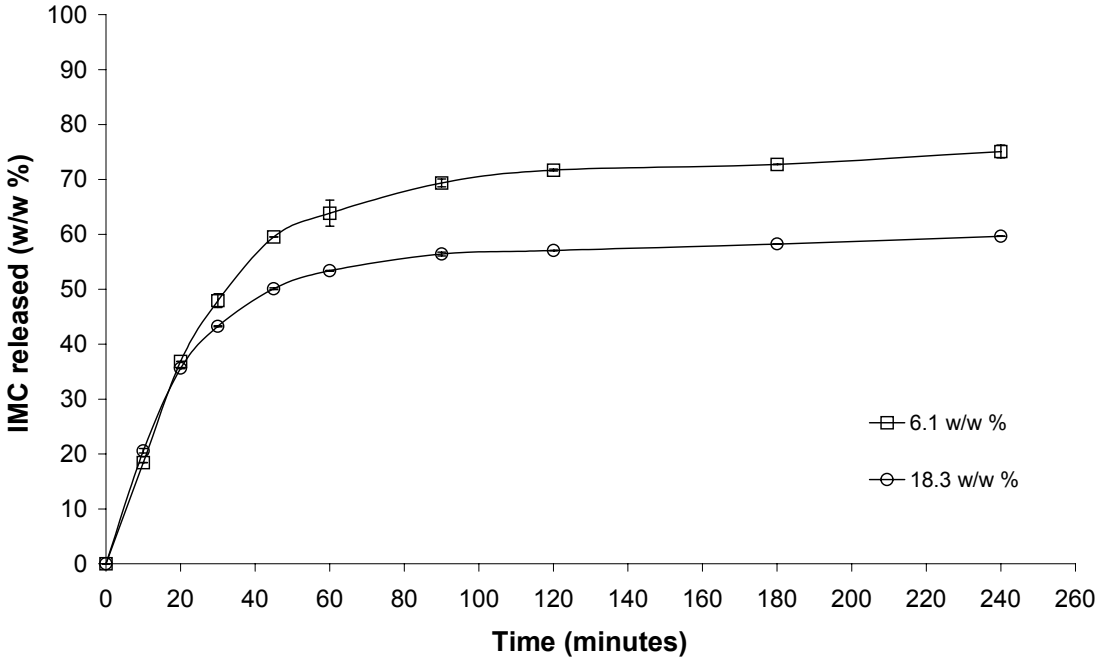

Figure 4.46 Release of IMC from P(NIPAAm-*co*-DMAAm-*co*-OA) core-shell nanoparticles with different drug loading levels in PBS (pH 7.4) at 20°C

CHAPTER 5 CONCLUSIONS AND RECOMMENDATIONS

5.1 Conclusions

Temperature-sensitive core-shell nanoparticles

A new type of thermally responsive core-shell nanoparticles were successfully formed using cholesteryl end-capped P(NIPAAm-*co*-DMAAm) polymer. The core-shell nanoparticles were spherical and had a size of less than 100 nm in diameter. The amphiphilic polymer possessed a low CAC value, which was 20 mg/L. The CAC value was reduced in PBS. The LCST value of core-shell nanoparticles was lower in PBS (pH 7.4) than that in ultra pure water. The presence of serum albumin further reduced the LCST value. This core-shell nanoparticles system provided great capacity for loading of hydrophobic drug. Although there were a number of factors that influence drug encapsulation efficiency, drug precipitation was the dominant factor. Drug precipitation caused by rapid solvent removal at high temperatures and high initial drug contents led to low drug encapsulation efficiency. However, low fabrication temperature yielded a longer swollen phase, resulting in better drug entrapment. It was demonstrated that CyA release from the cholesteryl end-capped P(NIPAAm-*co*-DMAAm) core-shell nanoparticles was faster at a temperature below the LCST. The core-shell nanoparticles system developed would make an important carrier for targeted delivery of hydrophobic drugs.

Temperature/pH-sensitive core-shell nanoparticles

Novel temperature and pH responsive core-shell nanoparticles, which can solubilise poorly water-soluble drugs, were successfully synthesised using P(NIPAAm-*co*-

DMAAm-*co*-OA). The nanoparticles had a small size (less than 200 nm), low CAC (64 mg/L in water) and a good stability in the presence of serum proteins. The nanoparticles demonstrated reversibility of thermoresponsive aggregation/dispersion and deformation/reformation of structure in heating/cooling thermal cycles through the LCST. The drug entrapment efficiencies were shown to be dependent on temperature, pH and initial drug loading. The release behaviours of IMC and CyA from the nanoparticles were affected by pH, temperature and drug loading. The IMC-loaded nanoparticles exhibited rapid release while the CyA-loaded nanoparticles showed significant slow and sustained release characteristics. The release rate of IMC was increased by increasing pH and temperature but decreased in higher drug loading levels. On the other hand, higher CyA release rate was obtained at a lower temperature. The physical state of the drug and core had a great influence on the release behaviour of drugs from the nanoparticles. These nanoparticles have shown potential for drug targeting in both passive and active manner, enhancing site-specific drug accumulation and release induced by external pH and temperature stimuli.

In conclusion, a new type of stimuli-sensitive core-shell nanoparticles based on thermally responsive cholesteryl end-capped poly(*N*-isopropylacrylamide-*co*-*N,N*-dimethylacrylamide), as well as pH and thermally responsive poly(*N*-isopropylacrylamide-*co*-*N,N*-dimethylacrylamide-*co*-oleic acid) amphiphilic polymers were successfully designed and utilised to encapsulate cyclosporin A (CyA) and/or indomethacin (IMC). Coupling with the EPR effect, the thermally and/or pH responsive core-shell nanoparticles systems may provide a good approach to targeting drugs to tumour and inflamed tissues.

5.2 Recommendations

The ultimate goal of drug delivery systems capable of releasing hydrophobic drugs in response to temperature and/or pH is to provide higher drug release at low pH and high temperatures above the LCST, since tumours, inflamed tissues or endosomal compartments are often associated with lower pH and/or higher temperatures than normal tissues. Therefore, suitable drugs, whose water solubility is not sensitive to temperature and pH, should be chosen to study drug release kinetics.

It is of primary importance to determine the core radius of the core-shell nanoparticles, viscosity of the inner core, and changes of pyrene fluorescence lifetimes with temperature to provide more detailed information on the effects of pH, polymer concentration and core-forming blocks on drug entrapment and release kinetics, physical state of the inner core, and the actual location of pyrene when the temperature is altered.

Finally, it is also of interest to determine the cytotoxicity and biocompatibility of the polymers, plasma clearance and biodistribution of the core-shell nanoparticles, and the stability of the core-shell nanoparticles in physiological saline solutions.

REFERENCES

Adam, M.L. and G.S. Kwon. Relative Aggregation State and Hemolytic Activity of Amphotericin B Encapsulated by Poly(ethylene oxide)-*Block*-Poly(*N*-hexyl-L-aspartamide)-Acyl Conjugate Micelles: Effects of Acryl Chain Length, Journal of Controlled Release, *87*, pp. 23-32. 2003.

Alberts, B., D. Bray, J. Lewis, M. Raff, K. Roberts and J.D. Watson. (ed). Molecular Biology of the Cell. New York: Garland Publishing Incorporation. 1989.

Alexandridis, P., J.F. Holzwarth and T. A. Hatton. Micellization of Poly(ethylene oxide)-poly(propylene oxide)-poly(ethylene oxide) Triblock Copolymers in Aqueous, Macromolecules, *27*, pp. 2414-2425. 1994.

Allen, C., D. Maysinger and A. Eisenberg. Nano-Engineering Block Copolymer Aggregates for Drug Delivery, Colloids and Surfaces B: Biointerfaces, *16*, pp. 3-27. 1999a.

Allen, C., J. Han, Y. Yu, D. Maysinger and A. Eisenberg. Polycaprolactone-*b*-Poly(ethylene oxide) Copolymer Micelles as a Delivery Vehicle for Dihydrotestosterone, Journal of Controlled Release, *63*, pp. 275-286. 2000.

Allen, C., Y. Yu, A. Eisenberg and D. Maysinger. Cellular Internalization of PCL_{20}-*b*-PEO_{44} Block Copolymer Micelles, Biochimica et Biophysica Acta, *1421*, pp. 32-38. 1999b.

Allen, T.M. Interactions of Liposomes and Other Drug Carriers with the Mononuclear Phagocyte System. In Liposomes as Drug Carriers, ed by G. Gregoriadis, pp. 37-50. Toronto: John Wiley and Sons. 1988.

Alonso, M.J. Drug and the Pharmaceutical Sciences. In Microparticulate Systems for the Delivery of Proteins and Vaccines, Vol. 77, ed by S. Cohen and H. Bernstein, pp. 203-242. New York: Marcel Dekker Incorporation. 1996.

Astafieva, I., K. Khougaz and A. Eisenberg. Micellization in Block Polyelectrolyte Solutions. 2. Fluorescence Study of the Critical Micelle Concentration as a Function of Soluble Block Length and Salt Concentration, Macromolecules, *28*, pp. 7127-7134. 1995.

Astafieva, I., X.F. Zhong and A. Eisenberg. Critical Micellization Phenomenon in Block Polyelectrolyte Solutions, Macromolecules, *26*, pp. 7339-7352. 1993.

Audus, K.L. Targeted Drug Delivery. In Handbook of Experimental Pharmacology, Vol. 100, ed by R.L. Juliano. New York: Springer-Verlag. 1991.

Augustijns, P.F., S.C. Brown, D.H. Willard, T.G. Consler, P.P. Annaert, R.W. Hendren and T.P. Bradshaw. Hydration Changes Implicated in the Remarkable Temperature-Dependent Membrane Permeation of Cyclosporin A, Biochemistry, *39*, pp. 7621-7630. 2000.

Bader, H., H. Ringsdorf and B. Schmidt. Water Soluble Polymers in Medicine, Angewandte Makromolekulare Chemie, *123/124*, pp. 457-485. 1984.

Bahadur, P., N.V. Sastry and Y.K. Rao. Interaction Studies of Styrene-Ethylene Oxide Block Copolymers with Ionic Surfactants in Aqueous Solutions, Colloids and Surfaces, *29*, pp. 343-358. 1988.

Benoit, J.P., F. Courteille and C. Thies. A Physiochemical Study of the Morphology of Progesterone-Loaded Poly(D,L-lactide) Microspheres, International Journal of Pharmaceutics, *29*, pp. 95-102. 1986.

Benrebouh, A., D. Avoce and X.X. Zhu. Thermo- and pH- Sensitive Polymers Containing Cholic Acid Derivatives, Polymer, *42*, pp. 1471-1479. 2001.

Berti, D., P.L. Luisi and P. Baglioni. Molecular Recognition in Supramolecular Structures Formed by Phosphatidylnucleosides-Based Amphiphiles, Colloids and Surfaces A: Physicochemical and Engineering Aspects, *167*, pp. 95-103. 2000.

Brannon-Peppas, L. Polymers in Controlled Drug Delivery, Medical Plastics and Biomaterials, pp. 34. 1997.

Brannon-Peppas, L. Recent Advances on the Use of Biodegradable Microparticles and Nanoparticles in Controlled Drug Delivery, International Journal of Pharmaceutics, *116*, pp. 1-9. 1995.

Burt, H.M., X. Zhang, P. Toleikis, L. Embree and W.L. Hunter. Development of Copolymers of Poly(D,L-lactide) and Methoxypolyethylene Glycol as Micellar Carriers of Paclitaxel, Colloids and Surfaces B: Biointerfaces, *16*, pp. 161-171. 1999.

Cammas, S., K. Suzuki, C. Sone, Y. Sakurai, K. Kataoka and T. Okano. Thermo-Responsive Polymer Nanoparticles with a Core-Shell Micelle Structure as Site-Specific Drug Carriers, Journal of Controlled Release, *48*, pp. 157-164. 1997.

Cartier, S., T.A. Horbett and B.D. Ratner. Glucose-Sensitive Membrane Coated Porous Filters for Control of Hydraulic Permeability and Insulin Delivery from a Pressurized Reservoir, Journal of Membrane Science, *106*, pp. 17-24. 1995.

Cavallaro, G., M. Fresta, G. Giammona, G. Puglish and A. Villari. Entrapment of β-lactams Antibiotics in Polyethylcyanoacrylate Nanoparticles: Studies on the Possible *In Vivo* Application of this Colloidal Delivery System, International Journal of Pharmaceutics, *111*, pp. 31-41. 1994.

Chilkoti, A., M.R. Dreher, D.E. Meyer and D. Raucher. Targeted Drug Delivery by Thermally Responsive Polymers, Advanced Drug Delivery Reviews, *54*, pp. 613-630. 2002.

Chiu, H.C., A.T. Wu and Y.F. Lin. Synthesis and Characterization of Acrylic Acid-Containing Dextran Hydrogels, Polymer, *42*, pp. 1471-1479. 2001.

Cho, C.S., M.Y. Chang, H.C. Lee, S.C. Song, M. Goto and T. Akaike. Release of Dehydroepiandrosterone from Nanoparticles Composed of Poly(L-lactic acid) and Poly(ethylene oxide) Diblock Copolymer Endcapped With Sugar Moiety, Proceeding of International Symposium on Controlled Release of Bioactive Materials, *25*, pp. 721-722. 1998.

Christova, D., R. Velichkova, W. Loos, E.J. Goethals and F.D. Prez. New Thermo-Responsive Polymer Materials Based on Poly(2-ethyl-2-oxazoline) Segments, Polymer, *44*, pp. 2255-2261. 2003.

Chung, J.E., M. Yokoyama, K. Suzuki, T. Aoyagi, Y. Sakurai and T. Okano. Reversibly Thermo-Responsive Alkyl-Terminated Poly(*N*-isopropylacrylamide) Core-Shell Micellar Structures, Colloids and Surfaces B: Biointerfaces, *9*, pp. 37-48. 1997.

Chung, J.E., M. Yokoyama, M. Yamato, T. Aoyagi, Y. Sakurai and T. Okano. Thermo-Responsive Drug Delivery from Polymeric Micelles Constructed Using Block Copolymers of Poly(*N*-isopropylacrylamide) and Poly(butylmethacrylate), Journal of Controlled Release, *62*, pp. 115-127. 1999.

Chung, J.E., M. Yokoyama, T. Aoyagi, Y. Sakurai and T. Okano. Effect of Molecular Architecture of Hydrophobically Modified Poly(*N*-isopropylacrylamide) on the

Formation of Thermoresponsive Core-Shell Micellar Drug Carriers, Journal of Controlled Release, *53*, pp. 119-130. 1998.

Chung, J.E., M. Yokoyama and T. Okano. Inner Core Segment Design for Drug Delivery Control of Thermo-Responsive Polymeric Micelles, Journal of Controlled Release, *65*, pp. 93-103. 2000.

Cowie, J.M.G. (ed). Polymers: Chemistry and Physics of Modern Materials. New York: Blackie Academic and Professional. 1994.

Creutz, S., J. van Stam, F. C. De Schryver and R. Jerome. Dynamics of Poly((dimethylamino)alkyl methacrylate-*block*-sodium methacrylate) Micelles. Influence of Hydrophobicity and Molecular Architecture on the Exchange Rate of Copolymer Molecules, Macromolecules, *31*, pp. 681-689. 1998.

Dean, J.A. (ed). Lange's Handbook of Chemistry. pp. 104-113, New York: McGraw-Hill. 1999.

Dhara, D. and P.R. Chatterji. Phase Transition in Linear and Cross-Linked Poly(*N*-isopropylacrylamide) in Water: Effect of Various Types of Additives, Journal of Macromolecular Science Reviews in Macromolecular Chemistry and Physics, *40*, pp. 51-68. 2000.

Ding, J. and G. Liu. Water-Soluble Hollow Nanospheres as Potential Drug Carriers, Journal of Physical Chemistry B, *102*, pp. 6107-6113. 1998.

Donbrow, M. (ed). In Vitro Release from Microcapsules and Microspheres. In Microcapsules and Nanoparticles in Medicine and Pharmacy. Boca Raton: CRC Press. 1991.

Dong, D.C. and M.A. Winnik. The Py Scale of Solvent Polarities, Canadian Journal of Chemistry, *62*, pp. 2560-2565. 1984.

Duncan, R. Drug-Polymer Conjugates: Potential for Improved Chemotherapy, Anticancer Drugs, *3*, pp. 175-210. 1992.

Duncan, R. and J. Kopechek. Soluble Synthetic Polymers as Potential Drug Carriers, Advanced Polymer Science, *57*, 51-101. 1984.

Eekman, F., A.J. Moës and K. Amighi. Surfactant Induced Drug Delivery Based on the Use of Thermosensitive Polymers, Journal of Controlled Release, *88*, pp. 105-116. 2003.

Ehrlich, P. Collected Studies on Immunity. pp. 441, New York: John Wiley. 1906.

Eisenberg, S.R. and A.J. Grodzinsky. Electrically Modulated Membranes Permeability, Journal of Membrane Science, *19*, pp. 173-194. 1984.

Evans, D.F., G. Pye, R. Bramley, A.G. Clark, T.J. Dyson and J.D. Hardcastle. Measurement of Gastrointestinal pH Profiles in Normal Ambulant Human Subjects, Gut, *29*, pp. 1035-1041. 1988.

Feil, H., Y.H. Bae, J. Feijen and S.W. Kim. Effect of Comonomer Hydrophilicity and Ionization on the Lower Critical Solution Temperature of *N*-Isopropylacrylamide Copolymers, Macromolecules, *26*, pp. 2496-2500. 1993.

Fukushima, S., M. Machida, T. Akutsu, K. Shimizu, S. Tanaka, K. Okamoto, H. Mashiba, M. Yokoyama, T. Okano, Y. Sakurai and K. Kataoka. Roles of Adriamycin and Adriamycin Dimer in Antitumor Activity of the Polymeric Micelle Carrier System, Colloids and Surfaces B: Biointerfaces, *16*, pp. 227-236. 1999.

Gabizon, A.A. Liposome Circulation Time and Tumor Targeting: Implications for Cancer Chemotherapy, Advanced Drug Delivery Reviews, *16*, pp. 285-294. 1995.

Gadelle, F., W.J. Koros and R.S. Schechter. Solubilization of Aromatic Solutes in Block Copolymers, Macromolecules, *28*, pp. 4883 – 4892. 1995.

Gautier, S., M. Boustta and M. Vert. Alkylated Poly(L-lysine citramide) as Models to Investigate the Ability of Amphiphilic Macromolecular Drug Carriers to Physically Entrap Lipophilic Compounds in Aqueous Media, Journal of Controlled Release, *60*, pp. 235-247. 1999.

General, S. and A.F. Thünemann. pH-Sensitive Nanoparticles of Poly(amino acid) Dodecanoate Complexes, International Journal of Pharmaceutics, *230*, pp. 11-24. 2001.

Gerasimov, O.V., J.A. Boomer, M.M. Qualls and D.H. Thompson. Cytosolic Drug Delivery Using pH and Light-Sensitive Liposomes, Advanced Drug Delivery Review, *38*, pp. 317-338. 1999.

Gessner, A., A. Lieske, B.R. Paulke and R.H. Müller. Influence of Surface Charge Density on Protein Adsorption on Polymeric Nanoparticles: Analysis by Two-Dimensional Electrophoresis, European Journal of Pharmaceutics and Biopharmaceutics, *54*, pp. 165-170. 2002.

Goodby, J.M. Liquid Crystals and Life, Liquid Crystals, *24*, pp. 25-38. 1998.

Govender, T., T. Riley, T. Ehtezazi, M.C. Garnett, S. Stolnik, L. Illum and S.S. Davis. Defining the Drug Incorporation Properties of PLA-PEG Nanoparticles, International Journal of Pharmaceutics, *199*, pp. 95-110. 2000.

Govender, T., S. Stolnik, C. Xiong, S. Zhang, L. Illum and S.S. Davis. Drug-Polyionic Block Copolymer Interactions for Micelle Formation: Physicochemical Characterisation, Journal of Controlled Release, *75*, pp. 249-258. 2001.

Gref, R., Y. Minamitake, M.T. Peracchia, V. Trubetskoy, V. Torchilin and R. Langer. Biodegradable Long-Circulating Polymeric Nanospheres, Science, *263*, pp. 1600-1603. 1994.

Ha, J.C., S.Y. Kim and Y.M. Lee. Poly(ethylene oxide)-Poly(propylene oxide)-Poly(ethylene oxide) (Pluronic)/Poly(ε-caprolactone) (PCL) Amphiphilic Block Copolymeric Nanospheres I. Preparation and Characterization, Journal of Controlled Release, *62*, pp. 381-392. 1999.

Han, S.K., K. Na and Y.H. Bae. Sulfonamide Based pH-Sensitive Polymeric Micelles: Physicochemical Characteristics and pH-Dependent Aggregation, Colloids and Surfaces A: Physicochemical and Engineering Aspects, *214*, pp. 49-59. 2003.

Harada, A. and K. Kataoka. Novel Polyion Complex Micelles Entrapping Enzyme Molecules in the Core. 2. Characterization of the Micelles Prepared at Non-Stoichiometric Mixing Ratios, Langmuir, *15*, pp. 4208-4212. 1999.

Harada, A. and K. Kataoka. Novel Polyion Complex Micelles Entrapping Enzyme Molecules in the Core. Preparation of Narrowly-Distributed Micelles from Lysozyme and Poly(ethylene glycol)-Poly(aspartic acid) Block Copolymer in Aqueous Medium, Macromolecules, *31*, pp. 288-294. 1998.

Harada, A. and K. Kataoka. Pronounced Activity of Enzymes Through the Incorporation into the Core of Polyion Complex Micelles Made from Charged Block Copolymers, Journal of Controlled Release, *72*, pp. 85-91. 2001.

Helmlinger, G., F. Huan, M. Dellian and R.K. Jain. Interstitial pH and pO_2 Gradients in Solid Tumors in Vivo: High-Resolution Measurements Reveal a Lack of Correlation, Nature Medicine, *3*, pp. 177-182. 1997.

Hruska, Z., M. Piton, A. Yekta, J. Duhamel, M.A. Winnik, G. Riess and M.D. Croucher. Study of Block Copolymer Micelles. 6. Exit and Reentry Kinetics of Bromoacetonaphthone in Aqueous Polystyrene-Poly(ethylene oxide) Block Copolymer Micelles, Macromolecules, 26, pp. 1825-1828. 1993.

Huang, S.K., P.R. Stauffer, K. Hong, J.W.H. Guo, T.L. Phillips, A. Huang and D. Papahadjopoulos. Liposomes and Hyperthermia in Mice: Increased Tumor Uptake and Therapeutic Efficacy of Doxorubicin in Sterically Stabilized Liposomes, Cancer Research, *54*, pp. 2186-2191. 1994.

Husseini, G.A., D.A. Christensen, N.Y. Rapoport and W.G. Pitt. Ultrasonic Release of Doxorubicin from Pluronic P105 Micelles Stabilized with an Interpenetrating Network of *N*,*N*-diethylacrylamide, Journal of Controlled Release, *83*, pp. 303-305. 2002.

Husseini, G.A., R.I. El-Fayoumi, K.L. O'Neill, N.Y. Rapoport and W.G. Pitt. DNA Damage Induced by Micellar-Delivered Doxorubicin and Ultrasound: Comet Assay Study, Cancer Letters, *154*, pp. 211-216. 2000.

Inoue, T., G. Chen, K. Nakamae and A.S. Hoffman. An AB Block Copolymer of Oligo(methyl methacrylate) and Poly(acrylic acid) for Micellar Delivery of Hydrophobic Drugs, Journal of Controlled Release, *51*, pp. 221-229. 1998.

Ismailos, G., C. Reppas, J.B. Dressman and P. Macheras. Unusual Solubility Behaviour of Cyclosporin A in Aqueous Media, Journal of Pharmacy and Pharmacology, *43*, pp. 287-289. 1991.

Jeong, B., Y.H. Bae and S.W. Kim. Biodegradable Thermosensitive Micelles of PEG-PLGA-PEG Triblock Copolymers, Colloids and Surfaces B: Biointerfaces, *16*, pp. 185-193. 1999.

Jeong, J.H. and T.G. Park. Poly(L-lysine)-G-Poly(D,L-lactide-co-glycolic acid) Micelles for Low Cytotoxic Biodegradable Gene Delivery Carriers, Journal of Controlled Release, *82*, pp. 159-166. 2002.

Jeong, Y.I., J.B. Cheon, S.H. Kim, J.W. Nah, Y.M. Lee, Y.K. Sung, T. Akaike and C.S. Cho. Clonazepam Release from Core-Shell Type Nanoparticles in Vitro, Journal of Controlled Release, *51*, pp. 169-178. 1998.

Jones, M.C. and J.C. Leroux. Polymeric Micelles – A New Generation of Colloidal Drug Carriers, European Journal of Pharmaceutics and Biopharmaceutics, *48*, pp. 101-111. 1999.

Junginger, H.E. (ed). Drug Targeting and Delivery: Concepts in Dosage Form. New York: Ellis Horwood, 1992.

Kabanov, A.V., E.V. Batrakova, N.S. Melik-Nubarov, N.A. Fedoseev, T.Y. Dorodnich, V.Y. Alakhov, V.P. Chekhonin, I.R. Nazarova and V.A. Kabanov. A New Class of Drug Carriers: Micelles of Poly(oxyethylene)-Poly(oxypropylene) Block Copolymers as Microcontainers for Drug Targeting from Blood in Brain, Journal of Controlled Release, *22*, pp. 141-158. 1992.

Kabanov, A.V., I.R. Nazarova, I.V. Astafieva, E.V. Batrakova, V.Y. Alakhov, A.A. Yaroslavov and V.A. Kabanov. Micelle Formation and Solubilization of Fluorescent-Probes in Poly(oxyethylene-*b*-oxypropylene-*b*-oxyethylene) Solutions, Macromolecules, *28*, pp. 2303-2314, 1995.

Kabanov, A.V., V.P. Chekhonin, V.Y. Alakhov, E.V. Batrakova, A.S. Lebedev, N.S. Melik-Nubarov, S.A. Arzhakov, A.V. Levashov, G.V. Morozov, E.S. Severin and V.A. Kabanov. The Neuroleptic Activity of Haloperidol Increases After Its Solubilization in Surfactant Micelles: Micelles as Microcontainers for Drug Targeting, FEBS Letters, *258*, pp. 343-345. 1989.

Kabanov, A.V. and V.Y. Alakhov. Micelles of Amphiphilic Block Copolymers as Vehicles for Drug Delivery. In Amphiphilic Block Copolymers: Self-Assembly and Applications, ed by P. Alexandridis and B. Lindman, pp. 347-376. New York: Elsevier. 2000.

Kalyanasundaram, K. and J.K. Thomas. Environmental Effects on Vibronic Band Intensities in Pyrene Monomer Fluorescence and Their Application in Studies of Micellar Systems, Journal of the American Chemical Society, *99*, pp. 2039-2044. 1977.

Kaneko, Y., K. Sakai and T. Okano. Temperature-Responsive Hydrogels as Intelligent Materials. In Biorelated Polymers and Gels, ed by T. Okano, pp. 29-69. New York: Academic Press. 1998.

Kang, S.I. and Y.H. Bae. pH-Induced Volume-Phase Transition by Reversible Crystal Formation, Macromolecules, *34*, pp. 8173-8178. 2001.

Kataoka, K. Design of Nanoscopic Vehicles for Drug Targeting Based on Micellization of Amphiphilic Block Copolymers, Journal Of Macromolecular Science Pure And Applied Chemistry, *11*, pp. 1759-1769. 1994.

Kataoka, K., G.S. Kwon, M. Yokoyama, T. Okano and Y. Sakurai. Block-Copolymer Micelles as Vehicles for Drug Delivery, Journal of Controlled Release, *24*, pp. 119-132. 1993.

Kataoka, K., H. Togawa, A. Harada, K. Yasugi, T. Matsumoto and S. Katayose. Spontaneous Formation of Polyion Complex Micelles with Narrow Distribution from Antisense Oligonucleotide and Cationic Block Copolymer in Physiological Saline, Macromolecules, *29*, pp. 8556-8557, 1996.

Kataoka, K., T. Matsumoto, M. Yokoyama, T. Okano, Y. Sakurai, S. Fukushima, K. Okamoto and G.S. Kwon. Doxorubicin-Loaded Poly(ethylene glycol)-Poly(β-benzyl-L-aspartate) Copolymer Micelles: Their Pharmaceutical Characteristics and Biological Significance, Journal of Controlled Release, *64*, pp. 143-153. 2000.

Katayama, S. and A. Ohata. Reentrant Phase Transition in Acrylamide-Derivative Copolmer Gels, Macromolecules, *18*, pp. 2782-2784. 1985.

Katayose, D. and K. Kataoka. Water Soluble Polyion Complex Associates of DNA and Poly(ethylene glycol)-Poly(L-lysine) Block Copolymer, Bioconjugate Chemistry, *8*, pp. 702-707. 1997.

Katayose, S. and K. Kataoka. PEG-Poly(lysine) Block Copolymer as a Novel Type of Synthetic Gene Vector with Supramolecular Structure. In Advanced Biomaterials in Biomedical Engineering and Drug Delivery Systems, ed by N. Ogata, S.W. Kim, J. Feijen and T. Okano, pp. 319-320. Tokyo: Springer. 1996.

Kathmann, E.E.L., L.A. White and C.A. McCormick. Water-Soluble Polymers. 73. Electrolyte- and pH-Responsive Zwitterionic Copolymers of 4-[(2-Acrylamido-2-methylpropyl)-dimethylammonio]butanoate with 3-[(2-Acrylamido-2-methyl-propyl)dimethylammonio]propanesulfonate, Macromolecules, *30*, pp. 5297-5304. 1997.

Kim, S.Y., J.C. Ha and Y.M. Lee. Poly(ethylene oxide)-Poly(propylene oxide)-Poly(ethylene oxide)/Poly(ε-caprolactone) (PCL) Amphiphilic Block Copolymeric Nanospheres II. Thermo-Responsive Drug Release Behaviours, Journal of Controlled Release, *65*, pp. 345-358. 2000a.

Kim, I.S., Y.I. Jeong, C.S. Cho and S.H. Kim. Core-Shell Type Polymeric Nanoparticles Composed of Poly(L-lactic acid) and Poly(*N*-isopropylacrylamide), International Journal of Pharmaceutics, *211*, pp. 1-8. 2000b.

Kim, I.S., Y.I. Jeong, C.S. Cho and S.H. Kim. Thermo-Responsive Self-assembled Polymeric Micelles for Drug Delivery In Vitro, International Journal of Pharmaceutics, *205*, pp. 165-172. 2000c.

Kim, S.Y., I.G. Shin and Y.M. Lee. Amphiphilic Diblock Copolymeric Nanospheres Composed of Methoxy Poly(ethylene glycol) and Glycolide: Properties, Cytotoxicity and Drug Release Behaviour, Biomaterials, *20*, pp. 1033-1042. 1999.

Kim, S.Y., I.G. Shin, Y.M. Lee, C.S. Cho and Y.K. Sung. Methoxy Poly(ethylene glycol) and ϵ-caprolactone Amphiphilic Block Copolymeric Micelle Containing Indomethacin II. Micelle Formation and Drug Release Behaviours, Journal of Controlled Release, *51*, pp. 13-22. 1998.

Kim, Y.H., Y.H. Bae and S.W. Kim. pH/Temperature-Sensitive Polymers for Macromolecular Drug Loading and Release, *28*, pp. 143-152. 1994.

Kohori, F., K. Sakai, T. Aoyagi, M. Yokoyama, Y. Sakurai and T. Okano. Preparation and Characterisation of Thermally Responsive Block Copolymer Micelles Comprising Poly(*N*-isopropylacrylamide-*b*-DL-lactide), Journal of Controlled Release, *55*, pp. 87-98. 1998.

Kohori, F., M. Yokoyama, K. Sakai and T. Okano. Process Design for Efficient and Controlled Drug Incorporation into Polymeric Micelle Carrier Systems, Journal of Controlled Release, *78*, pp. 155-163. 2002.

Kost, J. Intelligent Drug Delivery Systems. In Encyclopedia of Controlled Drug Delivery, Vol. 1, ed by E. Mathiowitz, pp. 445-461. New York: Wiley-Interscience. 1999.

Kreuter, J. Evaluation of Nanoparticles as Drug-Delivery-Systems II: Comparison of the Body Distribution of Nanoparticles with the Body Distribution of Microspheres (Diameter > 1 µm), Liposomes, and Emulsions, Pharmaceutica Acta Helvetiae, *58*, pp. 217-226. 1983.

Kwon, G., M. Naito, M. Yokoyama, T. Okano, Y. Sakurai and K. Kataoka. Block Copolymer Micelles for Drug Delivery: Loading and Release of Doxorubicin**,** Journal of Controlled Release, *48*, pp. 195-201. 1997.

Kwon, G., M. Naito, M. Yokoyama, T. Okano, Y. Sakurai and K. Kataoka. Micelles Based on AB Block Copolymers of Poly(ethylene oxide) and Poly(β-benzyl L-aspartate), Langmuir, *9*, pp. 945-949. 1993a.

Kwon, G, S. Suwa, M. Yokoyama, T. Okano, Y. Sakurai and K. Kataoka. Enhanced Tumor Accumulation and Prolonged Circulation Times of Micelle-Forming Poly(ethylene oxide-aspartate) Block Copolymer-Adriamycin Conjugates, Journal of Controlled Release, *29*, pp. 17-23. 1994a.

Kwon, G.S. and K. Kataoka. Block Copolymer Micelles as Long-Circulating Drug Vehicles, Advanced Drug Delivery Reviews, *16*, pp. 295-309. 1995.

Kwon, G.S., M. Naito, K. Kataoka, M. Yokoyama, Y. Sakurai and T. Okano. Block Copolymer Micelles as Vehicles for Hydrophobic Drugs, Colloids and Surfaces B: Biointerfaces, *2*, pp. 429-434. 1994b.

Kwon, G.S., M. Naito, M. Yokoyama, T. Okano, Y. Sakurai and K. Kataoka. Physical Entrapment of Adriamycin in AB Block Copolymer Micelles, Pharmaceutical Research, *12*, pp. 192-195. 1995.

Kwon, G.S., M. Yokoyama, T. Okano, Y. Sakurai and K. Kataoka. Biodistribution of Micelle-Forming Polymer-Drug Conjugates, Pharmaceutical Research, *10*, pp. 970-974. 1993b.

Kwon, G.S. and T. Okano. Polymeric Micelles as New Drug Carriers, Advanced Drug Delivery Reviews, *21*, pp. 107-116. 1996.

Kwon, G.S. and T. Okano. Soluble Self-Assembled Block Copolymers for Drug Delivery, Pharmaceutical Research, *16*, pp. 597-600. 1999.

Kwon, I.C., Y.H. Bae and S.W. Kim. Electrically Erodible Polymer Gel for Controlled Release of Drugs, Nature, *354*, pp. 291-293. 1991.

Kyriakides, T.R., C.Y. Cheung, N. Murthy, P. Bornstein, P.S. Stayton and A.S. Hoffman. pH-Sensitive Polymers that Enhance Intracellular Drug Delivery In Vivo, Journal of Controlled Release, *78*, pp. 295-303. 2002.

La, S.B., T. Okano and K. Kataoka. Preparation and Characterization of the Micelle-Forming Polymeric Drug Indomethacin-Incorporated Poly(ethylene oxide)-Poly(β-

benzyl L-aspartate) Block Copolymer Micelles, Journal of Pharmaceutical Sciences, *85*, pp. 85-90. 1996.

Lasic, D.D. Doxorubicin in Sterically Stabilized Liposomes, Nature, *380*, pp. 561-562. 1996.

Lavasanifar, A., J. Samuel and G.S. Kwon. Micelles of Poly(ethylene oxide)-*Block*-Poly(*N*-alkyl stearate L-aspartamide): Synthetic Analogues of Lipoproteins for Drug Delivery, Journal Of Biomedical Materials Research, *52*, pp. 831-835. 2000.

Lavasanifar, A., J. Samuel and G.S. Kwon. Micelles Self-Assembled from Poly(ethylene oxide)-*Block*-Poly(*N*-hexyl stearate L-aspartamide) by a Solvent Evaporation Method: Effect on the Solubilization and Haemolytic Activity of Amphotericin B, Journal of Controlled Release, *77*, pp. 155-160. 2001a.

Lavasanifar, A., J. Samuel and G.S. Kwon. Poly(ethylene oxide)-*Block*-Poly(L-amino acid) Micelles for Drug Delivery, Advanced Drug Delivery Reviews, *54* pp. 169-190. 2002a.

Lavasanifar, A., J. Samuel and G.S. Kwon. The Effect of Alkyl Core Structure on Micellar Properties of Poly(ethylene oxide)-Block-Poly(L-aspartamide) Derivatives, Colloids and Surfaces B: Biointerfaces, *22*, pp.115-126. 2001b.

Lavasanifar, A., J. Samuel and G.S. Kwon. The Effect of Fatty Acid Substitution on the In Vitro Release of Amphotericin B from Micelles Composed of Poly(ethylene oxide)-*Block*-Poly(*N*-hexyl stearate-L-aspartamide), Journal of Controlled Release, *79*, pp. 165-172. 2002b.

Leroux, J.C., E. Roux, D.L. Garrec, K. Hong and D.C. Drummond. *N*-isopropylacrylamide Copolymers for the Preparation of pH-Sensitive Liposomes and Polymeric Micelles, Journal of Controlled Release, *72*, pp. 71-84. 2001.

Leroux, J.C., R.M. Cozens, J.L. Roesel, B. Galli, E. Doelker and R. Gurny. pH-Sensitive Nanoparticles: An Effective Means to Improve the Oral Delivery of HIV-1 Protease Inhibitors in Dogs, Pharmaceutical Research, *13*, pp. 485-487. 1996.

Li, Y. and G.S. Kwon. Methotrexate Esters of Poly(ethylene oxide)-*Block*-Poly(2-hydroxyethyl-L-Aspartamide). Part 1: Effects of the Level of Methotrexate Conjugation on the Stability of Micelles and on Drug Release, Pharmaceutical Research, *17*, pp. 607-611. 2000.

Li, Y. and G.S. Kwon. Micelle-like Structures of Poly(ethylene oxide)-*Block*-Poly(2-hydroxyethyl aspartamide)-Methotrexate Conjugates, Colloids and Surfaces B: Biointerfaces, *16*, pp. 217-226. 1999.

Linhardt, R.J. Biodegradable Polymers for Controlled Release of Drugs. In Controlled Release of Drugs: Polymers and Aggregate Systems, ed by M. Rosoff, pp. 53-95. New York: VCH Publishers. 1989.

Liu, S., J.V.M. Weaver, Y. Tang, N.C. Billingham and S.P. Armes. Synthesis of Shell Cross-Linked Micelles with pH-Responsive Cores Using ABC Triblock Copolymers, Macromolecules, *35*, pp. 6121-6131. 2002.

Liu, X.M., Y.Y. Yang and K.W. Leong. Thermally Responsive Polymeric Micellar Nanoparticles Self-Assembled from Cholesteryl End-Capped Random Poly(*N*-isopropylacrylamide-co-*N,N*-dimethylacrylamide): Synthesis, Temperature-Sensitivity and Morphologies, Journal of Colloid and Interface Science, *266*, pp. 295-303. 2003.

Loosli, H.R., H. Oschkinat, H.P. Weber, T.J. Petcher and A. Widmer. The Conformation of Cyclosporin A in the Crystal and Solution, Helvetica Chimica Acta, *68*, pp. 682-704. 1985.

Maeda, H., J. Wu, T. Sawa, Y. Matsumura and K. Hori. Tumor Vascular Permeability and the EPR Effect in Macromolecular Therapeutics: A Review, Journal of Controlled Release, *65*, pp. 271-284. 2000.

Marin, A., H. Sun, G.A. Husseini, W.G. Pitt, D.A. Christensen and N.Y. Rapoport. Drug Delivery in Pluronic Micelles: Effect of High-Frequency Ultrasound on Drug Release from Micelles and Intracellular Uptake, Journal of Controlled Release, *84*, pp. 39-47. 2002.

Marin, A., M. Muniruzzaman and N. Rapoport. Mechanism of the Ultrasonic Activation of Micellar Drug Delivery, Journal of Controlled Release, *75*, pp. 69-81. 2001.

Matsumura, Y. and H. Maeda. A New Concept for Macromolecular Therapeutics in Cancer Chemotherapy: Mechanism of Tumoritropic Accumulation of Proteins and the Antitumor Agent Smancs, Cancer Research, *46*, pp. 6387-6392. 1986.

Meyer, D.E., B.C. Shin, G.A. Kong, M.W. Dewhirst and A. Chilkoti. Drug Targeting using Thermally Responsive Polymers and Local Hyperthermia, Journal of Controlled Release, *74*, pp. 213-224. 2001.

Meyer, O., D. Papahadjopoulos and J.C. Leroux. Copolymers of *N*-Isopropylacrylamide Can Trigger pH Sensitivity to Stable Liposomes. FEBS Letters, *42*, pp. 61-64. 1998.

Mikos, A.G., R.M. Murphy, H. Bernstein and N.A. Peppas. Biomaterials for Drug and Cell Delivery. In Materials Research Society Symposium Proceedings, November 1993, Boston, Massachusetts, USA, Vol. 331.

Mizumura, Y., Y. Matsumura, T. Hamaguchi, N. Nishiyama, K. Kataoka, T. Kawaguchi, W.J.M. Hrushesky, F. Moriyasu and T. Kakizoe. Cisplatin-Incorporated Polymeric Micelles Eliminate Nephrotoxicity, While Maintaining Antitumor Activity, Japanese journal of cancer research, *92*, pp. 328-336. 2001.

Na, K., K.H. Park, S.W. Kim and Y.H. Bae. Self-Assembled Hydrogel Nanoparticles from Curdlan Derivatives: Characterization, Anti-Cancer Drug Release and Interaction with a Hepatoma Cell Line (HepG2), Journal of Controlled Release, *69*, pp. 225-236. 2000.

Na, K., E.S. Lee and Y.H. Bae. Adriamycin Loaded Pullulan Acetate/Sulfonamide Conjugate Nanoparticles Responding to Tumor pH: pH-Dependent Cell Interaction, Internalization and Cytotoxicity in Vitro, Journal of Controlled Release, *87*, pp. 3-13. 2003.

Nagarajan, R. and K. Ganesh. Block Copolymer Self-Assembly in Selective Solvents: Theory of Solubilization in Spherical Micelles, Macromolecules, *22*, pp. 4312-4325. 1989.

Nagarajan, R., M. Barry and E. Ruckenstein. Unusual Selectivity in Solubilization by Block Copolymer Micelles, Langmuir, *2*, pp. 210-215. 1986.

Nah, J.W., Y.I. Jeong and C.S. Cho. Clonazepam Release from Core-Shell Type Nanoparticles Composed of Poly(γ-benzyl L-glutamate) as the Hydrophobic Part and Poly(ethylene oxide) as the Hydrophilic Part, Journal of Polymer Science: Part B: Polymer Physics, *36*, pp. 415-423. 1998.

Nakajima, A. Solvent Effect on the Vibrational Structures of the Fluorescence and Absorption Spectra of Pyrene, Bulletin of the Chemical Society of Japan, *44*, pp. 3272-3277. 1971.

Niwa, T., H. Takeuchi, T. Hino, M. Nahara and Y. Kawashima. Biodegradable Submicron Carriers for Peptide Drugs: Preparation of DL-Lactide Glycolide

Copolymer (PLGA) Nanospheres with Nafarelin Acetate by a Novel Emulsion-Phase Separation Method in an Oil System, International Journal of Pharmaceutics, *121*, pp. 1123-1130. 1995.

Palmer, T.N., V.J. Caride, M.A. Caldecourt, J. Twickler and V. Abdullah. The Mechanism of Liposome Accumulation in Infarction, Biochimica Et Biophysica Acta, *797*, pp. 363-368. 1984.

Park, K. (ed). Controlled Drug Delivery: Challenges and Strategies. pp. 49-67, Washington, DC: American Chemical Society. 1997.

Pratten, M.K. and J.B. Lloyd. Micelle-Forming Block Copolymers: Pinocytosis by Macrophages and Interaction with Model Membranes, Makromolekulare Chemie, *186*, pp. 725-733. 1985.

Příborský, J., K. Takayama and T. Nagai. Influence of Acute Uraemia on Percutaneous Absorption of Nonsteroidal Anti-Inflammatory Drugs, Acta Universitatis Palackinae Olomucensis Faculty of Medicine, *141*, pp. 35-38. 1998.

Price, C. Micelle Formation by Block Copolymer in Organic Solvents, Pure and Applied Chemistry, *55*, pp. 1563-1572. 1983.

Prochaska, K., D. Kiserow, C. Ramireddy, Z. Tuzar, P. Munk and S.E. Webber. Time-Resolved Fluorescence Studies of the Chain Dynamics of Naphthalene-Labelled Polystyrene-Block-Poly(methacrylic acid) Micelles in Aqueous Media, Macromolecules, *25*, pp. 454-460. 1992.

Rapoport, N.Y., J.N. Herron, W.G. Pitt and L. Pitina. Micellar Delivery of Doxorubicin and its Paramagnetic Analog, Ruboxyl, to HL-60 Cells: Effect of Micelle Structure and Ultrasound on the Intracellular Drug Uptake, Journal of Controlled Release, *58*, pp. 153-162. 1999.

Riley, T., T. Govender, S. Stolnik, C.D. Xiong, M.C. Garnett, L. Illum and S.S. Davis. Colloidal Stability and Drug Incorporation Aspects of Micellar-Like PLA-PEG Nanoparticles, Colloids and Surfaces B: Biointerfaces, *16*, pp. 147-159. 1999.

Ringsdorf, H., J. Venzmer and F.M. Winnik. Fluorescence Studies of Hydrophobically Modified Poly(*N*-isopropylarylamides), Macromolecules, *24*, pp. 1678-1686. 1991.

Roland, A., J.E. O'Mullane, P. Goddard, L. Brookman and K. Petrak. New Macromolecular Carriers for Drugs, I. Preparation and Characterization of Poly(oxyethylene-*b*-isoprene-*b*-oxyethylene) Block Copolymer Aggregates, Journal Of Applied Polymer Science, *44*, pp. 1195-1203. 1992.

Sakata, M., M. Todokoro, T. Kai, M. Kunitake and C. Hirayama. Effect of Cationic Polymer Adsorbent pK_a on the Selective Removal of Endotoxin from an Albumin Solution, Chromatographia, *53*, pp. 619-623. 2001.

Schroeder, H.G., G.H. Simmons and P.P. Deluca. Distribution of Radiolabelled Subsieve Microsphres After Intravenous Administration to Beagle Dogs, Journal of Pharmaceutical Sciences, *67*, pp. 504-507. 1978.

Serres, A., M. Baudyš and S.W. Kim. Temperature and pH-Sensitive Polymers for Human Calcitonin Delivery, Pharmaceutical Research, *13*, pp. 196-201. 1996.

Seymour, L.W., K. Kataoka and A.V. Kabanov. Cationic Block Copolymers as Self-Assembling Vectors for Gene Delivery. In Self-Assembling Complexes for Gene Delivery from Laboratory to Clinical Trial, ed by A.V. Kabanov, L.W. Seymour and P. Felgner, pp. 219-239. Chichester: John Wiley. 1998.

Shin, I.G., S.Y. Kim, Y.M. Lee, C.S. Cho and Y.K. Sung. Methoxy Poly(ethylene glycol)/ϵ-Caprolactone Amphiphilic Block Copolymeric Micelle Containing Indomethacin I. Preparation and Characterization, Journal of Controlled Release, *51*, pp. 1-11. 1998.

Siegal, T., A. Horowitz and A. Gabizon. Doxorubicin Encapsulation in Sterically Stabililized Liposomes for the Treatment of a Brain Tumor Model: Biodistribution and Therapeutic Efficacy, Journal of Neurosurgery, *83*, pp. 1029-1037. 1995.

Sinko, P. and J. Kohn. Polymeric Drug Delivery Systems: An Overview. In Polymeric Delivery Systems: Properties and Applications, ed by M.A. El-Nokaly, D.M. Piatt and B.A. Charpentier, pp. 18-41. Washington: American Chemical Society. 1993.

Stolnik, S., M.C. Garnett, M.C. Davies, L. Illum, M. Bousta, M. Vert and S.S. Davis, The Colloidal Properties of Surfactant-Free Biodegradable Nanospheres from Poly(*β*-malic acid-*co*-benzyl malate)s and Poly(lactic acid-*co*-glycolide), Colloids and Surfaces A : Physicochemical and Engineering Aspects, *97*, pp. 235-245. 1995.

Suzuki, A. And T. Tanaka. Phase Transition in Polymer Gels Induced by Visible Light, Nature, *346*, pp. 345-347. 1990.

Taillefer, J., M.C. Jones, N. Brasseur, J.E. van Lier and J.C. Leroux. Preparation and Characterization of pH-Responsive Polymeric Micelles for the Delivery of Photosensitizing Anticancer Drugs, Journal of Pharmaceutical Sciences, *89*, pp. 52-62. 2000.

Takeoka, Y., T. Aoki, K. Sanui, N. Ogata, M. Yokoyama, T. Okano, Y. Sakurai and M. Watanabe. Electrochemical Control of Drug Release from Redox-Active Micelles, Journal of Controlled Release, *33*, pp. 79-87. 1995.

Tanaka, N., M. Takemura, T. Konnu and S. Kunugi. Pressure Effect on the Chain Shrinkage of Poly(vinylpyrrolidone) Induced by Complexation with a Hydrophobic Compound in Aqueous Solution, Macromolecules, *31*, pp. 8840-8844. 1998.

Tardi, P.G., N.L. Boman and P.R. Cullis. Review: Liposomal Doxorubicin, Journal of Drug Targeting, *4*, pp. 129-140. 1986.

Tannock, I.F. and D. Rotin. Acid pH in Tumors and Its Potential for Therapeutic Exploitation, Cancer Research, *49*, pp. 4373-4384. 1989.

Teng, Y., M.E. Morrison, P. Munk and S.E. Webber. Release Kinetics Studies of Aromatic Molecules into Water from Block Polymer Micelles, Macromolecules, *31*, pp. 3578-3587. 1998.

Torchilin, V.P. Structure and Design of Polymeric Surfactant-Based Drug Delivery Systems, Journal of Controlled Release, *73*, pp. 137-172, 2001.

Ulbrich, K., C. Konak, Z. Tuzar and J. Kopecek. Solution of Drug Carriers Based on Poly[N-(2-hydroxypropyl)methacrylamide] Containing Biodegradable Bonds, Makromolekulare Chemie, *188*, pp. 1261-1272. 1987.

Ulbrich, K., T. Etrych, P. Chytil, M. Jelínková and B. Říhová. HPMA Copolymers with pH-Controlled Release of Doxorubicin In Vitro Cytotoxicity and In Vivo Antitumor Activity, Journal of Controlled Release, *87*, pp. 33-47, 2003.

Urry, D.W. Physical Chemistry of Biological Free Energy Transduction As Demonstrated by Elastic Protein-Based Polymers, Journal of Physical Chemistry B, *101*, pp. 11007-11028. 1997.

Van den Berg, A.P., J.L. Wike-Hooley, A.E. van den Berg-Blok, J. van der Zee and H.S. Reinhold. Tumor pH in Human Mammary Carcinoma, European Journal of Cancer and Clinical Oncology, *18*, pp. 457-462. 1982.

Wang, Y., R. Balaji, P. Quirk and W.L. Mattice. Detection of the Rate of Exchange Between Micelles Formed by Diblock Copolymers in Aqueous Solution, Polymer Bulletin, *28*, pp. 333-338. 1992.

Weinstein, J.N. Liposomes in the Diagnosis and Treatment of Cancer. In Liposomes: from Biophysics to Therapeutics, ed by M.J. Ostro, pp. 277-338. New York: Dekker. 1987.

Weinstein, J.N. and W. van Osdol. The Macroscopic and Microscopic Pharmacology of Monoclonal Antibodies, International Journal of Immunopharmacology, *14*, pp. 457-463. 1992.

Weissig, V., K.R. Whiteman and V.P. Torchilin. Accumulation of Protein-Loaded Long-Circulating Micelles and Liposomes in Subcutaneous Lewis Lung Carcinoma in Mice, Pharmaceutical Research, *15*, pp. 1552-1556. 1998.

Wilczek-Vera, G., P.O. Danis and A. Eisenberg. Individual Block Length Distributions of Block Copolymers of Polystyrene-Block-Poly(α-methylstyrene) by MALDI/TOF Mass Spectrometry, Macromolecules, *29*, pp. 4036-4044. 1996.

Wilhelm, M., C.L. Zhao, Y. Wang, R. Xu and M.A. Winnik. Poly(styrene-ethylene oxide) Block Copolymer Micelle Formation in Water: A Fluorescence Probe Study, Macromolecules, *24*, pp. 1033-1040. 1991.

Winnik, F.M., A.R. Davidson, G.K. Hamer and H. Kitano. Amphiphilic Poly(N-isopropylacrylamides) Prepared by Using a Lipophilic Radical Initiator: Synthesis and Solution Properties in Water, Macromolecules, *25*, pp. 1876-1880. 1992.

Xing, L. and W.L. Mattice. Strong Solubilization of Small Molecules by Triblock-Copolymer Micelles in Selective Solvents, Macromolecules, *30*, pp. 1711-1717. 1997.

Xu, R., M. Winnik, F.R. Hallett, G. Riess and M.D. Croucher. Light Scattering Study of the Association Behaviour of Sytrene-Ethylene Oxide Block Copolymers in Aqueous Solution, Macromolecules, *24*, pp. 87-93. 1991.

Yamamoto, Y., K. Yasugi, A. Harada, Y. Nagasaki and K. Kataoka. Temperature-Related Change in the Properties Relevant to Drug Delivery of Poly(ethylene glycol)-Poly(D,L-lactide) Block Copolymer Micelles in Aqueous Milieu, Journal of Controlled Release, *82*, pp. 359-371. 2002.

Yamamoto, Y., Y. Nagasaki, M. Kato and K. Kataoka. Surface Charge Modulation of Poly(ethylene glycol)-Poly(D,L-lactide) Block Copolymer Micelles: Conjugation of Charged Peptides, Colloids and Surfaces B: Biointerfaces, *16*, pp. 135-146. 1999.

Yamamoto, Y., Y. Nagasaki, Y. Kato, Y. Sugiyama and K. Kataoka. Long-Circulating Poly(ethylene glycol)- Poly(D,L-lactide) Block Copolymer Micelles with Modulated Surface Charge, Journal of Controlled Release, *77*, pp. 27-38. 2001.

Yang, H. and W.F. Elmquist. The Binding of Cyclosporin A to Human Plasma: An In Vitro Microdialysis Study, Pharmaceutical Research, *13*, pp. 622-627. 1996.

Yasugi, K., T. Nakamura, Y. Nagasaki, M. Kato and K. Kataoka. Sugar-Installed Polymer Micelles: Synthesis and Micellization of Poly(ethylene glycol)-Poly(D,L-lactide) Block Copolymers Having Sugar Groups at the PEG Chain End, Macromolecules, *32*, pp. 8024-8032. 1999.

Yokoyama, M. Novel Passive Targetable Drug Delivery with Polymeric Micelles. In Biorelated Polymers and Gels: Controlled Release and Applications in Biomedical Engineering, ed by T. Okano, pp. 193-229. New York: Academic Press. 1998.

Yokoyama, M., A. Satoh, Y. Sakurai, T. Okano, Y. Matsumura, T. Kakizoe and K. Kataoka. Incorporation of Water-Insoluble Anticancer Drug into Polymeric Micelles and Control of Their Particle Size, Journal of Controlled Release, *55*, pp. 219-229. 1998a.

Yokoyama, M., G.S. Kwon, T. Okano, Y. Sakurai, M. Naito and K. Kataoka. Influencing Factors on In Vitro Micelle Stability of Adriamycin-Block Copolymer Conjugates, Journal of Controlled Release, *28*, pp. 59-65. 1994a.

Yokoyama, M., M. Miyauchi, N. Yamada, T. Okano, Y. Sakurai and K. Kataoka. Characterization and Anticancer Activity of the Micelle-Forming Polymeric Anticancer Drug Adriamycin-Conjugated Poly(ethylene glycol)-Poly(aspartic acid) Block Copolymer, Cancer Research, *50*, pp. 1693-1700. 1990.

Yokoyama, M., S. Fukushima, R. Uehara, K. Okamoto, K. Kataoka, Y. Sakurai and T. Okano. Characterization of Physical Entrapment and Chemical Conjugation of

Adriamycin in Polymeric Micelles and Their Design for in Vivo Delivery to a Solid Tumor, Journal of Controlled Release, *50*, pp. 79-92. 1998b.

Yokoyama, M., T. Okano and K. Kataoka. Improved Synthesis of Adriamycin-Conjugated Poly(ethylene oxide)-Poly(aspartic acid) Block Copolymer and Formation of Unimodal Micellar Structure with Controlled Amount of Physically Entrapped Adriamycin, Journal of Controlled Release, *32*, pp. 269-277. 1994b.

Yokoyama, M., T. Okano, Y. Sakurai, S. Suwa and K. Kataoka. Introduction of Cisplatin into Polymeric Micelles, Journal of Controlled Release, *39*, pp. 351-356. 1996.

Yokoyama, M., T. Sugiyama, T. Okano, Y. Sakurai, M. Naito and K. Kataoka. Analysis of Micelle Formation of an Adriamycin-Conjugated Poly(ethylene glycol)-Poly(aspartic acid) Block Copolymer by Gel Permeation Chromatography, Pharmaceutical Research, *10*, pp. 895-899. 1993.

Yoo, H.S. and T.G. Park. Biodegradable Polymeric Micelles Composed of Doxorubicin Conjugated PLGA-PEG Block Copolymer, Journal of Controlled Release, *70*, pp. 63-70. 2001.

Yoo, H.S., E.A. Lee and T.G. Park. Doxorubicin-Conjugated Biodegradable Polymeric Micelles Having Acid-Cleavable Linkages, Journal of Controlled Release, *82*, pp. 17-27. 2002.

Yu, B.G., T. Okano, K. Kataoka and G. Kwon. Polymeric Micelles for Drug Delivery: Solubilization and Haemolytic Activity of Amphotericin B, Journal of Controlled Release, *53*, pp. 131-136. 1998.

Yu, L. and G.S. Kwon. Micelle-like Structures of Poly(ethylene oxide)-*Block*-Poly(2-hydroxyethyl aspartamide)-Methotrexate Conjugates, Colloids and Surfaces B: Biointerfaces, *16*, pp. 217-226. 1999.

Yu, L. and G.S. Kwon. Methotrexate Esters of Poly(Ethylene Oxide)-*Block*-Poly(2-hydroxyethyl-L-aspartamide). Part 1: Effects of the Level of Methotrexate Conjugation on the Stability of Micelles and on Drug Release, Pharmaceutical Research, *17*, pp. 607-611. 2000.

Yu, Y. and A. Eisenberg. Control of Morphology through Polymer-Solvent Interactions in Crew-Cut Aggregates of Amphiphilic Block Copolymers, Journal of the American Chemical Society, *119*, pp. 8383-8384. 1997.

Yu, Y., L. Zhang and A. Eisenberg. Multiple Morphologies of Crew-Cut Aggregates of Polybutadiene-*b*-poly(acrylic acid) Diblocks with Low T_g Cores, Langmuir, *13*, pp. 2578-2581. 1997.

Yuan, F., M. Leuning, S.K. Huang, D.A. Berk, D. Papahadjopoulos and R.K. Jain. Microvascular Permeability and Interstitial Penetration of Sterically Stabilized (Stealth) Liposomes in a Human Tumor Xenograft, Cancer Research, *54*, pp. 3352-3356. 1994.

Yuk, S.H., S.H. Cho and S.H. Lee. pH/Temperature-Responsive Polymer Composed of Poly(*N*,*N*-dimethylamino)ethyl methacrylate-co-ethylacryamide, Macromolecules, *30*, pp. 6856-6859. 1997.

Zhang, L. and A. Eisenberg. Morphogenic Effect of Added Ions on Crew-Cut Aggregates of Polystyrene-*b*-poly(acrylic acid) Block Copolymers in Solutions, Macromolecules, *29*, pp. 8805-8815. 1996a.

Zhang, L. and A. Eisenberg. Multiple Morphologies and Characteristics of "Crew-Cut" Micelle-like Aggregates of Polystyrene-*b*-poly(acrylic acid) Diblock Copolymers in Aqueous Solutions, Journal of the American Chemical Society, *118*, pp. 3168-3181. 1996b.

Zhang, L. and A. Eisenberg. Structures of "Crew-Cut" Aggregates of Polystyrene-*b*-poly(acrylic acid) Diblock Copolymers, Macromolecular Symposia, *113*, pp. 221-232. 1997.

Zhang, L., K. Yu and A. Eisenberg. Ion-Induced Morphological Changes in "Crew-Cut" Aggregates of Amphiphilic Block Copolymers, Science, *272*, pp. 1777-1779. 1996a.

Zhang, X., J.K. Jackson and H.M. Burt. Development of Amphiphilic Diblock Copolymers as Micellar Carriers of Taxol, International Journal of Pharmaceutics, *132*, pp. 195-206. 1996b.

APPENDIX A

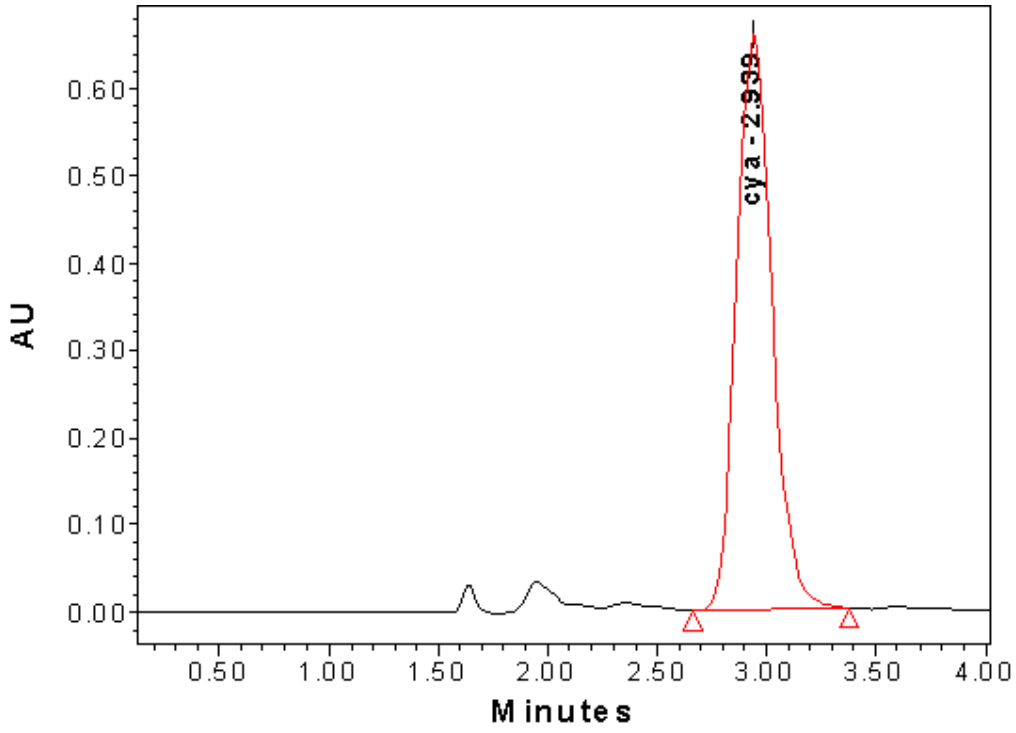

Figure A.1 HPLC chromatogram of a CyA standard solution (Concentration: 30 ppm)

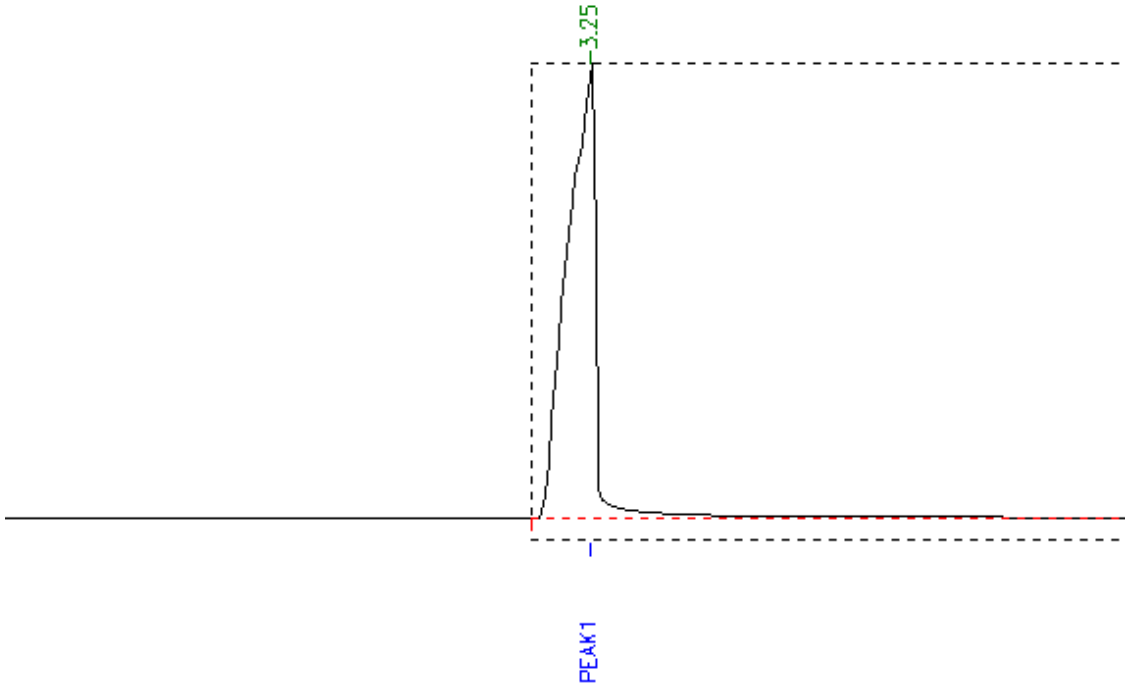

Figure A.2 GC gaschromatogram of a DMF standard solution (Concentration: 30 ppm)

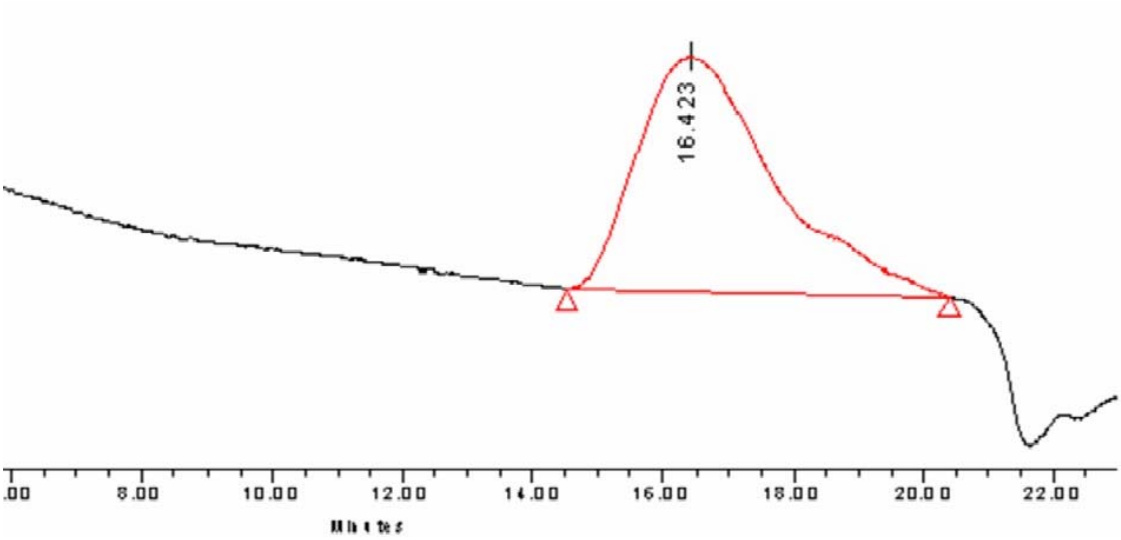

Figure A.3 GPC chromatogram of P(NIPAAm-*co*-DMAAm-*co*-OA) in THF